Combustion Instabilities:

Issues in Modeling and Control

Thesis by

Claude Seywert

In partial fulfillment of the requirements for the degree of

Doctor of Philosophy

California Institute of Technology

Pasadena, California

2001

(Defended February 20, 2001)

Acknowledgments

At the beginning of this thesis I would like to extend my thanks to various people who have helped me during my time as a graduate student at Caltech.

Foremost among these is my thesis advisor, Dr. F.E.C. Culick, who provided me with motivation and guidance throughout my graduate studies.

I would like to thank Dr. Richard Murray, Dr. Mory Gharib and Dr. Hans Hornung for accepting to serve on my thesis committee and the GALCIT faculty in general for supporting my studies and my research.

I gratefully acknowledge the financial support for the research reported herein by the Air Force Office of Scientific Research, the Advanced Gas Turbines System Research program of the Department of Energy, the Italian power company ENEL and the California Institute of Technology.

My fellow students at the Jet Propulsion Center deserve a lot of credit. Without the numerous discussions with Winston Pun, Steve Palm, and Grant Swensson, none of this work would have been completed. For valuable ideas and contributions I would like to thank Sanjeev Malhorta and Konstantin Matveev. I also benefited from talks with Guido Poncia during his stay at Caltech. Most of the work presented in this thesis complements the research done by Giorgio Isella. Besides providing me with help and advice, he helped

me relax during our daily coffee break at the Red Door Cafe. Thanks also belong to Olivier Duchemin who has been my office mate during my stay at Caltech.

I need to recognize the encouragement of all those other people who were not directly involved with my work but helped create an environment that fostered my development. Ying, Luis, Stefan, Tobias, Sandeep and the rest of the gang: your support was greatly appreciated.

Last but not least there's all those who made my stay in Southern California an unforgettable experience: the various members of the Aero soccer team whose proud captain I was and who gave me an excuse to exercise; the directors of the Graduate Student Council with whom I had the pleasure to serve; the wonderful people I got to know and cherish through the Life Teen program at the St. Philip the Apostle Catholic Church; the friends I made at the Tilden Study Center. Thanks to everyone of you: I will truly treasure the memories of our time together.

And then there's my parents and my family. Without them I wouldn't be finishing a thesis today. What can I say? Thanks a lot!

Abstract

This study deals with various aspects in the development of active control of combustion instabilities.

A low-order model is developed, reconciling along the way two different approaches taken by researchers to attack the description of combustion instabilities. The model is demonstrated with application to a Rijke tube and compared to experiments. The Rijke burner experiments suggest two major discrepancies with the model: the presence of a hysteresis loop is unaccounted for and the model does not describe the seemingly random fluctuations in the amplitude of the pressure oscillations in the 'unstable' regime. So far no explanation for the hysteresis can be given; however, this phenomenon is successfully exploited by using a novel nonlinear control technique to expand the stable operating range of the burner.

The origin of the 'noise' in the pressure trace is explained by considering entropy and vorticity waves in the combustor. Their presence leads to a slight modification of the original model, introducing stochastic source terms into the oscillator equations. The consequences of the presence of these terms is analyzed by means of simulations. One interesting result is that they allow for the identification of model parameters from a single experimental run of a stable combustion system.

Finally, a unified approach to controlling combustion instabilities is presented. The formu-

lation and analysis account for truncation to a few modes; uncertainties in the description of the system (including uncertain sensing and actuating); external disturbances; and intrinsic noise sources. An explicit expression is derived against which any controller can be checked for stability.

Contents

List of Figures

List of Tables

Chapter 1

Introduction

Conventional propulsion and power systems convert chemical into kinetic energy by burning the fuel. In this work we are concerned with rocket engines, afterburners (solid or liquid fuels) and gas turbines (liquid or gaseous fuel). These very different systems can be treated by a common analysis since the main feature is common to all of them: a substantial amount of energy is released within a small spacial volume. It should not be surprising that the resulting enormous power densities are accompanied by relatively small fluctuations. These oscillations are usually negligible with respect to steady thrust or power produced. That's because even at the highest amplitudes observed in practice these oscillations consume only a small fraction of the total available chemical energy. Nevertheless these fluctuations of pressure or thrust, when sustained, can lead to serious problems (e.g., structural vibrations) or annoying effects (e.g., production of pollutants).

A famous example of this sort of oscillations are the POGO oscillations that occurred in the Apollo launch vehicle; in that case there was a strong coupling between the combustion chamber pressure oscillations and the propellant feed system. Air-breathing propulsion systems also suffer from these oscillations; in ramjets, for instance, their influence on the

shock system in the inlet diffuser can reduce the inlet stability margin.

More recently the occurrence of sustained pressure fluctuations in the main combustor of gas turbines has attracted a lot of attention. This is ultimately due to an increased global interest in clean power generation. Among the characteristics of gas turbines making them more attractive for use in stationary power generation than traditional power plants are higher efficiency and lower production of pollutants, especially oxides of nitrogen(NO_x). Limits on the efficiency and emission level attainable in practice are set by operating conditions for which combustion can be successfully sustained. To achieve the low levels of NO_x mandated by law, most gas turbine vendors have developed some form of lean-premix combustion. In these devices the fuel/air ratio typically approaches one-half the ideal stoichiometric level (i.e., twice as much air is supplied as is actually needed to burn the fuel). The excess air is a key to limiting NO_x formation since very lean conditions cannot produce the high temperatures that create thermal NO_x (the dominant mechanism of NO_x production).

Pressure oscillations driven by combustion have been a repeated problem in the development of low-emission premix combustors. This problem is due to specific changes made to the combustor to accommodate the premix approach. In premix systems, most of the combustion air is sent through the fuel injector, eliminating the need for downstream combustion air holes; unfortunately, this eliminates acoustic damping that reduces the likelihood of oscillations. Furthermore, in premix systems, slight disturbances in pressure create immediate changes in the airflow, producing a subsequent change in reaction stoichiometry. Near the lean combustion limit even minor changes in reaction stoichiometry can lead to significant variations in heat release – which, if synchronized with the resonant pressure,

can sustain an oscillating combustion. Finally, because the fuel and air are mixed before arriving at the combustion chamber, the flame anchoring is purely aerodynamical. Oscillations can be severe enough to momentarily reverse the flow and create a flame flashback, driving the flame towards the fuel injector. It is therefore essential to eliminate oscillations in commercial engines. With sufficient amplitude, the vibration and enhanced heat transfer that accompany pressure oscillations can lead to fatigue failure of the combustor liner in a matter of hours.

The difficulties in preventing the occurrence of these pressure oscillations, known as 'combustion instabilities' (though this term might be misleading since in almost all instances the combustion processes themselves are stable), arise due to poor understanding and inability to model the underlying processes such as unsteady combustion, coupling with feed systems, and acoustics involving mean flow and nonlinear effects. Given the highly complex and uncertain nature of the problem, predictive tools to model the stability and nonlinear behavior of combustion chambers are impossible to develop. Hence the purpose of the theory is to provide a framework for interpreting observations; to improve the base for understanding the fundamental principles that govern the physical behavior; to formulate guidelines for designing new combustion chambers; and to provide methods and tools for attacking the problem of oscillations during the development of new combustion chambers.

The framework used here reduces the description of combustion instabilities to a low order dynamical system. This formulation allows quick simulations of the system and assessment of its dynamical behavior and changes thereof as a result of modifications in geometry, propellent, etc. (this assumes a model of these various components exists that can be included in the general framework). Furthermore, this formulation is a natural starting

point to apply control techniques to the combustion system.

Controlling combustion instabilities, reducing their amplitude or preventing them from occurring in the first place, is a major focus of current research. Historically, if a combustion instability is encountered in the developmental stage of a system, it is eliminated by trial and error procedures involving changes in the feed system or the combustor geometry, or introduction of devices to produce additional damping such as baffles and resonance rods. These procedures are expensive and time consuming, and any 'knowledge' obtained while tuning a specific system cannot in general be transfered to another combustor. Furthermore, these methods, labeled *passive* control methods, are not always effective in controlling instabilities. Therefore, *active* control is widely viewed as a promising approach for avoiding problems of combustion instability.

An active control system is characterized by the presence of an actuator, a dynamic component that perturbs the combustor to achieve the desired performance. In a closed-loop approach a sensor monitors the state of the combustor (usually by recording pressure in the chamber) and feeds its output to a control algorithm that computes and sends an appropriate control signal to the actuator. Examples of actuators are loudspeakers that produce pressure fluctuations in the combustor or fuel injectors that modulate part of the fuel flow (usually through secondary injection) thereby affecting the heat release in the chamber directly. Reviews of approaches to active control, ranging from the simplest choice of a constant gain and phase shift controller to applications of modern robust control theory, are given by Candel (1992); McManus, Poinsot and Candel (1993); Hong, Yang and Ray (1998); and in AGARD (1996).

As mentioned, the controller development is based on a low order model of the combustion

system. This underlying simplified model is necessary if the controller is to be easily implementable on a commercial combustion system. How can the complex processes in the combustion chamber be captured by such a simple model? The answer resides in the fact that if the amplitudes are small, the vibrations within the chamber are related to classical acoustic behavior possible in the absence of combustion and mean flow. Therefore, we can reduce the dynamics of the combustion chamber to the evolution of a few *modes*. It is important to realize that in applying this reduction, a substantial amount of information has been neglected: while frequency spectra of experimentally obtained pressure traces show indeed the peaks corresponding to the various modes, there's also a substantial broadband *noise* present. This component has been largely neglected in the literature so far; however, its influence on the design of an appropriate controller can be significant. Furthermore, the sources responsible for the appearance of this noise might have a substantial effect on the dynamics of the combustion system itself and could be responsible for the so-called 'triggering' phenomenom. This arises when a combustion system is linearly stable, meaning that small disturbances will decay and disappear, but can be excited to produce a sustained oscillation when hit by a finite-sized fluctuation. In the language of dynamical systems this behavior is characterized by a 'subcritical Hopf-bifurcation'. An example of triggering is shown in figure 1.1.

The figure shows the firing of two identical (same geometry, same propellant) solid propellant test motors, preformed at the China Lake Naval Air Warfare Center Weapons Division by Fred S. Blomshield in August 1997. Motor 1 was pulsed lightly at $t = 1s$ and $t = 2s$ with a pressure disturbance of 3.9% and 3.1% of the mean level respectively. Both pulses decayed. Motor 2 was pulsed at a 9.7% pressure disturbance level; the disturbance grew into a limited

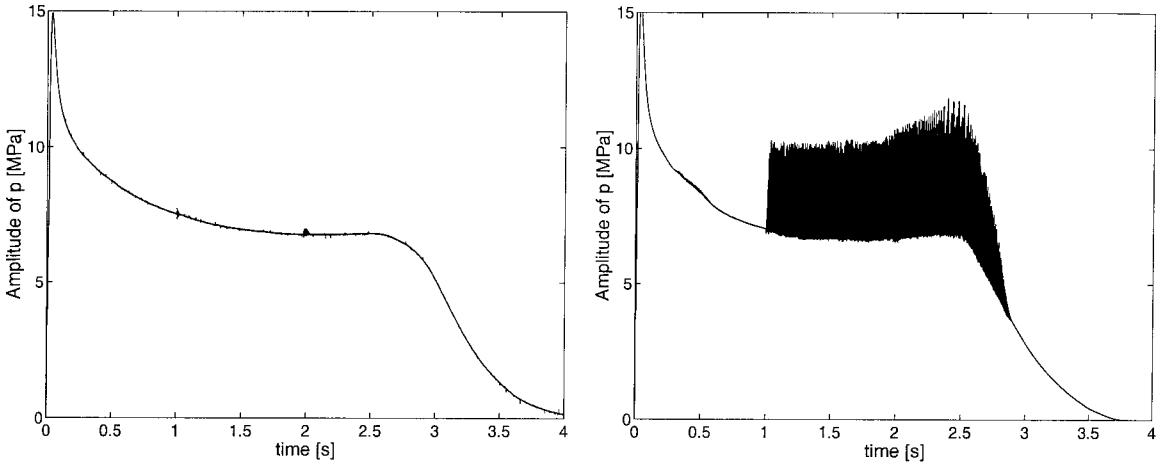

(a) Motor No.1 (b) Motor No.2

Figure 1.1: Test firings of solid propellant rocket motors, illustrating 'triggering' cycle. This shows that linearly stable combustion systems can be unstable to 'large enough' disturbances in the chamber.

Outline of the Thesis

In chapter 2 the mathematical framework used to obtained the reduced order model of the combustion system is exposed. The text gives a brief description of the framework as developed over the years by Culick and his students. This review serves only to establish the underlying equations for this work and is far from complete. In particular, the technique of time-averaging to further simplify the second-order equations to a first-order system has been omitted because we will not use it. An essential part of the procedure as developed by Culick is an iterative solution which is based on a two parameter expansion of the equations. The two parameters in question are the mean flow speed and the amplitude of the oscillations. While we will refer to the 'order' of the equations, the reader is referred to other works for the details of this ordering procedure. We also present an alternative application

of the idea of spatial averaging as developed independently by Zinn and students. We show that when applied to the same equation, the two methods lead to the same formal result. However, the approach taken by this second method (the 'modified Galerkin method') can be applied to more general cases and we discuss a few different applications.

Chapter 3 shows how the equations can be applied to what is arguably the simplest of all combustion devices: a Rijke tube. The novel feature of the model is the introduction of transfer functions for the heat release response into the framework developed in the previous chapter. Simulations of a reduced order model for an electrical Rijke heater and a Rijke burner are presented and compared with experiment. In the Rijke burner experiment, a new type of control making use of the non linear behavior of the system (hysteresis) is successfully demonstrated.

The experiments show some obvious deficiencies of the model. In chapter 4 we try to make the model more realistic by including extra sources (noise) in the equation. The origin of those terms is explained and their effect on the system dynamics analyzed. It is shown that the presence of the noise sources allows for a convenient method of system identification of a stable combustor, meaning that it allows to quantify stability margins without the need of repeated experiments.

Control of combustion instabilities is the subject of chapter 5. We derive an analytical expression which assures the effectiveness of control and against which any controller can be checked. In this equation all factors affecting the reduced order model are taken into account: the neglected modes and their dynamics; noise sources; uncertainties in the model parameters and in the sensing and actuation processes. This is extremely useful as it does not place any restriction on the design of the controller and thus any procedure (usually

depending on the performance one wants to achieve) leading to a controller can be used. To our knowledge this represents the first time that the stability of the closed-loop system has been analyzed under the simultaneous influence of all these effects.

Finally our findings are summarized in chapter 6.

Chapter 2

Analytical Framework

The model structure used in this study is the result of an approximate analysis whose development was initiated three decades ago by Culick (1971). This formulation is very common in the combustion instability literature and has been covered in many other works, e.g., see Culick (1994) for a review.

2.1 Pressure Wave Equation

The analysis starts (as it must) from the fluid mechanical conservation equations. In the cases of a liquid or solid rocket, a rigorous analysis needs to consider a multi-phase flow, but it can be shown that even with these considerations the equations are in the form of a single medium with mass-averaged properties of the various phases. Therefore, these cases can be treated in the same way as the gaseous combustion in gas turbines and we can write:

$$\text{mass}: \quad \frac{\partial \rho}{\partial t} + (\vec{u} \cdot \nabla)\rho = \mathcal{W} \tag{2.1}$$

$$\text{momentum}: \quad \rho\left[\frac{\partial \vec{u}}{\partial t} + (\vec{u}\dot{\nabla})\vec{u}\right] = -\nabla p + \vec{\mathcal{F}} \tag{2.2}$$

$$\text{energy}: \quad \frac{\partial p}{\partial t} + \gamma p \nabla \vec{u} = -\vec{u} \cdot \nabla p + \mathcal{P} \tag{2.3}$$

For convenience the energy equation has been stated with the pressure as the independent variable since the analysis makes use of experimentally observed properties of the pressure which is often the only variable recorded in combustion tests. For a multiphase flow the source terms on the right-hand side of the equations include interaction terms between the phases, but these are ignored here and thus we define

$$\mathcal{W} = -\rho\nabla\cdot\vec{u} \tag{2.4}$$

$$\vec{\mathcal{F}} = \nabla\cdot\vec{\tau} \tag{2.5}$$

$$\mathcal{P} = (\gamma-1)\left[\nabla\cdot\vec{q}+Q-\vec{u}\cdot(\nabla\cdot\vec{\tau})\right] \tag{2.6}$$

To formally make use of the fact that combustion instabilities are closely related to acoustics, a wave equation for the pressure is derived. This is achieved by first writing all variables as sums of averaged and small-amplitude fluctuating parts.

$$\begin{aligned} p(t) &= \bar{p}+p'(t) \\ \rho(\vec{x},t) &= \bar{\rho}(\vec{x})+\rho'(\vec{x},t) \\ \vec{u}(\vec{x},t) &= \vec{\bar{u}}(\vec{x})+\vec{u}'(\vec{x},t) \end{aligned} \tag{2.7}$$

Introducing the splitting (2.7) into the momentum and energy equations yields:

$$\begin{aligned} \bar{\rho}\frac{\partial\vec{u}'}{\partial t}+\nabla p' &= -\rho'\left(\vec{\bar{u}}\dot{\nabla}\vec{u}'+\vec{u}'\cdot\nabla\vec{\bar{u}}+\vec{u}'\cdot\nabla\vec{u}'\right) \\ &\quad -\rho'\left(\vec{\bar{u}}\cdot\nabla\vec{\bar{u}}+\vec{\bar{u}}\cdot\vec{u}'+\vec{u}'\cdot\nabla\vec{\bar{u}}\right)+\vec{\mathcal{F}}' \end{aligned} \tag{2.8}$$

$$\frac{\partial p'}{\partial t}+\gamma\bar{p}\nabla\cdot\vec{u}' = -\gamma p'\nabla\cdot\vec{\bar{u}}-\gamma p'\nabla\cdot\vec{u}'-\vec{\bar{u}}\cdot\nabla p'-\vec{u}'\cdot\nabla\bar{p}-\vec{u}'\cdot\nabla p'+\mathcal{P}' \tag{2.9}$$

Now equation (2.9) is differentiated with respect to time and $\frac{\partial\vec{u}'}{\partial t}$ substituted from equation (2.8) to get

$$\nabla^2 p'-\frac{1}{\bar{a}^2}\frac{\partial^2 p'}{\partial t^2} = h$$

$$
\begin{aligned}
= \; & -\bar{\rho}\nabla\cdot(\vec{\bar{u}}\cdot\nabla\vec{u}'+\vec{u}'\cdot\nabla\vec{\bar{u}})+\frac{1}{\bar{a}^2}\vec{\bar{u}}\cdot\nabla\frac{\partial p'}{\partial t}+\frac{\gamma}{\bar{a}^2}\frac{\partial p'}{\partial t}\nabla\cdot\vec{\bar{u}} \\
& -\bar{\rho}\nabla\cdot\left(\vec{u}'\cdot\nabla\vec{u}'+\frac{p'}{\gamma\bar{p}}\frac{\partial\vec{u}'}{\partial t}\right)+\frac{1}{\bar{a}^2}\frac{\partial}{\partial t}(\vec{u}'\cdot\nabla p') \\
& +\frac{\gamma}{\bar{a}^2}\frac{\partial}{\partial t}(p'\nabla\cdot\vec{u}')+\nabla\cdot\vec{\mathcal{F}}'-\frac{1}{\bar{a}^2}\frac{\partial\mathcal{P}'}{\partial t}
\end{aligned}
\tag{2.10}
$$

A corresponding boundary condition for p' is derived by taking the scalar product of the outward normal vector $\vec{n}$ with equation (2.8).

$$
\begin{aligned}
-\vec{n}\cdot\nabla p' &= f \\
&= \bar{\rho}\frac{\partial\vec{u}'}{\partial t}\cdot\vec{n}+\bar{\rho}\left(\vec{\bar{u}}\cdot\nabla\vec{u}'+\vec{u}'\cdot\nabla\vec{\bar{u}}\right)\cdot\vec{n} \\
&\quad +\bar{\rho}(\vec{u}'\cdot\nabla\vec{u}')\cdot\vec{n}+\frac{p'}{\bar{a}^2}\frac{\partial\vec{u}'}{\partial t}\cdot\vec{n}-\vec{\mathcal{F}}'\cdot\vec{n}
\end{aligned}
\tag{2.11}
$$

The functions h and f contain *all* relevant physical processes including motion of the boundary, but every process included requires modeling, a separate matter.

2.2 Spatial Averaging

The idea of the approximate analysis is to transform the partial differential equations into a set of equivalent ordinary differential equations. That transformation and the subsequent expansion of the solution is especially useful in the context of control as it allows a reduction (through truncation) of the problem to a small number of degrees of freedom (states of the system). The transformation is achieved by spatially averaging the equations (2.10) and (2.11).

In addition to the choice of the partial differential equation(s) to be spatially averaged there are three essential defining features of the kind of approach used here: choice of the independent variable(s) to be expanded; choice of the spatial functions used in the series

expansion; choice of the weighting functions with respect to which the spatial averaging is done, usually chosen to be the same as the expansion functions.

We will start by describing the analysis commonly used (at least implicitly) in most studies and then compare it to an alternate approach proposed by Zinn and Powell (1970a), the 'modified Galerkin method'. Finally we will briefly mention a popular method, proper orthogonal decomposition, that can be used to get empirical expansion functions that are based on the measured behavior of the system.

2.2.1 Using the Unperturbed Problem

In the first instance, spatial averaging is closely tied to the idea that any unsteady disturbance in a chamber can be synthesized from an infinite set of basis functions; the expectation is that a small, finite number of these functions is sufficient to get a good approximate description of the disturbance. Examination of the frequency content of experimental pressure traces of combustion instabilities reveals that this idea applies well to the pressure fluctuations as only frequencies close to the acoustic frequencies of the chamber are present. Based on that observation, the weighting functions for the spatial averaging are chosen to be the unperturbed wave modes ψ_n predicted by classical acoustics for the same combustion chamber with rigid boundaries and no combustion or mean flow. They are obtained by setting $h = f = 0$ in the preceding equations.

$$\nabla^2\psi_n + k_n^2\psi_n = 0 \tag{2.12}$$

$$\vec{\hat{n}} \cdot \nabla\psi_n = 0 \tag{2.13}$$

Here the wave number for the n^{th} mode has been denoted k_n. The actual averaging step is done by multiplying equation (2.10) by ψ_n, multiplying equation (2.12) by p', subtracting

the results and integrating over the volume of the combustion chamber. Applying Greene's theorem and substituting for the boundary conditions, the final expression is found:

$$\frac{1}{\bar{a}^2}\int \psi_n \frac{\partial^2 p'}{\partial t^2}\, dV + k_n^2 \int \psi_n p'\, dV = -\int \psi_n h\, dV - \oint \psi_n f\, dS \tag{2.14}$$

At this point the unsteady pressure p' is expanded and written as a synthesis of the acoustic modes with time-varying amplitudes $\eta_n(t)$.

$$p'(\vec{x},t) = \bar{p}\sum_{n=1}^{N} \eta_n(t)\psi_n(\vec{x}) \tag{2.15}$$

Note that the zeroth mode (ψ_o = constant) is missing from (2.15). The omission means that excursions of the mean pressure ('DC shifts') cannot be computed with this theory; that is a deficiency that can be easily corrected but has not yet been treated.

Substitution in (2.14) leads eventually to a set of coupled oscillator equations

$$\begin{aligned} \frac{d^2\eta_n}{dt^2} + \omega_n^2 \eta_n &= F_n \\ &= -\frac{\bar{a}^2}{\bar{p}E_n^2}\left\{\int \psi_n h\, dV + \oint \psi_n f\, dS\right\} \end{aligned} \tag{2.16}$$

where $\int \psi_n \psi_m\, dV = \delta_{nm} E_n^2$.

Taking advantage of the presence of two small parameters appearing on the right-hand side (the Mach number of the averaged and fluctuating fields), one may devise an iteration/perturbation procedure to construct approximate sets of equations.

Coupled Oscillator Equations

Starting from equation (2.16) and replacing h and f by their respective definitions given in (2.10) and (2.11), the force F_n has the form (Burnley 1996, Burnley and Culick 2000):

$$\begin{aligned} \frac{-\bar{p}E_n^2}{\bar{a}} F_n &= \bar{\rho} I_1 + \frac{1}{\bar{a}^2} I_2 + \bar{\rho} I_3 + \frac{1}{\bar{a}^2} I_4 \\ &\quad + \int \left(\bar{\rho}\frac{\partial \vec{u}'}{\partial t} + \rho' \frac{\partial \vec{u}'}{\partial t}\right) \cdot \hat{n}\, \psi_n\, dS - \int \left[\frac{1}{\bar{a}^2}\frac{\partial \mathcal{P}'}{\partial t}\psi_n + \vec{\mathcal{F}}' \cdot \nabla \psi_n\right] dV \end{aligned} \tag{2.17}$$

with the definitions arising from gasdynamics:

$$
\begin{aligned}
I_1 &= \int (\vec{\bar{u}} \cdot \nabla \vec{u}' + \vec{u}' \cdot \nabla \bar{\vec{u}}) \cdot \nabla \psi_n dV \\
I_2 &= \frac{\partial}{\partial t} \int (\bar{\gamma} p' \nabla \cdot \bar{\vec{u}} + \bar{\vec{u}} \nabla \cdot p') \psi_n dV \\
I_3 &= \int \left(\vec{u}' \cdot \nabla \vec{u}' + \frac{\rho'}{\bar{\rho}} \frac{\partial \vec{u}'}{\partial t} \right) \cdot \nabla \psi_n dV \\
I_4 &= \frac{\partial}{\partial t} \int (\bar{\gamma} p' \nabla \cdot \vec{u}' + \vec{u}' \cdot \nabla p') \psi_n dV
\end{aligned}
\tag{2.18}
$$

In case of gas turbines the last term of equation (2.17) is the most relevant one for the driving of the instabilities as it relates the heat release of the combustion process in the chamber volume to the 'forcing' function F_n. For solid rocket applications the surface integral containing $\frac{\partial \vec{u}'}{\partial t} \cdot \hat{n}$ and representing all influences of motion at the boundary needs careful consideration. It is here that the dynamics of a burning surface enters (the propellant response function) and it is this term that also allows one to couple the unsteady motions within the chamber to motions of the case and of the surrounding structure such as a test stand or a parent vehicle. Moreover, this term allows one to accommodate random motions at the boundary, due, for example, to combustion of a heterogeneous material. The functions $\mathcal{P}'$ and $\vec{\mathcal{F}}'$ contain all other relevant processes within the volume and at the surface respectively. Therefore, with spatial averaging, this formulation captures the global effects in the chamber dynamics of all sources within the volume and on the boundary.

To evaluate the right-hand side of equation (2.16) we need to express F_n in terms of the expansion functions ψ_n. In order to do so we complement the expansion of p' into modes (see equation 2.15) with the corresponding velocity from classical acoustics:

$$
\vec{u}' = \sum_{j=1}^{\infty} \frac{\dot{\eta}_j(t)}{\bar{\gamma} k_j^2} \nabla \psi_j(\vec{r}) \tag{2.19}
$$

We also use the isentropic relation $p = C\rho^\gamma$ in order to eliminate the density fluctuations:

$$\rho' \approx \frac{p'}{\bar{a}^2} \tag{2.20}$$

Using these expansions, the gasdynamical part of F_n can be written as

$$F_n = -\sum_{i=1}^{\infty}\left(D_{ni}\dot{\eta}_i + E_{ni}\eta_i\right) - \sum_{i=1}^{\infty}\sum_{j=1}^{\infty}\left(A_{nij}\dot{\eta}_i\dot{\eta}_j + B_{nij}\eta_i\eta_j + M_{nij}\eta_i\dot{\eta}_j\right) \tag{2.21}$$

where

$$\begin{aligned}
D_{ni} &= \frac{1}{E_n^2}\int\left[\left(1+\frac{k_n^2}{k_i^2}\right)\psi_n\vec{\bar{u}}\cdot\nabla\psi_i + \gamma\psi_i\psi_n\nabla\cdot\vec{\bar{u}}\right. \\
&\qquad \left. -\frac{1}{k_i^2}\left(\nabla\psi_i\right)\times\left(\nabla\times\vec{\bar{u}}\right)\right)\cdot\nabla\psi_n\Bigg] \, dV \qquad (2.22)\\
E_{ni} &= \frac{1}{E_n^2}\left[\int\psi_i\left[\left(\vec{\bar{u}}\cdot\nabla\right)\vec{\bar{u}}\right]\cdot\nabla\psi_n\, dV - \bar{a}^2\oint\psi_n\nabla\psi_i\cdot\vec{\hat{n}}\, dS\right] \qquad (2.23)\\
A_{nij} &= \frac{1}{E_n^2}\int\left[\frac{1}{\gamma k_i^2}\left(\nabla\psi_i\cdot\nabla\psi_j - \gamma\psi_j\nabla^2\psi_i\right)\psi_n\right. \\
&\qquad \left. +\frac{1}{\gamma k_i^2 k_j^2}\left[\left(\nabla\psi_i\cdot\nabla\right)\nabla\psi_j\right]\cdot\nabla\psi_n\right] \, dV \qquad (2.24)\\
B_{nij} &= -\frac{1}{E_n^2}\int\frac{\bar{a}^2}{\gamma}\left[\left(\nabla\psi_i\cdot\nabla\psi_j + \gamma\psi_i\nabla^2\psi_j\right)\psi_n + \psi_i\nabla\psi_j\cdot\nabla\psi_n\right] \, dV \qquad (2.25)\\
M_{nij} &= \frac{1}{E_n^2}\int\frac{1}{\gamma k_j^2}\psi_i\nabla\left(\vec{\bar{u}}\cdot\nabla\psi_j\right)\cdot\nabla\psi_n\, dV \qquad (2.26)
\end{aligned}$$

2.2.2 Modified Galerkin Method

A different approach to spatial averaging was introduced by Zinn and Powell (1970a) who extended the classical Galerkin method to allow the spatial expansion functions to be independent of the boundary conditions for the system.

We consider a system described by the following two equations; the first one describing the behavior of the solution in the interior of the volume of interest V (the combustion chamber) and the second one specifying its boundary condition.

$$E_{\text{interior}}\left(\vec{x},t\right) = 0 \tag{2.27}$$

$$E_{\text{boundary}}\left(\vec{x},t\right) \;=\; 0 \tag{2.28}$$

In the Galerkin method an approximate solution $\vec{\tilde{x}} = \sum_1^N a_n\varphi_n$ to the problem is constructed in such a way that it fulfills the boundary conditions automatically (i.e., it is assumed that each expansion function φ_n satisfies the equations (2.28)). The 'best' $\vec{\tilde{x}}$ is then obtained by spatially averaging the remaining equations over the volume V with some weighting functions ϕ_n (usually taken to be the same as φ_n), thus solving the problem (2.29) for the unknowns a_n.

$$\int E_{\text{interior}}\left(\vec{\tilde{x}},t\right)\phi_n\, dV = 0 \tag{2.29}$$

By doing this expansion it is assumed that the functions φ_n form a complete set for the given boundary conditions and thus any solution to the problem can be expanded in this set.

The advantage of using a Galerkin expansion is the fact that in most applications the desired information can be obtained by using a truncated series that contains only a few terms. These terms describe the most important physical aspects of the problem while the remaining (neglected) terms only provide minor corrections. If the expansion of the solution $\vec{\tilde{x}}$ is truncated to N 'modes' then the following holds (if $\vec{x}$ is the correct solution):

$$\lim_{N\to\infty}\vec{\tilde{x}} = \lim_{N\to\infty}\sum_{n=1}^{N} a_n\varphi_n = \vec{x} \tag{2.30}$$

One major challenge in applying the Galerkin method is finding the appropriate expansion functions. According to Zinn and Powell (1970a) the condition that the expansion functions fulfill the stringent boundary conditions can be relaxed if those boundary conditions are accounted for in the weighting process itself; this should be done by solving the system

(2.31) instead of (2.29).

$$\int_0^T \left[\int E_{\text{interior}} \left(\vec{\tilde{x}}, t \right) \phi_n \, dV - \oint E_{\text{boundary}} \left(\vec{\tilde{x}}, t \right) \phi_n \, dS \right] \, dt = 0 \tag{2.31}$$

Connection to Section 2.2.1

In the problem of combustion instabilities we can start with the governing equations as given by (2.10) and (2.11) in the interior of the combustion chamber and its boundaries respectively. Thus we can apply equation (2.31) to obtain:

$$\int E_{\text{interior}} \left(\vec{\tilde{x}}, t \right) \phi_n \, dV \quad - \quad \oint E_{\text{boundary}} \left(\vec{\tilde{x}}, t \right) \phi_n \, dS = 0 \tag{2.32}$$

$$\int \left(\nabla^2 p' - \frac{1}{\bar{a}^2} \frac{\partial^2 p'}{\partial t^2} - h \right) \phi_n \, dV \quad - \quad \oint \left(\vec{\tilde{n}} \cdot \nabla p' + f \right) \phi_n \, dS = 0 \tag{2.33}$$

This last equation can be rewritten to give:

$$\frac{1}{\bar{a}^2} \int \frac{\partial^2 p'}{\partial t^2} \phi_n \, dV - \int \nabla^2 p' \phi_n \, dV + \oint \vec{\tilde{n}} \cdot \nabla p' \phi_n \, dS = - \int h \phi_n \, dV - \oint f \phi_n \, dS \tag{2.34}$$

Making use of Greene's theorem we get

$$- \int \nabla^2 p' \phi_n \, dV = \oint \left(p' \nabla \phi_n - \phi_n \nabla p' \right) \cdot \vec{\tilde{n}} \, dS - \int p' \nabla^2 \phi_n \, dV \tag{2.35}$$

If the weighting functions ϕ_n are now chosen to coincide with the functions ψ_n as defined and used above (equations (2.12) and (2.13)), this last equation turns into

$$- \int \nabla^2 p' \phi_n dV = \oint \left(0 - \psi_n \nabla p' \cdot \vec{\tilde{n}} \right) \, dS + k_n^2 \int p' \psi_n \, dV \tag{2.36}$$

Substituting (2.36) in equation (2.34) the integral equation for the pressure as given by equation (2.14) is recovered:

$$\frac{1}{\bar{a}^2} \int \psi_n \frac{\partial^2 p'}{\partial t^2} \, dV + k_n^2 \int \psi_n p' \, dV = - \int \psi_n h \, dV - \oint \psi_n f \, dS \tag{2.37}$$

This shows that equation (2.31) is compatible with the above averaging procedure; in particular the boundary conditions are incorporated into the solution in the same manner.

It is worth noting at this point that not only do the expansion functions ψ_n not satisfy those boundary conditions but so does any expansion solution we obtain. This is a consequence of the fact that while the functions ψ_n form a complete set for the acoustic boundary conditions, they do *not* form a complete set for the *nonlinear* boundary conditions. Thus any approximate solution $\tilde{p}'$ obtained by using expansion functions such as these will not converge pointwise to the full solution p'; (2.30) is no longer valid. Instead the convergence is achieved in an integral sense:

$$\lim_{N\to\infty} \int \left[p'(\vec{x},t) - \sum_{n=1}^{N} \eta_n(t)\psi_n(\vec{x}) \right]^2 dV = 0 \tag{2.38}$$

Other Applications of the Modified Galerkin Approach

The modified Galerkin approach is obviously very general and can be applied to a variety of problems. Some applications in the context of combustion instabilities are briefly mentioned (Zinn and Powell 1970a, Zinn and Powell 1970b, Powell 1970, Powell and Zinn 1971, Lores and Zinn 1973).

Velocity Potential Wave Equation

When the Mach number of the mean flow is small (assuming $\vec{u}$ and $\vec{u}'$ are of same order ϵ) the unsteady flow in the combustor can be described to second order in ϵ by a wave equation (2.39) for the velocity potential Φ (for a careful derivation of this equation see (Powell 1970)). It is permissible to write $\vec{u}' = \nabla\Phi$ since it can be shown that up to the second order considered the perturbation flow field is irrotational.

$$\nabla^2\Phi - \frac{\partial^2\Phi}{\partial t^2} = 2\vec{u}\cdot\nabla\frac{\partial\Phi}{\partial t} + \gamma(\nabla\cdot\vec{u})\frac{\partial\Phi}{\partial t} + 2\nabla\Phi\cdot\nabla\frac{\partial\Phi}{\partial t} + (\gamma-1)\frac{\partial\Phi}{\partial t}\nabla^2\Phi + W'_m \tag{2.39}$$

In this equation the source term W'_m accounts for the combustion process.

The variable to be expanded in this approach is the velocity potential Φ and we write:

$$\Phi(\vec{x},t) = \sum_{n=1}^{N} A_n(t)\phi_n(\vec{x}) \tag{2.40}$$

Using the same functions ϕ as weighting functions, the modified Galerkin method can then be applied to equation (2.39). The appropriate boundary condition (Q_m is an unsteady mass source at the boundary) reads:

$$Q'_m + \left(\nabla\Phi - \vec{u}\frac{\partial\Phi}{\partial t} - \frac{\partial\Phi}{\partial t}\nabla\Phi\right)\cdot\vec{n} \tag{2.41}$$

This procedure leads to a set of N second order differential equations for the $A_n(t)$ (for detailed expressions of the resulting equations see Zinn and Powell (1970b)). Just as in section 2.2.1, Zinn and Powell (1970b) use the classical acoustic modes ψ_n of the combustion chamber as expansion functions ϕ_n.

After solving for Φ the pressure perturbation field is obtained through the second-order momentum equation (2.42).

$$p'(\vec{x},t) = \gamma\left[\frac{1}{2}\left(\frac{\partial\Phi}{\partial t}\right)^2 - \frac{\partial\Phi}{\partial t} - \vec{u}\cdot\nabla\Phi - \frac{1}{2}\nabla\Phi\cdot\nabla\Phi\right] \tag{2.42}$$

Comparing this solution to the previous section it is noticeable that the unsteady pressure field does not necessarily vanish on the boundaries anymore and thus could in principle accommodate equation (2.11). However, in this approach the limitation is on the boundary condition for Φ and thus does not improve the quality of the solution.

While this approach is very attractive, it does have some drawbacks. It is constrained to irrotational flow and the underlying equation (2.39) cannot be augmented to account for higher order terms. Furthermore, the assumption that the mean flow field is of the same order of magnitude as the perturbation fields is a severe restriction when compared to the previous method.

Application to the Full Equations of Motion

The 'modified Galerkin method' is not restricted to be used on a single equation but can be applied to a collection of equations describing the solution.

The unsteady flow field in a combustion chamber is described by a system of five partial differential equations (the equation of continuity, 3 components of the momentum equation and the energy equation) and the equation of state. In the preceding approaches this system has been reduced to a single equation before applying a Galerkin type analysis. Powell and Zinn (1971) skip this reduction and apply the analysis directly to the equations of motion. The independent variables to be expanded in this case are the density fluctuation ρ', pressure fluctuation p', enthalpy fluctuation h' and the three components of the velocity perturbation u',v',w'. In order to be able to use the same expansion functions (e.g., the acoustic modes) for all perturbed quantities the velocity components are expressed in terms of 'quasi-potentials' (φ, η, ξ) - this is because the velocity disturbance is out of phase with the pressure disturbance (the same 'trick' is used in the approach used in this work by putting $\vec{u}' \sim \nabla\psi$; see equation (2.19)):

$$u' = \frac{\partial\varphi}{\partial x} \qquad v' = \frac{\partial\eta}{\partial y} \qquad w' = \frac{\partial\xi}{\partial z} \tag{2.43}$$

These 'quasi potentials' are then expanded alongside ρ', p', and h', i.e. we write

$$\begin{aligned} \varphi &= \sum A_{\varphi}^{(n)}(t)\phi_n(\vec{x}) & \eta &= \sum A_{\eta}^{(n)}(t)\phi_n(\vec{x}) & \xi &= \sum A_{\xi}^{(n)}(t)\phi_n(\vec{x}) \\ \rho' &= \sum A_{\rho}^{(n)}(t)\phi_n(\vec{x}) & p' &= \sum A_{p}^{(n)}(t)\phi_n(\vec{x}) & h' &= \sum A_{h}^{(n)}(t)\phi_n(\vec{x}) \end{aligned} \tag{2.44}$$

At this point it should be noted that this use of 'quasi potentials' allows for a general representation of any velocity disturbance and thus rotational flows can be studied. It is easy to see that the traditional Helmholtz decomposition is equivalent to the use of the

'quasi potentials'. If we write

$$\vec{u}' = \nabla\Phi + \nabla \times \vec{\mathcal{A}} \qquad \text{with} \qquad \vec{\mathcal{A}} = (\mathcal{A}_1 \quad \mathcal{A}_2 \quad \mathcal{A}_3) \tag{2.45}$$

then we can always find functions $\mathcal{X}$, $\mathcal{Y}$, and $\mathcal{Z}$ such that

$$\frac{\partial}{\partial x}\mathcal{X} = \frac{\partial}{\partial y}\mathcal{A}_3 - \frac{\partial}{\partial z}\mathcal{A}_2 \qquad \frac{\partial}{\partial y}\mathcal{Y} = \frac{\partial}{\partial z}\mathcal{A}_1 - \frac{\partial}{\partial x}\mathcal{A}_3 \qquad \frac{\partial}{\partial z}\mathcal{Z} = \frac{\partial}{\partial x}\mathcal{A}_2 - \frac{\partial}{\partial y}\mathcal{A}_1 \tag{2.46}$$

Therefore, the equivalence is given by defining $\varphi = \Phi + \mathcal{X}$, $\eta = \Phi + \mathcal{Y}$, and $\xi = \Phi + \mathcal{Z}$.

Powell and Zinn (1971) use this approach to study the radial and tangential modes in a cylindrical combustion chamber. In that investigation the Galerkin expansion series is limited to one term - the acoustic mode being studied. Thus the 'expansion' is $\rho' = A_\rho(t)\cos(m\theta)J_m(s_{mn}r)$, etc. Here $J_m(x)$ is the Bessel function of order m and s_{mn} is the nth nonzero root of the equation $J'_m(x) = 0$.

This procedure will provide first order differential equations for $\frac{dA_\rho}{dt}$, $\frac{dA_\varphi}{dt}$, $\frac{dA_\eta}{dt}$, $\frac{dA_\xi}{dt}$, $\frac{dA_h}{dt}$ (stemming from the equations of continuity, momentum and energy) as well as one algebraic relation for A_h (from the equation of state). This last equation is used to eliminate A_h and numerically integrate the remaining system.

Note that just as before care needs to be taken in the ordering procedure. Powell and Zinn (1971) assume that all perturbed quantities are of the same order, i.e., $O(\varphi) = O(\eta) = O(\xi) = O(p') = O(\rho') = O(h') = \epsilon$; furthermore, the mean flow field is assumed to be of the same order.

This approach of expanding six different quantities is much more complex than the previous approaches; this explains the short expansion series used. In the way it is presented here and has been studied in (Powell and Zinn 1971) there is another point of concern: the averaging procedure has been applied to the equation of state. Thus the equation of state

is not fulfilled at each point anymore (as it must) but instead is fulfilled in an average sense. As shown below this 'smearing out' effect affects the nonlinear terms of the system of equations and can alter their dynamical behavior.

Numerical results suggest indeed that the dynamics of the system change depending on whether the enthalpy h' is eliminated from the systems of equations before or after applying the Galerkin approach. The different behavior is solely due to the spatial averaging procedure.

To try to understand this qualitative change let's look at two-dimensional modes ($u' = 0$) in a cylindrical chamber. For that case the energy equation and equation of state read respectively:

$$(\bar{\rho}+\rho')\frac{\partial h_t'}{\partial t} + (\bar{\rho}+\rho')\left[\frac{\partial h_t'}{\partial r} + \frac{1}{r}w'\frac{\partial h_t'}{\partial \theta}\right] - \frac{\gamma-1}{\gamma}\frac{\partial p'}{\partial t} + \frac{d}{dz}(\bar{\rho}\bar{u})h_t' + W_m'h_t' = 0 \tag{2.47}$$

$$h_t' = \frac{1}{\bar{\rho}+\rho'}\left(p' - \rho'\bar{h}_t + \frac{\gamma-1}{2}\rho'\bar{u}^2\right) + \frac{\gamma-1}{2}\left(v'^2 + w'^2\right) \tag{2.48}$$

As mentioned above this approach has been applied with only 1 expansion mode. Therefore, consider $\psi_{mn} = J_m(s_{mn}r)\cos(m\theta)$ with $m = 1$. Then we get

$$\rho' \sim p' \sim h_t' \sim v' \sim \psi_{1n} \sim \cos\theta$$

$$w' \sim \tfrac{\partial}{\partial\theta}\psi_{1n} \sim \sin\theta \tag{2.49}$$

Focusing on the term $(\bar{\rho}+\rho')\frac{1}{r}w'\frac{\partial h_t'}{\partial\theta}$ of the energy equation we see that spatial averaging produces the term

$$\int_0^{2\pi}(\bar{\rho}+\rho')\frac{1}{r}w'\frac{\partial h_t'}{\partial\theta}\psi_{1n}d\theta \sim A_\rho A_\xi A_h \tag{2.50}$$

From the spatially averaged equation of state we get an expression for A_h (Powell and Zinn 1971) that can now be used in (2.50):

$$A_h = \alpha_1 A_p + \alpha_2 A_\rho + \alpha_3 A_\rho A_\eta^2 + \alpha_4 A_\rho A_\xi^2 \tag{2.51}$$

If on the other hand, we first substitute h_t' from equation of state and then do the spatial averaging with ψ_{1n} we end up with

$$\int_0^{2\pi} \left[\frac{\partial}{\partial\theta} \left(p' - \rho' \bar{h_t} + \frac{\gamma-1}{2} \rho' \bar{u}^2 \right) + \frac{\gamma-1}{2} (\rho' + \bar{\rho}) \frac{\partial}{\partial\theta} \left(v'^2 + w'^2 \right) \right] w' \psi_{1n} d\theta \sim \alpha A_\eta^2 A_\xi + \beta A_\xi^3 \tag{2.52}$$

It should be obvious that this type of discrepancy ($A_\rho A_\xi A_h$ in (2.50) versus $A_\eta^2 A_\xi + A_{\xi^3}$ in (2.52)), that changes the nature of the nonlinearities in the differential equations and thus their dynamical behavior, occurs also if $m \neq 1$ and thus qualitative changes occur also if other modes are considered.

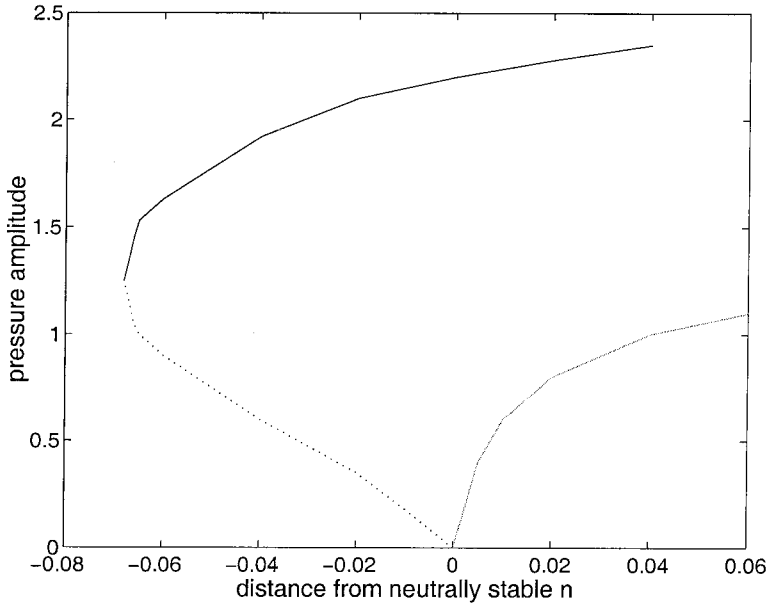

Figure 2.1: Bifurcation diagram for the 1R mode obtained by using the averaged equation of state (black) and by first eliminating h (grey)

The numerical example displayed in figure 2.1 illustrates these qualitative differences due to the averaging process. The calculations follow those in (Powell and Zinn 1971) and are done for a one mode expansion of the first radial mode in a cylindrical combustion chamber. The

combustion term is assumed to follow an $n-\tau$ model with fixed n and τ and the equations simulated include all terms up to $0(\epsilon^3)$.

As shown in figure 2.1, the subcritical Hopf bifurcation for the 1R mode, obtained by applying the spatial averaging to the equation of state, changes into a supercritical one if the state equation is eliminated before the averaging step (Appendix A provides a short introduction to the various type of bifurcations that occur in the context of this work). Thus triggering in the linearly stable regime is no longer possible with a 1 mode analysis. A similar effect is observed for the first tangential mode. Instead of reaching a limit cycle in the linearly unstable case as reported by Powell and Zinn (1971), the pressure oscillations grow indefinitely if the averaging of the equation of state is removed.

Accommodating the Boundary Conditions

The proper choice of terms to be used in the Galerkin expansion is crucial to the method. All the previously described approaches use the chamber's acoustic modes in the series expansion. This is well founded on experimental data which indicate that the behavior of high frequency combustion instabilities resembles those acoustic modes. Thus the expansions (in the 1-D case) read:

$$p' = \sum_{n=1}^{N} A_n(t)\psi_n(x) \qquad \rho' = \sum_{n=1}^{N} B_n(t)\psi_n(x) \qquad u'_{ac} = \sum_{n=1}^{N} C_n(t)\frac{\partial}{\partial x}\psi_n(x) \tag{2.53}$$

In general those expansions do not satisfy the boundary conditions set by the problem. If the complete equations of motion are used in the analysis, the velocity perturbation u' can be modified in such a way as to fulfill the boundary conditions by writing

$$u' = u'_{ac} + u'_b \tag{2.54}$$

Lores and Zinn (1973) study the longitudinal modes in a cylindrical combustion chamber

closed at one end and a choked nozzle at the other one. The quasi-steady nozzle boundary condition for the nozzle (at $x = 1$) reads

$$u'(1,t) - \frac{\gamma-1}{2\gamma}\bar{u}_e p'(1,t) + \frac{\gamma-1}{\gamma^2}\bar{u}_e p'^2(1,t) = 0 \tag{2.55}$$

With the only other boundary condition (the problem is treated in one dimension only) being $u(0,t) = 0$ (closed front end), both conditions can easily be fulfilled by choosing

$$u'_b(x,t) = \left[\frac{\gamma-1}{2\gamma}\bar{u}_e p'(1,t) + \frac{\gamma-1}{\gamma^2}\bar{u}_e p'^2(1,t)\right] x \tag{2.56}$$

In a more general case we would have $u'_b = f(p', \rho')$. The Galerkin method (without the boundary residuals which have now been eliminated) can then be applied to the equations of continuity, momentum and energy as above with the ψ_n as weighting functions.

The resulting differential equations for $A_n(t)$, $B_n(t)$ and $C_n(t)$ contain some new terms which didn't appear before: the introduction of the boundary term into the expansion creates an additional 'self-coupling' (terms like A_n^2, $A_n \frac{dA_n}{dt}$, ...) among the modes. Whereas these self-coupling terms are present in the previous approaches, they are of higher order and are generally introduced through the combustion model. By accounting for boundary conditions in the expansion itself, the dynamics of the system (especially for a low order analysis) are substantially changed. The presence of the self-coupling terms allows for triggering in the linearly stable region, a phenomenon not possible without them.

In the one-dimensional approach used by Lores and Zinn (1973), the expression for u'_b is easily found. In a general three-dimensional case such an expression is virtually impossible to derive. Therefore, the application of this approach to real systems is severely limited.

2.2.3 Proper Orthogonal Decomposition

As we have seen the choice of the expansion functions for the Galerkin method is critical. A commonly used tool for extracting coherent structures from data, either experimental or computational, is the Proper Orthogonal Decomposition (Holmes, Lumley and Berkooz 1996).

Given a set of data, represented as functions of space and time, the POD determines a basis set of orthogonal functions of space which span the data optimally in the L^2 sense. Thus, when $p(x,t)$ is a function of space and time, POD (also known as Karhunen-Loève decomposition) defines the functions $\psi_n(x), n = 1, 2, \ldots$, such that the truncation to the first N functions, $\tilde{p}$ (see equation (2.57)), has the smallest error. The functions ψ_n are called POD modes, Karhunen-Loève eigenfunctions, or empirical eigenfunctions.

$$\tilde{p}(x,t) = \sum_{n=1}^{N} \eta_n(t)\psi_n(x) \tag{2.57}$$

The error here is defined by

$$E[||p - \tilde{p}||^2] \tag{2.58}$$

where $E[\cdot]$ denotes the time average and $||\cdot||$ denotes the L^2 norm. It can be shown that the functions ψ_n that minimize this error are determined by the following equation:

$$\int K(x,y)\psi_n(y)dy = \lambda\psi(x) \tag{2.59}$$

The Kernel of the Fredholm integral equation is defined as

$$K(x,y) = E[p(x,t)p(y,t)] \tag{2.60}$$

Equation (2.59) reduces to a standard eigenvalue problem if the data, as is usually the case in practice, is discretized in both space and time. In such a case a numerically efficient

method to compute the POD modes is the so called 'method of snapshots'. In that method one uses a number k of 'snapshots' at times $t_i, i = 1, \ldots, k$ of the function $p(x,t)$ at the l discretized spatial points $x_i, i = 1, \ldots, l$ to construct the data matrix

$$A = \begin{pmatrix} p(x_1,t_1) & p(x_2,t_1) & \cdots & p(x_l,t_1) \\ p(x_1,t_2) & p(x_2,t_2) & \cdots & p(x_l,t_2) \\ \vdots & \vdots & \ddots & \vdots \\ p(x_1,t_k) & p)x_2,t_k) & \cdots & p(x_l,t_k) \end{pmatrix} \tag{2.61}$$

The POD modes are then the right singular vectors of A which can be easily computed by standard algorithms for singular value decomposition (attention needs to be paid that this gives the solutions to equation (2.59) only if the discretization in time and space is uniform).

The POD modes are 'optimal' for modeling or reconstructing the original signal – it can be proven that among all linear decompositions the POD is the most efficient, in the sense that, for a given number of modes the projection on the subspace used for modeling will contain the most energy possible in an averaged sense. In addition, the time series of the coefficients of the decomposition are uncorrelated.

To proceed the POD modes are used in lieu of the acoustic modes in the development given above.

2.3 Summary and Remarks

The derivation of the pressure wave equation and the coupled oscillator equations in section 2.2.1 is very straightforward. Unfortunately, this derivation does not provide a clear recipe for ordering the solutions according to the expansion in the two small parameters, mean

flow μ and perturbation amplitude ϵ. A more concise derivation can be based on a Green's function approach. While the final result is the same, it provides clearer guidelines to achieve an approximate solution by iteration. We chose not to give the full procedure here as it is rather lengthy; the reader is referred to Culick (1997).

As for the two parameter expansion, it is important to realize that the two parameters μ and ϵ have different physical origins. μ represents the intensity of the mean flow and the combustion while ϵ measures the amplitude of the unsteady motion. Therefore, we can selectively choose to retain terms having various order in ϵ and μ. Note that Zinn and students have not made that distinction but instead relate ϵ and μ in an arbitrary fashion. This explains some of the discrepancies found in the literature as, depending on which order in μ and ϵ is retained, different equations form the starting point for the Galerkin procedure. Culick (1997) provides the full details of the ordering procedure.

It has been pointed out that while the various approaches find the same linear stability limits, the non-linear behavior can differ between approaches. That difference seems to be mainly due to the coupling (and self-coupling) terms which depend on the expansion functions, the combustion model, and the underlying PDE(s). These inputs affect the structure of the equations derived and hence also the dynamical behavior of the system. Therefore, any conclusions drawn from numerical simulations are only valid within the scope of both the order of the parameter expansion and the accuracy of the combustion model.

From here onwards we will use the equations as derived in section 2.2.1. That approach seems to be the most consistent one as it allows for a clear ordering in the expansion terms and first reduces the equations of motion to one single PDE (the wave equation) before spatially averaging that equation, thus reducing the 'smearing out' effect.

Thus we will also use the acoustic modes of the chamber as expansion functions. While POD modes would be more 'efficient' by providing a more accurate model with the same number of modes, we simply have no way of knowing them a priori. We would need either finely resolved spatial and temporal experimental data of the pressure within the combustion chamber or compute a detailed direct numerical simulation of the combustion process. This is because the empirical eigenfunctions from the POD are only useful if the snapshots are representative of the dynamic characteristics of the system under consideration. However, the aim of the approach used in this work is to predict the approximate behavior of the system without having to do a detailed analysis and/or specific experiments for the special case under consideration. Furthermore, experience has shown that even a small number of the acoustic modes seems to be able to capture the main dynamics of the combustion system (Burnley 1996). If detailed data is available, proper orthogonal decomposition is the best method to obtain low-order models which then can be used for bifurcation analysis and control – an example of an application to self-sustained oscillations is given by Rowley, Colonius and Murray (2000). In that work POD modes are extracted from direct numerical simulations in order to obtain a low-order dynamical model of oscillations in the flow past an open cavity.

A further simplification of the dynamical model could be achieved by applying time-averaging to convert the second-order equations (2.16) into first-order equations. The motivation for this is the experimental observation that combustion instabilities usually have slowly varying amplitudes and phases of the modes contributing to the motions. We have not presented that approach here as we will not use it; the reason is that we will (in chapter 4) include noise sources in the equations and those sources are assumed to evolve on faster time scales.

Chapter 3

Application: Rijke Tube

One of the simplest generic geometries to study combustion instabilities is the so called Rijke tube; it gets its name from its discoverer, P.L. Rijke (Rijke 1859). Inside a Rijke tube a localized heat source is placed and there is a steady flow of gas (by means of natural convection or other). Depending on the position of that source (heated gauze, anchored flame) it can excite an acoustic oscillation. This oscillation is longitudinal, with a frequency close to an eigenmode of the tube. These 'singing flames' or 'gauze tones' have been observed and studied by numerous researchers (for a review, see for instance Raun, Beckstead, Finlinson and Brooks (1993)).

A general criterion for the acoustic instability to occur was first proposed by Rayleigh (1896). It states that when heat is released locally and periodically in a gaseous medium, an acoustic oscillation is amplified if the oscillating components of pressure and released heat flux are in phase. Therefore, it is crucially important to be able to describe the response of the rate of heat release to flow perturbations.

In this chapter we will apply the framework developed above to the Rijke tube. The Rijke tube example is instructive as it can be dealt with as a one-dimensional problem and thus

the computations are substantially simplified without losing the complex dynamical behavior of the system. We will show how the heat release is incorporated into the analytical framework by means of transfer functions that characterize the response of the heat source (e.g., flame) to fluctuations in velocity and pressure. These transfer functions can be computed analytically or measured experimentally for the heat source under consideration and are used here as inputs to the model. Results of the numerical integration of the model are compared to experiments.

The experiments with a burner described in section 3.3.2 show some interesting features that are not captured by the model. We show how the presence of an hysteresis loop in the dynamics of the combustion system can be exploited through a simple control algorithm to expand the stable operating range of the Rijke burner.

3.1 Applying the Analytical Framework

In a Rijke tube the heat release is concentrated in a region much smaller than the acoustic wavelength. In that case the system can be modeled by two uniform regions, split in between by the (infinitely thin) heat source. Furthermore, since the acoustic vibrations are longitudinal, a one-dimensional approach can be used to describe the problem.

We will therefore assume that the mean quantities (pressure, density, velocity, ...) are uniform throughout both sections. The region where heat is added to the flow is viewed as a discontinuity between the downstream and upstream sides across which the mean quantities 'jump'. Special attention needs to be attributed to these 'jump' conditions (matching conditions) at the interface between the constant regions.

A schematic of the Rijke tube is shown in figure 3.1. Quantities in the upstream volume

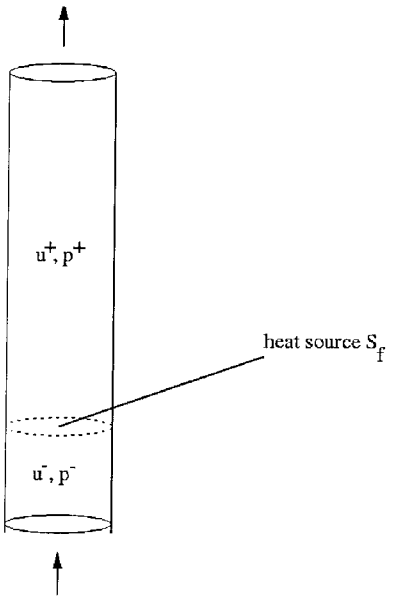

Figure 3.1: Rijke tube model

V^- are denoted with an $^-$ whereas downstream quantities are marked with an $^+$. Using the velocity fluctuations u' and pressure fluctuations p' as independent variables, the matching conditions across the discontinuity are defined in the most general way by

$$\begin{aligned} u'^+ - u'^- &= T(\omega)\, u'^- + Z(\omega)\, p'^- \\ p'^+ - p'^- &= R(\omega)\, u'^- + S(\omega)\, p'^- \end{aligned} \tag{3.1}$$

where $T(\omega)$, $Z(\omega)$, $R(\omega)$ and $S(\omega)$ are transfer functions across the heat source. As such they are imaginary quantities, which means that they carry both frequency dependent amplitude and phase information. These functions, along with the shapes of the various modes, are responsible for the selective driving of the modes depending on the position of the heat source in the tube.

Usually it is assumed that a flame does not support any pressure difference (thus putting $R(\omega)$ and $S(\omega)$ to 0) but depending on the device considered (e.g., a flame stabilized by a

porous gauze) it might be necessary to include this term (McIntosh 1987) and therefore we will carry it through in our calculations.

The equations (3.1) can be used to describe the most general case since they include the fundamental variables in the problem. In the literature one finds quite commonly models describing the fluctuating heat release q' in terms of u' and p'. The next paragraph shows how any such model can easily be recast in terms of the matching conditions (3.1) used here.

From the linearized energy equation we get the relation

$$u'^{+} - u'^{-} = \frac{\gamma - 1}{\gamma} \frac{q'}{\bar{p}} \tag{3.2}$$

Therefore, if we define the heat release fluctuation q' as

$$q' = T_u(\omega)\, u'^{-} + T_p(\omega)\, p'^{-} \tag{3.3}$$

we can define $T(\omega)$ and $Z(\omega)$ consistent with (3.1) as

$$T(\omega) = \frac{\gamma - 1}{\gamma \bar{p}} T_u(\omega) \qquad \text{and} \qquad Z(\omega) = \frac{\gamma - 1}{\gamma \bar{p}} T_p(\omega) \tag{3.4}$$

Other authors (Hathout, Annaswamy, Fleifil and Ghoniem 1998) express q' as a function of an equivalent flame speed, i.e.,

$$q' = Tr(\omega)\, u'_f \qquad \text{where} \qquad u'_f = \alpha\, u'^{-} + (1 - \alpha)\, u'^{+} \tag{3.5}$$

Once again this model is easily converted to the notation used here by defining

$$T(\omega) = \frac{(\gamma - 1) Tr(\omega)}{\gamma \bar{p} - (1 - \alpha)(\gamma - 1) Tr(\omega)} \tag{3.6}$$

Finally the 'classical' $n - \tau$ model defines the heat release fluctuation through

$$q' = n\, u'(t - \tau) \tag{3.7}$$

This fits into the framework described here as well, with a T that has an absolute value defined by n and its phase is given by τ. Note that we do not put any restrictions on n and τ and thus both the interaction index n and the time delay τ are allowed to be dependent on the frequency ω of the instability.

We see thus that any model describing the *linear* response of the heat source in terms of either u' or p' is described by the matching conditions (3.1). We emphasize linear, as the model described in this chapter does not take nonlinearities in the heat release into account (but we do include nonlinear gasdynamics). The simulations will show that this might be a major limitation in estimating the amplitude of pressure oscillations in the system.

The general equations derived by the procedure of spatial averaging in the previous chapter can now be applied to each section separately, i.e., the integration over the volume is interpreted as an integration over the sum of V^- and V^+. By doing so we have introduced a new boundary into the problem: the flame front S_f. Therefore, we need to be careful with the application of Green's theorem in the spatial averaging procedure.

Recall that

$$\begin{aligned} \nabla^2 p' - \frac{1}{\bar{a}^2}\frac{\partial^2 p'}{\partial t^2} &= h \qquad & \nabla^2\psi_n + k_n^2\psi_n &= 0 \\ \vec{\hat{n}}\cdot\nabla p' &= -f \qquad & \vec{\hat{n}}\cdot\nabla\psi_n &= g_n \end{aligned} \tag{3.8}$$

Note that the last equation has been modified to include g_n as we want to apply this condition at the interface S_f where $g_n \neq 0$.

Using these equations and assuming that g_n vanishes on the walls of the tube, the following relations hold (where S_1 and S_2 denote the upstream and downstream end surfaces of the

Rijke tube):

$$\oint_{S^+} (\psi_n \nabla p' - p' \nabla \psi_n) \cdot n \, dS = - \oint_{S_2} (\psi_n f + p' g_n) dS - \oint_{S_f} (\psi_n f + p' g_n) dS \tag{3.9}$$

$$\oint_{S^-} (\psi_n \nabla p' - p' \nabla \psi_n) \cdot n \, dS = - \oint_{S_1} (\psi_n f + p' g_n) dS - \oint_{S_f} (\psi_n f + p' g_n) dS \tag{3.10}$$

The integrals over S_1 and S_2 disappear since at the openings of the tube we have either $p' = 0$ and $\psi_n = 0$ (for an open end) or $f = 0$ and $g_n = 0$ (for a closed end). Therefore, the spatially averaged equation reads (compare with equation (2.14)):

$$\int_{V^- + V^+} \psi_n \frac{\partial^2 p'}{\partial t^2} dV + \int_{V^- + V^+} k_n^2 \psi_n p' dV = - \int \bar{a}^2 \psi_n h dV + \oint_{S_f} \left[\left(\psi_n^+ \bar{a}^{2+} f^+ - \psi_n^- \bar{a}^{2-} f^- \right) - \left(p'^+ \bar{a}^{2+} g_n^+ - \bar{p}'^- \bar{a}^{2-} g_n^- \right) \right] dS \tag{3.11}$$

At this point we follow the same procedure as before by expanding both pressure and velocity perturbations (h and f are functions of p' and u') into the modes ψ_n to finally arrive at a set of coupled oscillator equations:

$$\sum_{i=1}^{N} \left(C_{ni} \ddot{\eta}_i + \omega_n^2 C_{ni} \eta_i \right) = - \sum_{i=1}^{N} (D_{ni} \dot{\eta}_i + E_{ni} \eta_i) - \sum_{i=1}^{N} \sum_{j=1}^{N} (A_{nij} \dot{\eta}_i \dot{\eta}_j + B_{nij} \eta_i \eta_j + M_{nij} \eta_i \dot{\eta}_j) + \sum_{i=1}^{N} (F_{ni} \ddot{\eta}_i + G_{ni} \dot{\eta}_i + J_{ni} \eta_i) + \sum_{i=1}^{N} \sum_{j=1}^{N} (H_{nij} \dot{\eta}_i \dot{\eta}_j + K_{nij} \eta_i \eta_j + I_{nij} \eta_i \dot{\eta}_j) \tag{3.12}$$

Comparing with equation (2.21) we see that the second line of (3.12) is a result of the boundary terms introduced through the flame front. Thus the heat release modifies both linear terms (driving/damping and frequency shift) as well as the nonlinear terms (energy transfer between the modes). This is not in contradiction with the fact that we included only linear heat release dynamics; the nonlinear terms ($H_{nij}, K_{nij}, I_{nij}$) result from the interaction of the nonlinear gasdynamics with the linear heat release. Note that since the 'jump' in u' and p', as well as in the mean quantities at the interface, is taken into account

in determining the ψ_n, the matrix C_{ni} is not necessarily diagonal – this provides additional coupling between the various modes.

Starting from the definitions of f in (2.11) and h in (2.10), it is straightforward to write down an analytic expression for the various coefficients. Thus on the right-hand side of equation (3.11) we can write (note that we have dropped the $'$ to simplify the notation):

$$\begin{aligned}\frac{\bar{a}^{2+}}{\bar{p}}\psi_n^+ f^+ - \frac{\bar{a}^{2-}}{\bar{p}}\psi_n^- f^- &= \psi_n^- \left[\gamma\frac{\partial\left(u^-\right)}{\partial t} + \gamma\bar{u}^-\frac{\partial u^-}{\partial x} + \gamma u^-\frac{\partial u^-}{\partial x} + \frac{p^-}{\bar{p}}\frac{\partial u^-}{\partial t}\right] \\ &\quad -\psi_n^+ \left[\gamma\frac{\partial\left(u^+\right)}{\partial t} + \gamma\bar{u}^+\frac{\partial u^+}{\partial x} + \gamma u^+\frac{\partial u^+}{\partial x} + \frac{p^+}{\bar{p}}\frac{\partial u^+}{\partial t}\right] \quad (3.13)\end{aligned}$$

Now introduce the conditions (3.1), rearrange the terms, and drop the superscript (i.e., all quantities unless otherwise marked are $^-$ quantities) to get

$$\begin{aligned}\frac{\bar{a}^{2+}}{\bar{p}}\psi_n^+ f^+ - \frac{\bar{a}^{2-}}{\bar{p}}\psi_n^- f^- &= \psi_n \left[\gamma\frac{\partial}{\partial t}u + \gamma\bar{u}^-\frac{\partial}{\partial x}u + \gamma u\frac{\partial}{\partial x}u + \frac{p}{\bar{p}}\frac{\partial}{\partial t}u\right] \\ &\quad -\psi_n^+ \Bigg[\gamma T\frac{\partial u}{\partial t} + \gamma\frac{\partial u}{\partial t} \\ &\quad +\gamma Z\frac{\partial p}{\partial t} + \gamma\bar{u}^+ T\frac{\partial u}{\partial x} + \gamma\bar{u}^+\frac{\partial u}{\partial x} \\ &\quad +\gamma\bar{u}^+ Z\frac{\partial p}{\partial x} \\ &\quad +\gamma Tu\frac{\partial}{\partial x}Tu + \gamma Tu\frac{\partial}{\partial x}u + \gamma u\frac{\partial}{\partial x}Tu + \gamma u\frac{\partial}{\partial x}u + \frac{1}{\bar{p}}Ru\frac{\partial}{\partial t}Zp \\ &\quad +\gamma Tu\frac{\partial}{\partial x}Zp + \gamma u\frac{\partial}{\partial x}Zp + \gamma Zp\frac{\partial}{\partial x}Tu + \gamma Zp\frac{\partial}{\partial x}u + \frac{p}{\bar{p}}\frac{\partial}{\partial t}Zp + \frac{1}{\bar{p}}Ru\frac{\partial}{\partial t}Tu \\ &\quad +\frac{1}{\bar{p}}Ru\frac{\partial}{\partial t}Tu + \frac{1}{\bar{p}}Sp\frac{\partial}{\partial t}Zp \\ &\quad + \gamma Zp\frac{\partial}{\partial x}Zp + \frac{p}{\bar{p}}\frac{\partial}{\partial t}Tu + \frac{p}{\bar{p}}\frac{\partial}{\partial t}u + \frac{1}{\bar{p}}Sp\frac{\partial}{\partial t}Tu + \frac{1}{\bar{p}}Sp\frac{\partial}{\partial t}u\Bigg] \quad (3.14)\end{aligned}$$

Inserting the expansions (2.15) and (2.19) for p and u respectively leads straight to the formulas for F, H, I, and K. To get G and J we need to consider in addition the term

$$\begin{aligned}\frac{1}{\bar{p}}\left(p^+\bar{a}^{2+}g_n^+ - p^-\bar{a}^{2-}g_n^-\right) &= \frac{p}{\bar{p}}\left(\bar{a}^{2+}\left.\frac{\partial\psi_n}{\partial x}\right|^+ - \bar{a}^{2-}\left.\frac{\partial\psi_n}{\partial x}\right|^-\right) \\ &\quad +\frac{\bar{a}^{2+}}{\bar{p}}\left(Ru\left.\frac{\partial\psi_n}{\partial x}\right|^+ + Sp\left.\frac{\partial\psi_n}{\partial x}\right|^+\right) \quad (3.15)\end{aligned}$$

Finally we arrive at the following expressions:

$$C_{ni} = \int_0^L \psi_n \psi_i dx \tag{3.16}$$

$$D_{ni} = \int_0^L \left[\left(1 + \frac{k_n^2}{k_i^2} \right) \psi_n \bar{u}(x) \frac{\partial \psi_i}{\partial x} \right] dx \tag{3.17}$$

$$E_{ni} = 0 \tag{3.18}$$

$$A_{nij} = \int_0^L \left[\frac{1}{\gamma k_i^2} \left(\frac{\partial \psi_i}{\partial x} \frac{\partial \psi_j}{\partial x} - \gamma \psi_j \frac{\partial^2 \psi_i}{\partial x^2} \right) \psi_n + \frac{1}{\gamma k_i^2 k_j^2} \left(\frac{\partial \psi_i}{\partial x} \frac{\partial^2 \psi_j}{\partial x^2} \frac{\partial \psi_n}{\partial x} \right) \right] dx \tag{3.19}$$

$$B_{nij} = -\int_0^L \left[\frac{\bar{a}^2(x)}{\gamma} \left(\frac{\partial \psi_i}{\partial x} \frac{\partial \psi_j}{\partial x} + \gamma \psi_i \frac{\partial^2 \psi_j}{\partial x^2} \right) \psi_n + \psi_i \frac{\partial \psi_j}{\partial x} \frac{\partial \psi_n}{\partial x} \right] dx \tag{3.20}$$

$$M_{nij} = \int_o^L \frac{1}{\gamma k_j^2} \psi_i \bar{u}(x) \frac{\partial^2 \psi_j}{\partial x^2} \frac{\partial \psi_n}{\partial x} dx \tag{3.21}$$

$$F_{ni} = -\frac{1}{k_i^2} \psi_n(x_f^+) \frac{\partial \psi_i(x_f^-)}{\partial x} T(\omega_i) + \frac{1}{k_i^2} \frac{\partial \psi_i(x_f^-)}{\partial x} \left[\psi_n(x_f^-) - \psi_n(x_f^+) \right] \tag{3.22}$$

$$\begin{aligned} G_{ni} = & -\gamma \bar{p} \psi_n(x_f^+) \psi_i(x_f^-) Z(\omega_i) - \frac{\bar{u}^+}{k_i^2} \psi_n(x_f^+) \frac{\partial^2 \psi_i(x_f^-)}{\partial x^2} T(\omega_i) \\ & - \frac{\bar{a}^{2+}}{\gamma k_i^2 \bar{p}} \frac{\partial \psi_n(x_f^+)}{\partial x} \frac{\partial \psi_i(x_f^-)}{\partial x} R(\omega_i) \\ & + \frac{1}{k_i^2} \frac{\partial^2 \psi_i(x_f^-)}{\partial x^2} \left[\bar{u}^- \psi_n(x_f^-) - \bar{u}^+ \psi_n(x_f^+) \right] \end{aligned} \tag{3.23}$$

$$\begin{aligned} J_{ni} = & -\gamma \bar{u}^+ \bar{p} \psi_n(x_f^+) \frac{\partial \psi_i(x_f^-)}{\partial x} Z(\omega_i) - \bar{a}^{2+} \psi_i(x_f^-) \frac{\partial \psi_n(x_f^+)}{\partial x} S(\omega_i) \\ & + \psi_i(x_f^-) \left[\bar{a}^{2-} \frac{\partial \psi_n(x_f^-)}{\partial x} - \bar{a}^{2+} \frac{\partial \psi_n(x_f^+)}{\partial x} \right] \end{aligned} \tag{3.24}$$

$$\begin{aligned} H_{nij} = & -\frac{1}{\gamma k_i^2 k_j^2} \psi_n(x_f^+) \frac{\partial \psi_i(x_f^-)}{\partial x} \frac{\partial^2 \psi_j(x_f^-)}{\partial x^2} \left[T(\omega_i) T(\omega_j) + T(\omega_i) + T(\omega_j) \right] \\ & - \frac{1}{\gamma k_i^2} \psi_n(x_f^+) \frac{\partial \psi_i(x_f^-)}{\partial x} \psi_j(x_f^-) R(\omega_i) Z(\omega_j) \\ & + \frac{1}{\gamma k_i^2 k_j^2} \frac{\partial \psi_i(x_f^-)}{\partial x} \frac{\partial^2 \psi_j(x_f^-)}{\partial x^2} \left[\psi_n(x_f^-) - \psi_n(x_f^+) \right] \end{aligned} \tag{3.25}$$

$$\begin{aligned} I_{nij} = & -\frac{\bar{p}}{k_j^2} \psi_n(x_f^+) \left[\frac{\partial \psi_j(x_f^-)}{\partial x} \frac{\partial \psi_i(x_f^-)}{\partial x} + \psi_i(x_f^-) \frac{\partial^2 \psi_j(x_f^-)}{\partial x^2} \right] \left[T(\omega_j) Z(\omega_i) + Z(\omega_i) \right] \\ & - \bar{p} \psi_n(x_f^+) \psi_i(x_f^-) \psi_j(x_f^-) \left[S(\omega_i) Z(\omega_j) + Z(\omega_j) \right] \end{aligned}$$

$$+\frac{\bar{a}^{2-}}{\gamma^2\bar{p}k_j^2}\psi_n(x_f^+)\frac{\partial\psi_i(x_f^-)}{\partial x}\frac{\partial\psi_j(x_f^-)}{\partial x}\left[R(\omega_j)T(\omega_i)+R(\omega_j)\right] \tag{3.26}$$

$$K_{nij} = -\psi_n(x_f^+)\psi_i(x_f^-)\frac{\partial\psi_j(x_f^-)}{\partial x}\left[\gamma\bar{p}^2 Z(\omega_i)\,Z(\omega_j)-\frac{\bar{a}^{2-}}{\gamma}\left[T(\omega_j)+S(\omega_i)T(\omega_j)+S(\omega_i)\right]\right]$$
$$+\frac{\bar{a}^{2-}}{\gamma}\psi_i(x_f^-)\frac{\partial\psi_j(x_f^-)}{\partial x}\left[\psi_n(x_f^+)-\psi_n(x_f^-)\right] \tag{3.27}$$

As mentioned above, if the heat source is a flame it is usually assumed that $S(\omega)=0$ and $R(\omega)=0$ (and thus $\psi_k(x_f^+)=\psi_k(x_f^-)$) which considerably simplifies the nonlinear terms H_{nij}, I_{nij}, and K_{nij}. The remaining terms that have been introduced by the flame can then be traced to either one of the following sources (recall the matching conditions (3.1)):

- the jump in the mean quantities ($\bar{u}$, $\bar{a}$)
- a coupling of the heat source with the velocity fluctuations through $T(\omega)$
- a coupling of the heat source with the pressure fluctuations through $Z(\omega)$

All three of these factors contribute directly to the driving/damping of the various modes through G_{ni}.

For simulation purposes we convert the linear part of equation (3.12) into state-space form, a form commonly used for designing control laws (see for instance chapter 5). To achieve this the nonlinear part and any control commands are grouped into the input u to the system and thus the linear part of the system reads:

$$\sum_{i=1}^{N}\left[\left(C_{ni}-F_{ni}\right)\ddot{\eta}_i+\left(D_{ni}-G_{ni}\right)\dot{\eta}_i+\left(\omega_n^2 C_{ni}+E_{ni}-J_{ni}\right)\eta_i\right]=u_n \tag{3.28}$$

This system with input u , outputs η and $\dot{\eta}$, and states η and $\dot{\eta}$ takes on the following state-space form (we use the full state as an output of the system since the full information about the states is used as an input to the block describing the nonlinearities – see figure

3.2):

$$\begin{bmatrix} \dot{\eta} \\ \ddot{\eta} \end{bmatrix} = \begin{bmatrix} 0 & 1 \\ -(C-F)^{-1}(\omega^2 C + E - J) & -(C-F)^{-1}(D-G) \end{bmatrix} \begin{bmatrix} \eta \\ \dot{\eta} \end{bmatrix} + \begin{bmatrix} 0 \\ (C-F)^{-1} \end{bmatrix} u \tag{3.29}$$

$$\begin{bmatrix} \eta \\ \dot{\eta} \end{bmatrix} = 1 \cdot \begin{bmatrix} \eta \\ \dot{\eta} \end{bmatrix} + 0 \cdot u \tag{3.30}$$

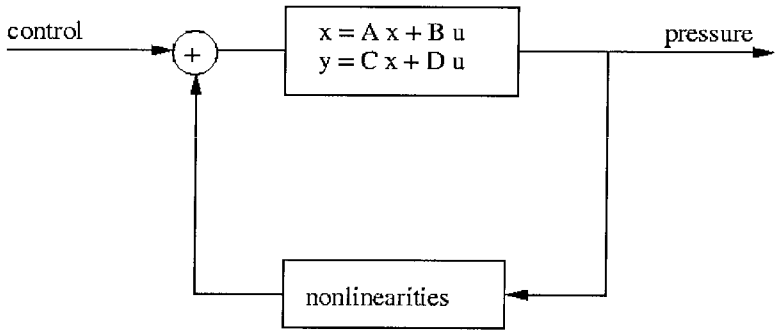

Figure 3.2: Isolating the linear part in state-space form

With this formulation the equations can be integrated by commercially available software. All simulations in this work have been done using the SIMULINK extension of MATLAB as this software has been designed especially with control applications in mind.

3.2 Electrical Rijke Tube

In this section the Rijke tube model developed above is applied for the case of an electrically heated Rijke tube and compared to experimental results. The experiments have been carried out in the Jet Propulsion Center at Caltech by Winston Pun and Konstantin Matveev and

are described in more detail by Pun (2001).

3.2.1 Experiment

The experimental apparatus used for this experiment is shown in figure 3.3. The main part of the apparatus is the rectangular steel tube (with a square cross section) which is placed horizontally in order to eliminate convection effects. Therefore, the air flow becomes an experimental parameter that is set by the operator through the use of a blower which 'sucks' the air out of the tube. A damping chamber has been added between this blower and the tube so as to dampen the blower noise and ensure a stable airflow. The heat source consists of an electrically powered nichrome gauze. The gauze is mounted on rods that feed the electrical power and allow for easy displacement of the heat source location within the tube.

Further characteristics of the tube are summarized in table 3.1.

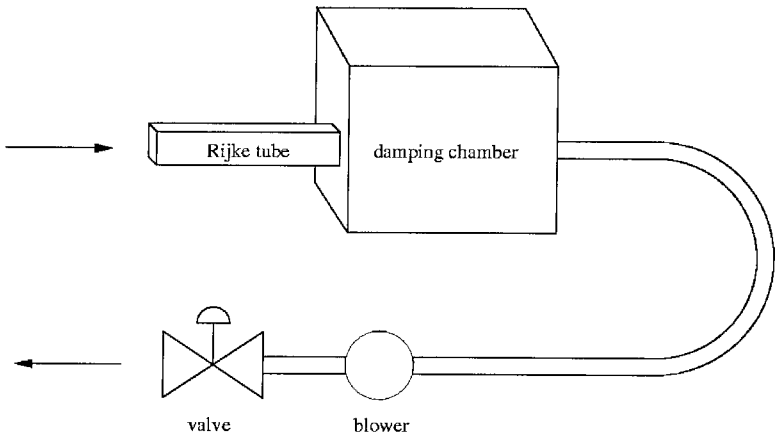

Figure 3.3: Layout of the electrical Rijke tube used in the JPC lab

The input variables that set the operation condition of the tube are thus given by the imposed airflow through the tube, the position of the heat source, and the electrical power

Tube length	$1.002m$
Cross section side	$10.16cm$
Inner cross section area	$.907dm^2$
Gauze wire number density	$15.75wires/cm$

Table 3.1: Electrical Rijke tube characteristics

provided to the gauze. These variables are set and/or measured by the data acquisition system which is installed on a PC.

The instrumentation on the tube consists of two piezoelectric pressure transducers mounted at a distance of $15cm$ and $80cm$ respectively from the upstream end of the tube, as well as sixteen thermocouples mounted along the length of the tube. During an experimental run these data, alongside the variables, are sampled at a rate of $7500Hz$ by a digital acquisition board mounted in a PC. This sampling rate is sufficient to capture the important acoustic modes of the tube, as the first mode associated with the pressure fluctuation is observed in the $100 - 200Hz$ range.

Poncia (1998) provides further details about the experimental apparatus, its instrumentation and the acquisition system.

The behavior of this electrical Rijke tube has been exhaustively investigated by varying the experimental conditions. Of interest here are the measured stability limits of the tube with the heater positioned at the $L/4$ location; they are displayed in figure 3.4. The measurements have been done by fixing the mass flow rate of air through the tube and varying the power supplied to the heater element. The symbols $\circ$ and $*$ mark the power level at which the transition between stable and unstable operation occurred while the power was increased, respectively decreased. While the stability limit seems to be independent

of the transition direction for most conditions, it is worth noting that for mass flow rates above $3g/s$, the two limits diverge. This occurs only on the upper end of the operating conditions of the tube, and further experiments, currently being conducted by Konstantin Matveev, will try to clarify this behavior.

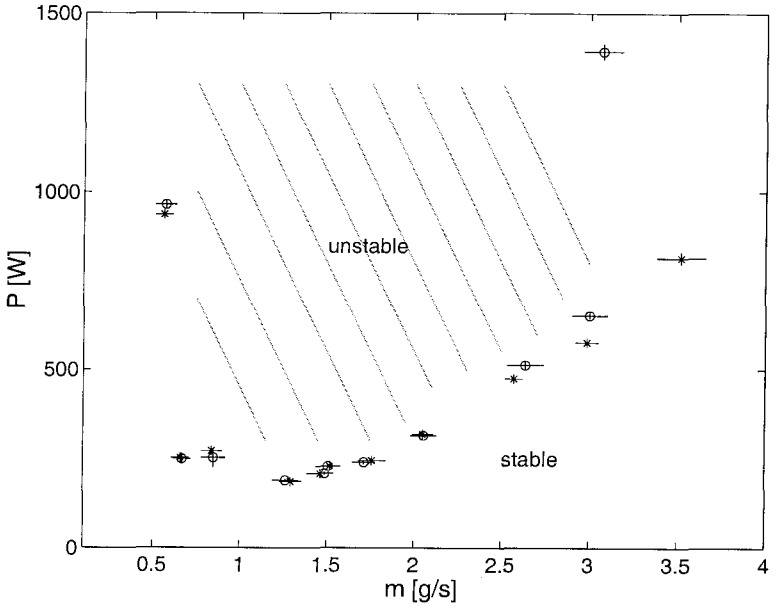

Figure 3.4: Stability diagram for the electric Rijke tube as measured in the laboratory (o: increasing power, $*$: decreasing power)

Another experimental result that we will be trying to model is the amplitude of the pressure oscillations when the tube is 'singing'. The observation is that the tube settles into a limit cycle whose amplitude is almost independent of the operating conditions (as long as we are in the unstable regime obviously). At a power level of $P = 500W$ the maximum of the pressure oscillation is about $.06psi$, or $p'/\bar{p} = .4\%$.

3.2.2 Model

While there are quite a few authors who have developed models for an electrically driven Rijke tube (Raun et al. 1993), we choose to follow the approach taken by Nicoli and Pelce (1989), chiefly because they derive a simple analytical expression that can be used directly in the formulation considered in section 3.1.

Nicoli and Pelce (1989) determine the transfer function $T(\omega)$ defined in equation (3.1) in the limit of small Mach number of the average flow. Their development is an expansion of earlier work by Carrier (1954) and Merk (1957). The generalization is done by taking into consideration the effects of gas compressibility, viscosity and temperature variation in the transport properties of the gas. The heating apparatus considered is a grid perpendicular to the tube axis, infinitely thin and conductive, heated at a constant temperature. An analysis of what happens to the stationary solution when a sound wave of frequency ω encounters the grid provides a differential equation for T that can be solved analytically if the quantity $\rho\mu/c_p$ is assumed to be constant. This analytical solution (equation (77) of Nicoli and Pelce (1989)) reads:

$$T(\omega) = \frac{2\gamma_T}{(1+\gamma_T)(1+\sqrt{1+4i\omega\tau}) - 2\gamma_T} \tag{3.31}$$

Where γ_T is defined as $\gamma_T = (T^+ - T^-)/T^-$ and $\tau = l_d/\bar{u}$ is the diffusive timescale, l_d is the thickness of the diffusion zone (the analysis shows that the main effects occur with a thin diffusion region around the grid through the mass flow rate perturbance of the incoming sound wave). The same analytical expression is also valid in the limit of small γ_T without any restrictions on the viscosity μ. Furthermore, Nicoli and Pelce (1989) show, through numerical calculations, that the dependence of μ on the temperature has little importance for the general form of the transfer function and therefore we assume that (3.31) is a good

description of the actual $T(\omega)$ and use it in our calculations. The behavior of the transfer function for various values of γ_T is illustrated in figure 3.5.

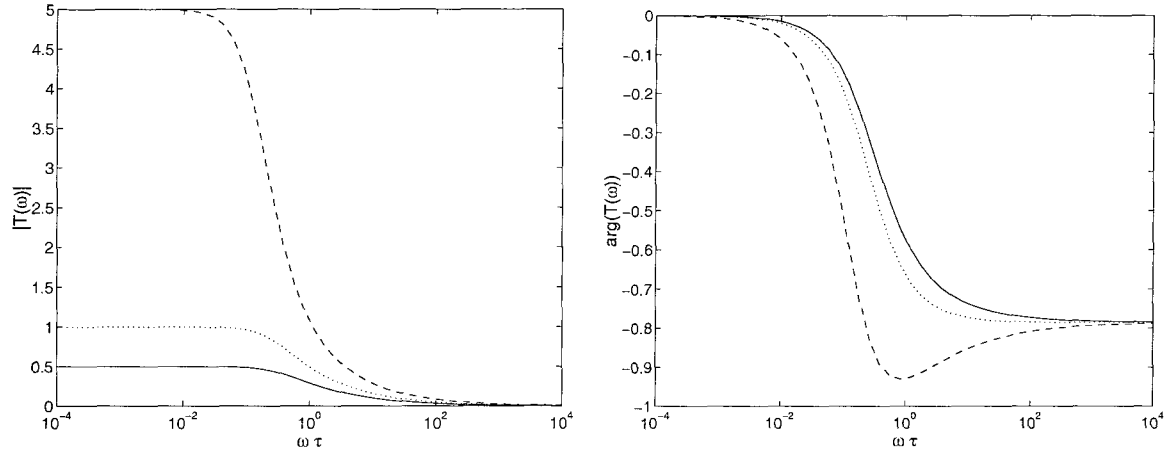

(a) Absolute value of T

(b) Argument of T

Figure 3.5: Transfer function T for an electric Rijke tube for various values of γ_T ($-$: $\gamma_T = .5$; $\cdots$: $\gamma_T = 1$; $\cdot-$: $\gamma_T = 5$)

Simulations

Using the transfer function given in (3.31), we numerically simulate a $1m$ long electrical Rijke tube with the heater located at the 1/4 location. The simulations were done using the first 4 longitudinal modes of the tube. The mode shapes and their respective frequencies are given in figure 3.6 for the case with $\bar{u} = .2m/s$ and $T^+ = 230C$.

The two parameters that affect the stability of the system - given the position of the heater, fixed at $L/4$ here - in our model are $\bar{u}$ and T^+ (the downstream temperature T^- is given by the room temperature). The limit between stable and unstable regions of operations is plotted in terms of these parameters in figure 3.7 and is in fact a straight line.

In the unstable region a random disturbance grows into a finite amplitude limit cycle. To

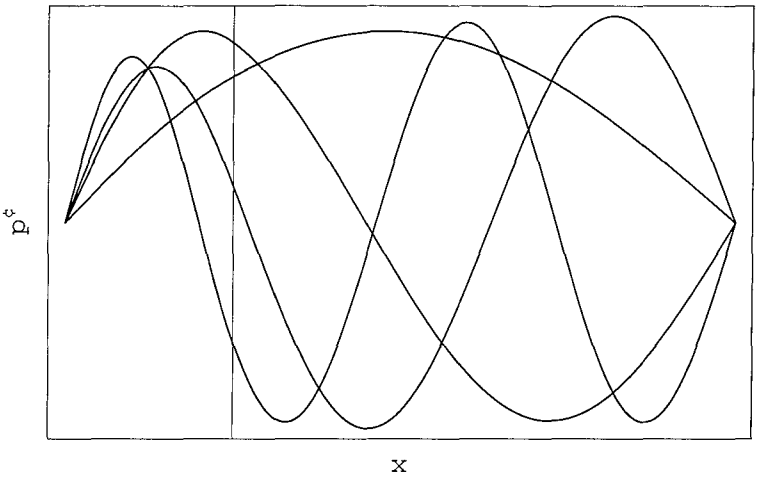

1^{st} mode	181 Hz
2^{nd} mode	243 Hz
3^{rd} mode	517 Hz
4^{th} mode	702 Hz

Figure 3.6: Mode shapes for the electrical Rijke tube (simulation)

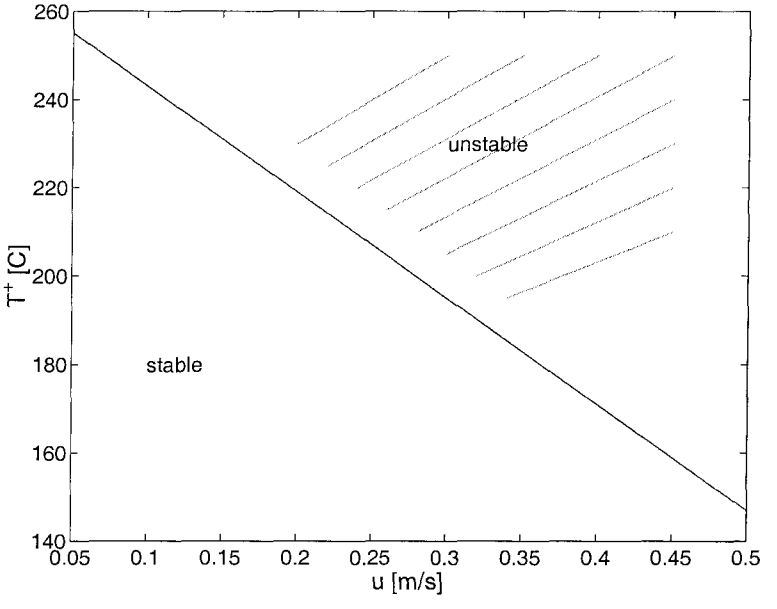

Figure 3.7: Stability diagram for the electric Rijke tube as predicted by the model

analyze the nonlinear behavior of the system, we trace this amplitude as mean speed and temperature are varied. The simulations are done at either fixed $\bar{u}$ or fixed T^+. The resulting bifurcation diagrams are given in figure 3.8 in terms of the remaining free parameter.

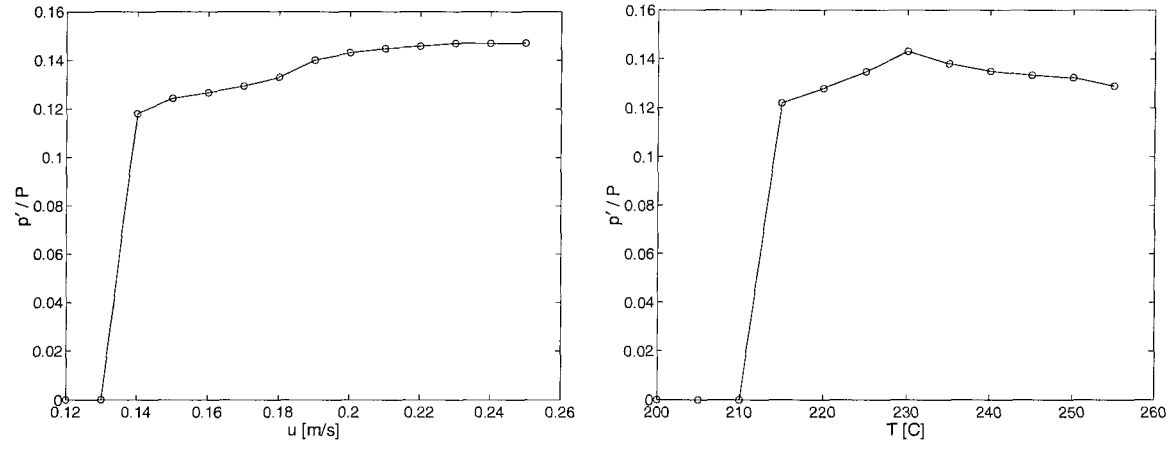

(a) constant T^+ of $230C$

(b) constant $\bar{u}$ of $.2m/s$

Figure 3.8: Limit cycle amplitude at $15cm$ from the upstream end of the Rijke tube as a function of mean flow and upstream temperature

3.2.3 Comparison with Experiment

Before we can compare the simulation results with the experimental data points, we need to relate the parameters used in the experiment (mass flow rate $\dot{m}$ and electrical power P) and in the simulation (mean flow speed $\bar{u}$ and downstream temperature T^+) to each other. Knowing the area A of the tube, we can readily convert the mass flow rate into a mean velocity by using the continuity equation:

$$\bar{u} = \frac{\dot{m}}{\rho A} \tag{3.32}$$

Relating the electrical power to $\bar{u}$ and T^+ is not that straightforward. To achieve this, T^+

has been measured as a function of $\dot{m}$ for different power levels (i.e., the measurements have been carried out at constant P). The results for two power levels are shown in figure 3.9.

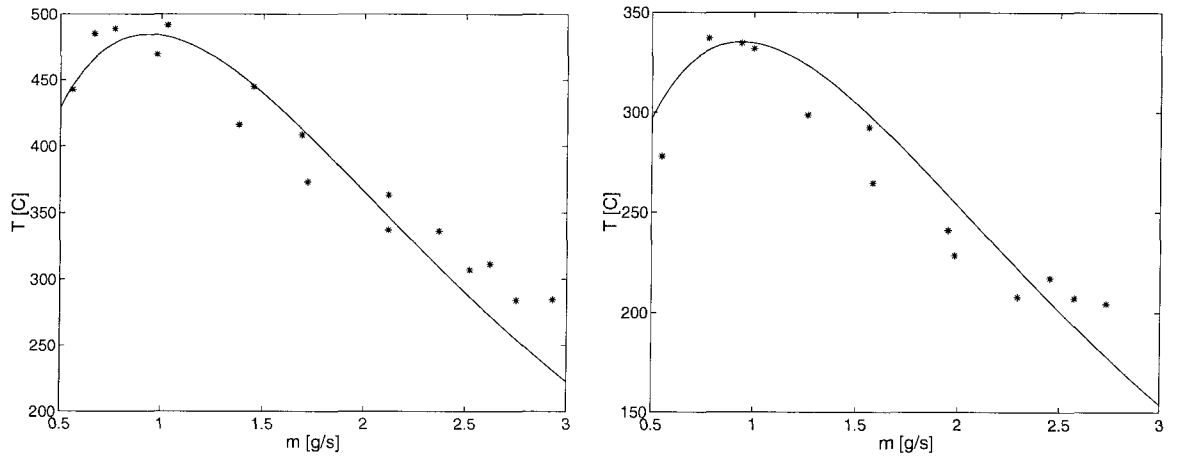

(a) $P = 500W$ (b) $P = 900W$

Figure 3.9: Temperature vs. mass flow rate at constant power

From the distribution of the data points we suggest the following functional form for $T^+(\dot{m}, P)$:

$$T^+ = (a \cdot P + b) \cdot \left(\dot{m}^c \cdot e^{-d \cdot \dot{m}}\right) \tag{3.33}$$

This relation is purely empirical and not based on any physical model. Nevertheless we find that by choosing $a = .83$, $b = 330$, $c = .75$, and $d = .8$, the resulting curves fit the observed behavior of T well for the various power levels. In figure 3.9 the suggested fit is shown as a solid line for two selected power settings.

Using relations (3.32) and (3.33) figure 3.7 can be mapped to the $\dot{m}-P$ plane. The predicted and measured linear stability limits for the electrical Rijke tube are compared in figure 3.10.

As seen in the figure the linear behavior of the Rijke tube is well described by the pre-

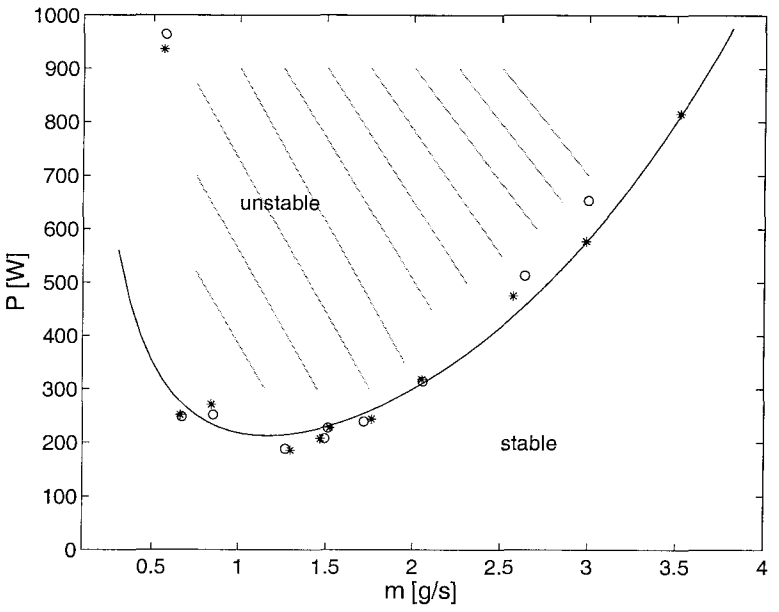

Figure 3.10: Comparison of simulated and measured stability diagrams for the electric Rijke tube

sented model. This shows that a rather simple transfer function for the heater element in combination with a low order gasdynamical model is sufficient to capture the stability characteristics.

To compare the nonlinear behavior of the model with the experiment, we take a look at the amplitudes of the limit cycles. From figure 3.8 it is obvious that those amplitudes are an order of magnitude too large and thus we conclude that the present model is not sufficient to capture the nonlinear dynamics of the system. We get an even stranger result if we make use of relations (3.32) and (3.33) and try to trace limit cycle amplitudes at a constant power level. The result of that attempt is seen in figure 3.11.

During the simulations it was noted that the model equations did not always converge towards a limit cycle. Therefore, the number of modes in the model was doubled to 8. This gave convergence over a broader range of parameter values but was still not sufficient

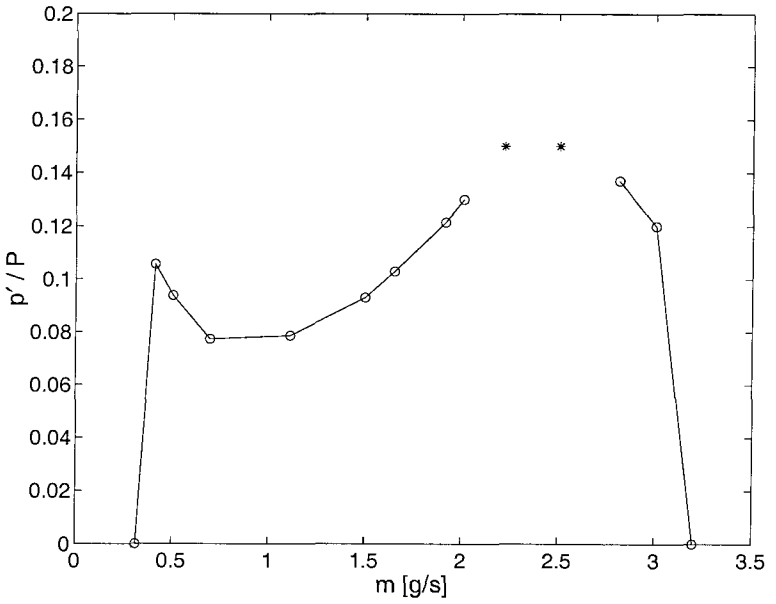

Figure 3.11: Pressure amplitude (from simulation) at $x = 15cm$ vs. mass flow rate for a constant power setting ($P = 500W$)

in all cases. The points marked by a $*$ in figure 3.11 did not give a limit cycle and thus the amplitudes are unknown for these mass flow rates. Since we already found that the nonlinear gasdynamics were not sufficient to explain the experimental observations, we did not try to include further modes.

It is therefore obvious that while a transfer function may be able to capture the linear behavior of the heater element, a much more complex model is needed to describe its nonlinear dynamics and its interaction with the flow field.

3.3 Rijke Burner

The same approach as above is now taken for a Rijke burner, i.e., the heat source consists of an actual flame. As before, we use a model based on transfer functions and compare its

predicted results to experiments.

3.3.1 Model

Clavin, Pelce and Longting (1990) derive a transfer function $Z(\omega)$ (the notation here is in accordance with equation (3.1)) that characterizes the feedback mechanism of the acoustic wave on a flat flame front. Assuming a flat flame and a simplified combustion model with a one-step reaction controlled by an Arrhenius law with an activation energy much larger than the thermal energy, Clavin et al. (1990) give the following analytical expression for $Z(\omega)$ (i.e., the coupling of the heat release to the pressure perturbations) as a function of the acoustic frequency ω. Note that diffusive and thermal effects within the flame are included in this model through the Lewis number.

$$Z(\Omega) = \frac{\beta}{2} M \frac{T^+}{T^-} \left(\frac{c_p - c_v}{c_v} \right) \cdot \left[\frac{\left(\sqrt{1+4i\Omega}-1\right) \cdot \left(\sqrt{1+4i\Omega} - \frac{\rho^+ - \rho^+}{\rho^-}\right) \cdot \sqrt{1+4i\Omega}}{\left(\sqrt{1+4i\Omega}-1\right) \cdot \sqrt{1+4i\Omega} - \frac{\beta}{2}(Le-1) \cdot \left(1 - \sqrt{1+4i\Omega} + 2i\Omega\right)} \right] \quad (3.34)$$

Here $\Omega = \omega \cdot \tau_t$ where $\tau_t = D_{th}/u_l^2$ is the transit time through the flame front with D_{th} the thermal diffusivity of the gas, u_l the laminar flame speed, and β is the reduced activation energy. The derivation of equation (3.34) is explained in detail in (Clavin et al. 1990) and the characteristics of the resulting function $Z(\omega)$ are displayed in figure 3.12.

Similarly we need to consider the effect of the acoustic acceleration on the geometry of the flame front. No flame is perfectly flat and instead most 'flat' flames exhibit a distinctive cellular pattern. The amplitude of these cellular structures is modulated by the periodic acoustic acceleration of the gas if an instability is present. This leads to a corresponding modulation of the total flame surface area and thus to a modulation of the global heat release rate. Pelce and Rochwerger (1992) use a laminar flame model with a planar (on

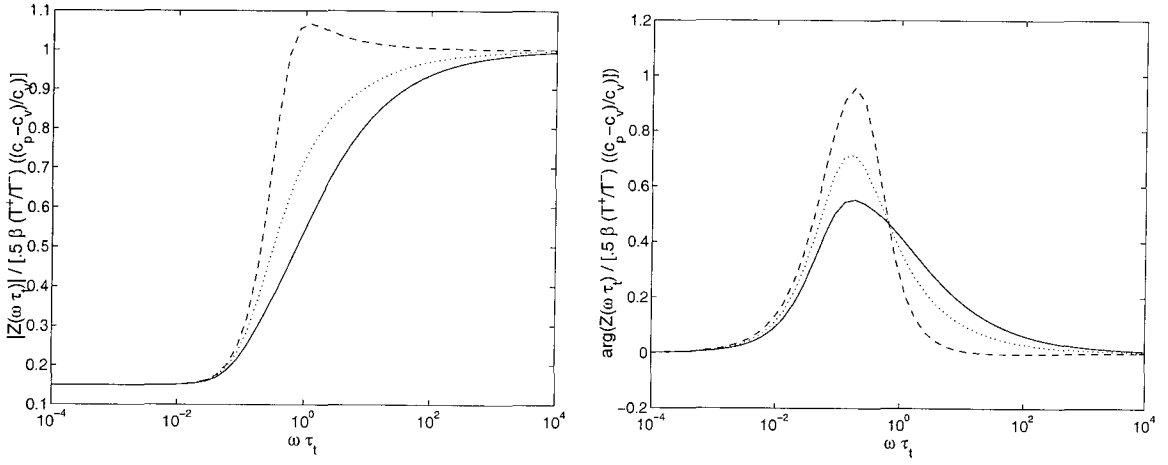

(a) Absolute value of Z

(b) Argument of Z

Figure 3.12: Transfer function Z for a flat flame for various values of Le ($-$: $Le = .8$; $\cdots$: $Le = 1$; $\cdot-$: $Le = 1.2$)

average) flame front that is perturbed by a two-dimensional sinusoidal wrinkling of small amplitude to derive an expression for the transfer function $T(\omega)$ which characterizes the coupling of the flame to the velocity perturbation introduced by the acoustic disturbance (see equation (3.1)). Clanet, Searby and Clavin (1999) extend that formulation to a flame model with temperature dependent diffusion coefficients and relax the assumption made by Pelce and Rochwerger (1992) that the cell size is given by the marginally unstable wavenumber k_c. However, these additions do not change the general behavior of $T(\omega)$ and thus we decide to use the (somewhat simpler) formulation of Pelce and Rochwerger (1992) given in equation (3.35) – the advantage being that this is an analytical expression that can be easily evaluated.

$$T(\omega) = \frac{(a_0 k_c)^2}{2} \cdot \frac{T^+ - T^-}{T^-} \cdot \frac{-i\omega\tau_t C(k_c d)}{-(\omega\tau_t)^2 A(k_c d) + i\omega\tau_t B(k_c d)} \tag{3.35}$$

The functions $A(k_c d)$, $B(k_c d)$, and $C(k_c d)$ depend on the temperatures T^+, T^- and on the

Markstein number; their expression and details on the derivation are given in the references cited above. Figure 3.13 illustrates the behavior of the transfer function.

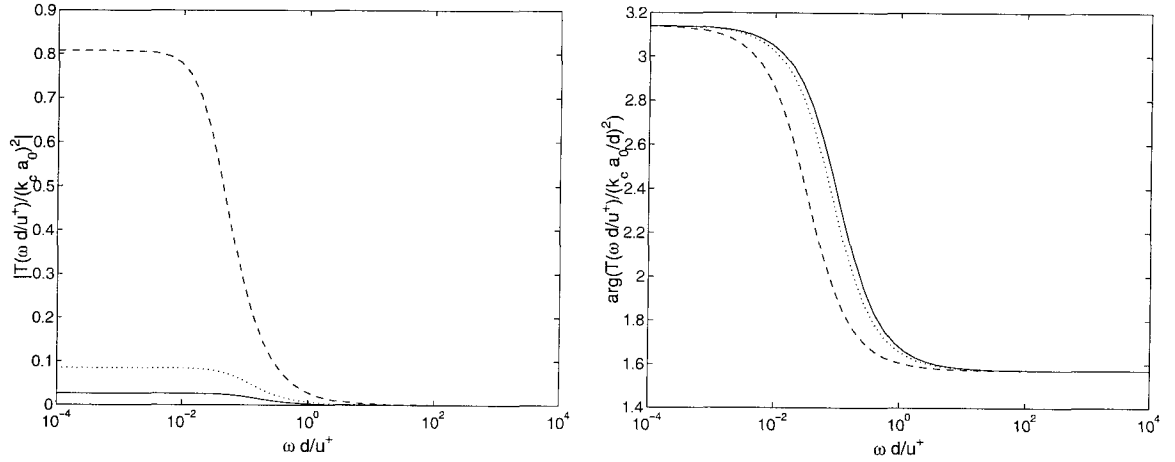

(a) Absolute value of T

(b) Argument of T

Figure 3.13: Transfer function T for a flat flame for various values of $\gamma_T = (T^+ - T^-)/T^-$ ($-$: $\gamma_T = .5$; $\cdots$: $\gamma_T = 1$; $\cdot-$: $\gamma_T = 5$)

Simulations

The above defined transfer functions $Z(\omega)$ and $T(\omega)$ have been used to numerically simulate a flat flame burning at the 1/4 location of a $1.5m$ long tube (as used in the experiment in section 3.3.2). The parameters used for the various expressions are given in table 3.2.

The simulations use the first four modes of the Rijke burner; it has been found that additional modes do not alter the results. These modes are illustrated in figure 3.14.

With these parameters and mode shapes, a random initial disturbance grows into an easily identifiable limit cycle. Figure 3.15 shows the pressure trace at the 3/4 location of the tube for the baseline case with $\bar{u} = .70m/s$ and $T^+ = 700K$.

Linear stability limits are determined by monitoring the first occurrence of the instability

temperature upstream	T^-	297	K
temperature downstream	T^+	700	K
reduced activation energy	β	20	
mean velocity (upstream)	$\bar{u}$	.7	m/s
flame transit time	τ_t	10^{-3}	s
laminar flame speed	u_l	.2	m/s
Lewis number	Le	1.2	
Markstein number	Ma	4.5	

Table 3.2: Parameters for simulation of Rijke burner

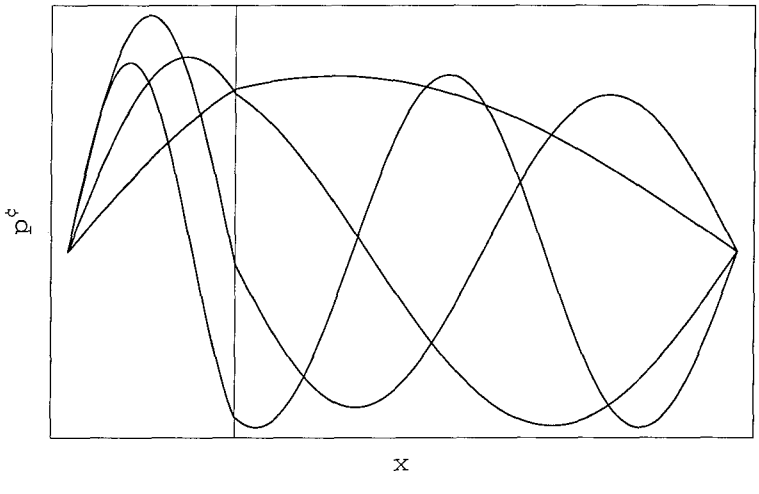

1^{st} mode	122.6 Hz
2^{nd} mode	266.7 Hz
3^{rd} mode	387.8 Hz
4^{th} mode	512.3 Hz

Figure 3.14: Mode shapes for the Rijke burner (simulation)

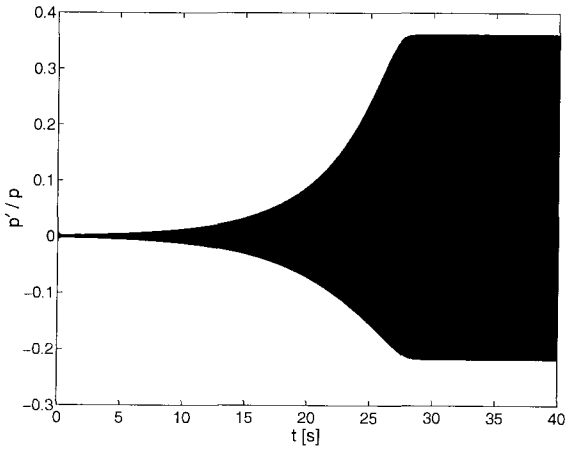

Figure 3.15: Pressure trace at 3/4 location for baseline case

as the model parameter $\bar{u}$ and T^+ are varied. Figure 3.16 presents the stability curve as predicted by the numerical simulations.

We obtain the bifurcation diagrams recording the final amplitude of the limit cycle (at the 3/4 location) as a function of the mean flow speed $\bar{u}$ and upstream temperature T^+. These diagrams are given in figure 3.17. The sudden appearance of a finite amplitude limit cycle is striking, a feature that is duplicated in the experiments (see figure 3.23). The amplitude of the limit cycle is comparable to the one measured in the experiment, a fact that might lead us to hope that in the case of a flame (as opposed to the electrical heater) the gasdynamics dominate the nonlinear behavior.

3.3.2 Experiment

The Rijke burner used in this experiment consists of a $1.5m$ vertical glass pipe, open at both ends, with a high temperature Bunsen burner positioned inside. Consistent with the theory the maximum driving is obtained with the heat release at the 1/4 location so in this experiment that's where the burner is placed. The experimental setup is displayed in figure

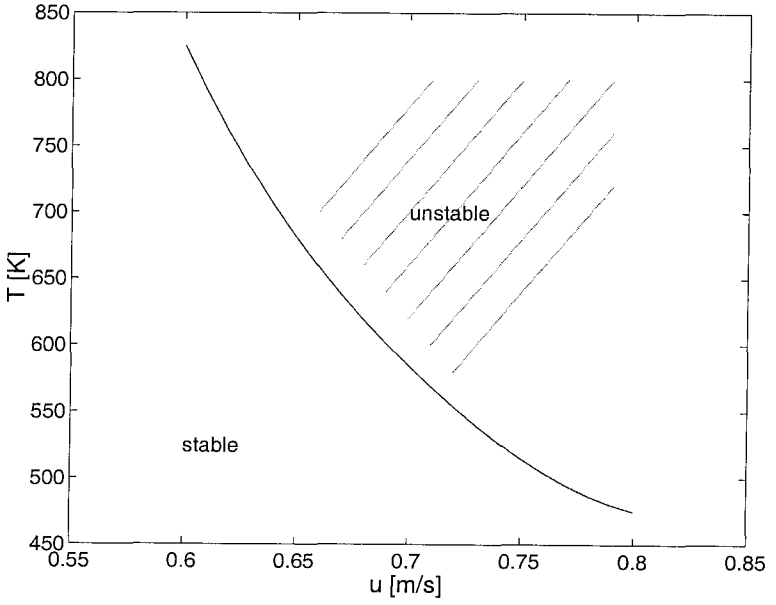

Figure 3.16: Stability diagram for the Rijke burner as predicted by the model

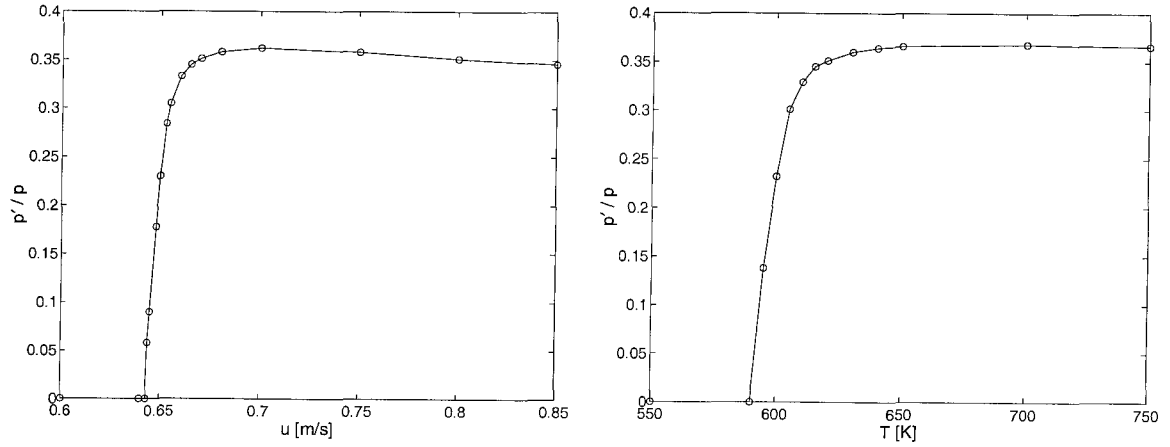

(a) constant T^+ of $700K$

(b) constant $\bar{u}$ of $.7m/s$

Figure 3.17: Limit cycle amplitude at the 3/4 location as a function of mean flow and upstream temperature

3.18. A photograph of the actual apparatus is shown in figure 3.19.

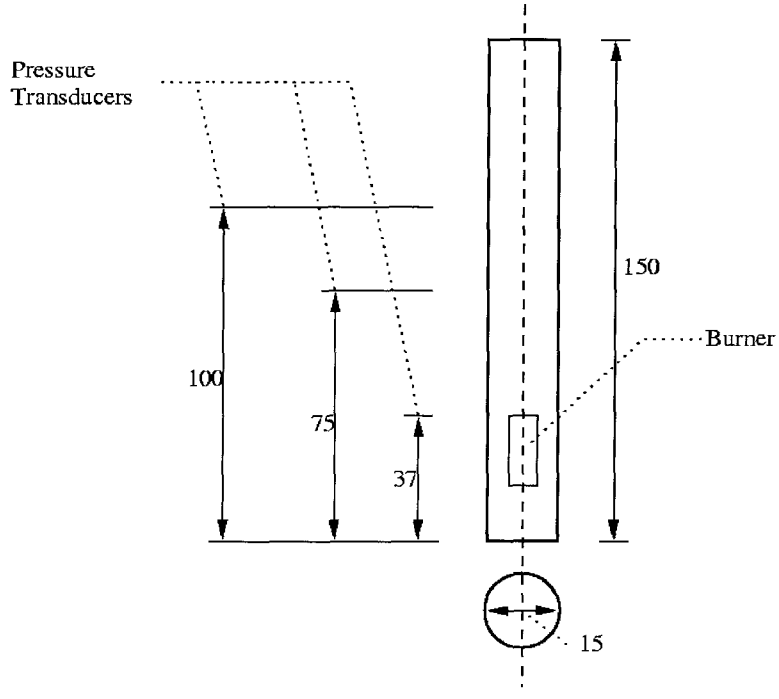

Figure 3.18: Layout of the Rijke burner

The apparatus exhibits two burning modes: stable combustion characterized by a very quiet burning process that does not couple with the acoustics of the tube and unstable combustion exhibiting large coherent pressure oscillations at the resonance frequencies of the tube. A pressure trace taken during these self-sustained oscillations is shown in figure 3.20. A minimum heat release is necessary to drive the oscillations. Several burner models, with different heat releases characteristics, were tested. In order to be able to achieve this lower limit, we settled on a Humboldt high temperature Bunsen burner. A picture of the burner is shown in figure 3.19. At the bottom of the burner a fuel jet entrains air which then mixes with the fuel inside the main burner body. When the self-sustained pressure oscillations inside the Rijke tube occur, the burning is extremely violent and flame

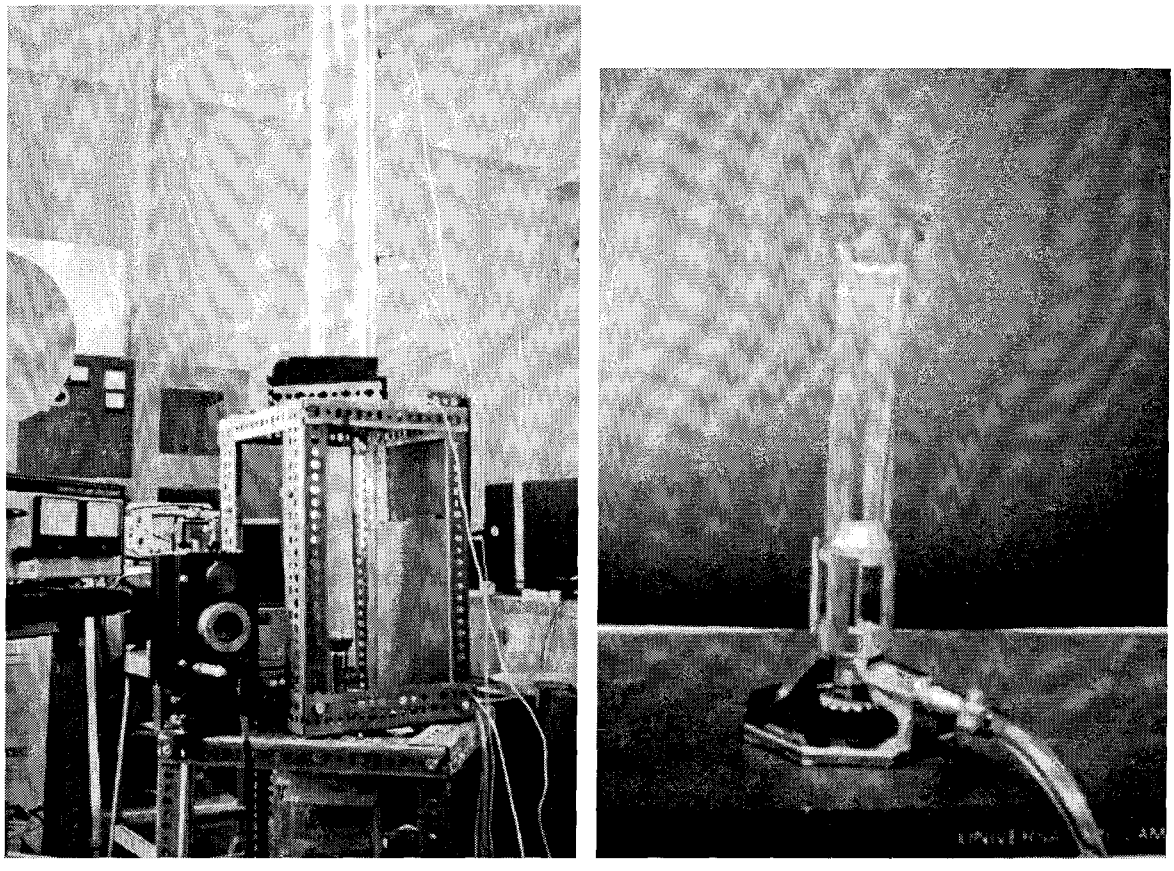

(a) Rijke burner apparatus

(b) Humboldt bunsen burner

Figure 3.19: Experimental Rijke burner

stabilization becomes an issue (the upwards velocity due to natural convection and the oscillating velocity when burning unstable initially caused severe flame blow-out problems). To provide additional flame anchoring, a metallic net was added at the top of the burner. The airflow through the tube is determined by natural convection and thus the parameters determining the operating condition of the tube are reduced to the position of the flame and the amount of fuel being burned (i.e., the strength of the flame). The fuel flow is set manually through valves and monitored via a digital mass airflow sensor.

The Rijke tube is instrumented with three piezoelectric pressure transducers positioned

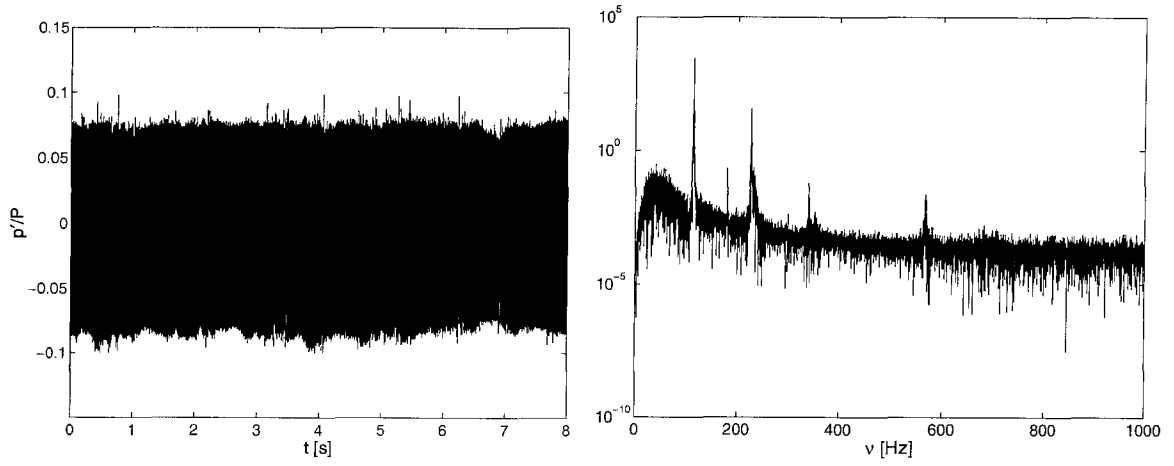

(a) (b)

Figure 3.20: Typical pressure trace (a) and spectra (b) when tube is 'singing'

respectively at 1/3, 1/2 and 3/4 of the length of the glass pipe. Their signals are amplified and acquired, with the fuel flow rate, via a digital acquisition board on a PC. The signals are sampled at $2000Hz$ which compares well with the $115Hz$ of the first acoustic mode of the tube.

Figure 3.21 illustrates the transition of the system from stable to unstable burning; the signal shown is the pressure at the 3/4 location. Shadowgraphs taken during the transition phase are given in figure 3.22. The photographs were taken in .2 second intervals at a shutter speed of 1/2000. Only half of the burner is shown (the dark area in the picture is the burner lip), the system being axisymmetric. The vertical lines are an effect of the non-uniform thickness of the wall of the cylindrical tube. The shadowgraph system uses an Hg-lamp with a pinhole screen as a point light source which is placed in the focal point of a spherical mirror. The mirror projects the light (coming out in parallel rays) through the glass tube section into the camera lenses. Thus the pictures shown are actually integrated

along the line of sight. Nevertheless they provide some interesting information as they clearly show that the vortex shedding from the lip of the burner plays an essential role and changes dramatically between both burning modes. Note that the edge of the photographs does not coincide with the tube wall; the tube has a $15cm$ diameter whereas the diameter of the burner is only $4.5cm$.

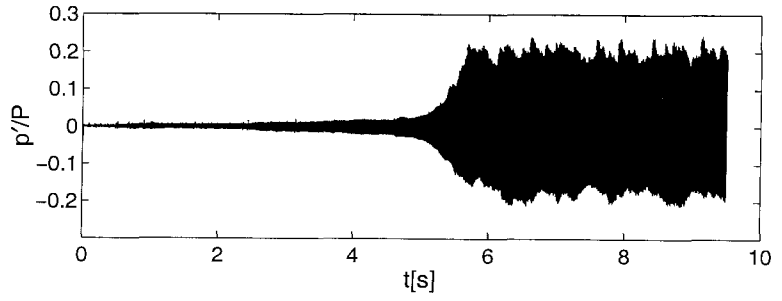

Figure 3.21: Transition from stable to unstable burning

A plot of the pressure amplitude against the fuel flow rate reveals a curious result: the Rijke tube presents a kind of hysteresis; that is, for certain values of the fuel flow rate the pressure amplitude can take on two distinct values depending on whether this operating point is reached from above by reducing the flow rate from a 'singing' state of the tube or from below by incrementing the heat release in a 'quiet' state. Figure 3.23 demonstrates this behavior.

3.3.3 Discussion

The appearance of an hysteresis loop is a novel result. The model proposed above is not capable of capturing any such effects; the nonlinearities included serve only to limit the amplitude of the pressure oscillations. The nonlinearities in the model produce a supercritical Hopf bifurcation, instead of a subcritical one accompanied with a saddle-node bifurcation

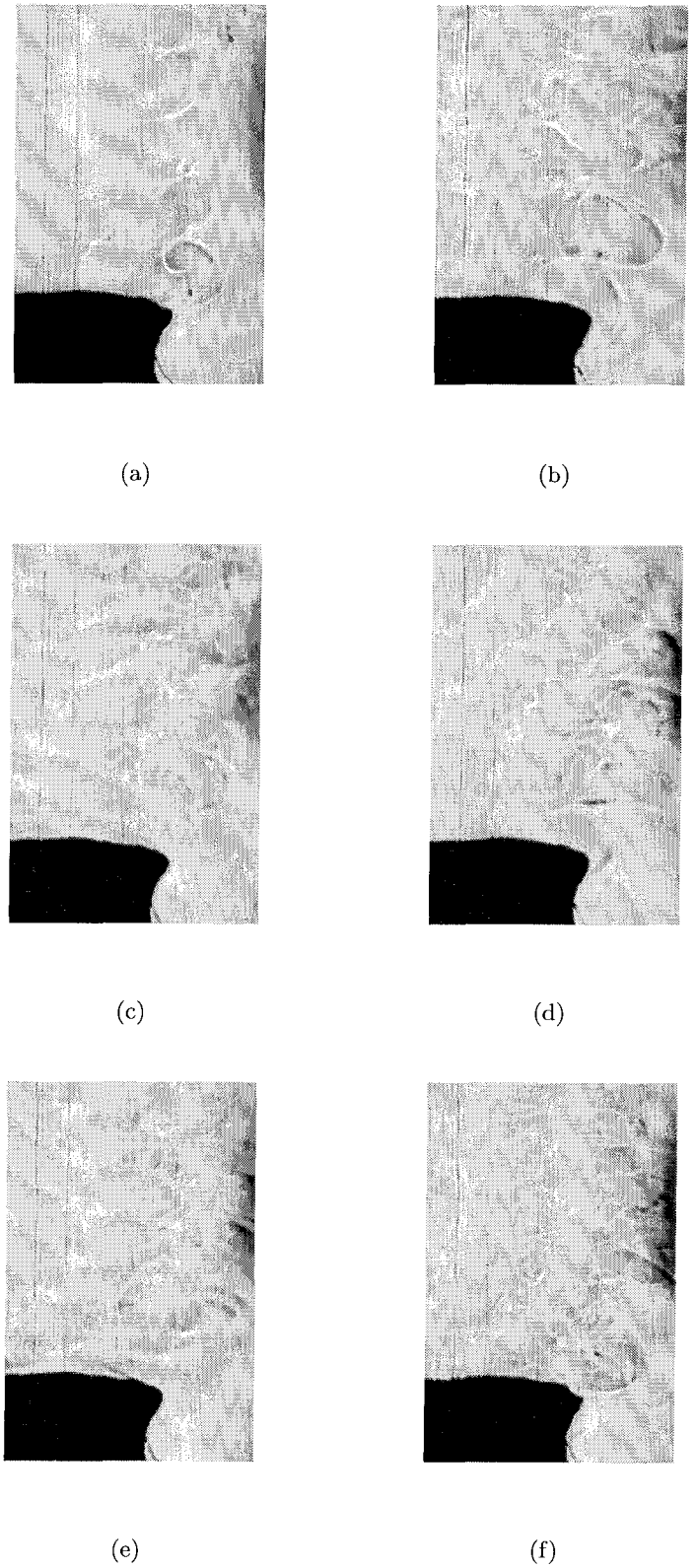

(a) (b)

(c) (d)

(e) (f)

Figure 3.22: Shadowgraph images taken at $.2s$ intervals during the transition period from (a) stable burning to (f) unstable burning

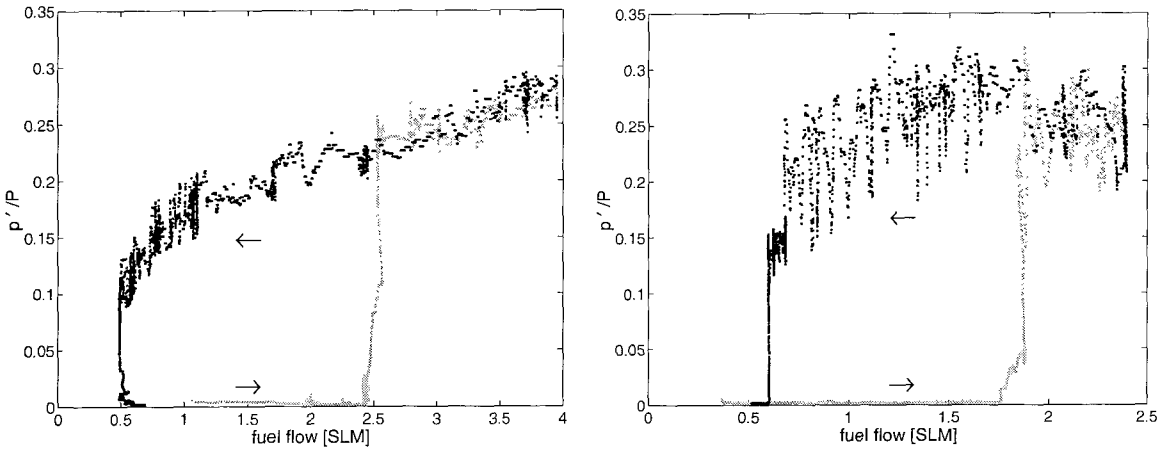

(a) Methane (b) Propane

Figure 3.23: Dependence of the pressure amplitude in the tube on the fuel flow rate for two different fuels (hysteresis); grey - increasing the fuel flow; black - decreasing the fuel flow

(see appendix A). Thus, effects such as triggering and hysteresis cannot be described. At this point it is unknown what causes this peculiar behavior and how widespread it is in combustion systems. Based on the shadowgraph visualization we speculate that the vortex shedding mechanism is a major factor. We have found a similar hysteresis in a dump combustor and there too the vortex shedding seems to dominate the flow dynamics. Results for the dump combustor have been reported by Isella, Seywert, Culick and Zukoski (1997).

The presence of two possible states of the system at the same operating condition allows for some interesting applications of control algorithms. In order to control the burner a secondary fuel line is added to the system. A two-way normally closed solenoid valve serves as the actuator of this secondary line and is controlled directly by the computer through a fast-response time solid state relay. The layout of the system is shown in figure 3.24.

The control of the system is achieved through a simple step modulation of the fuel supply

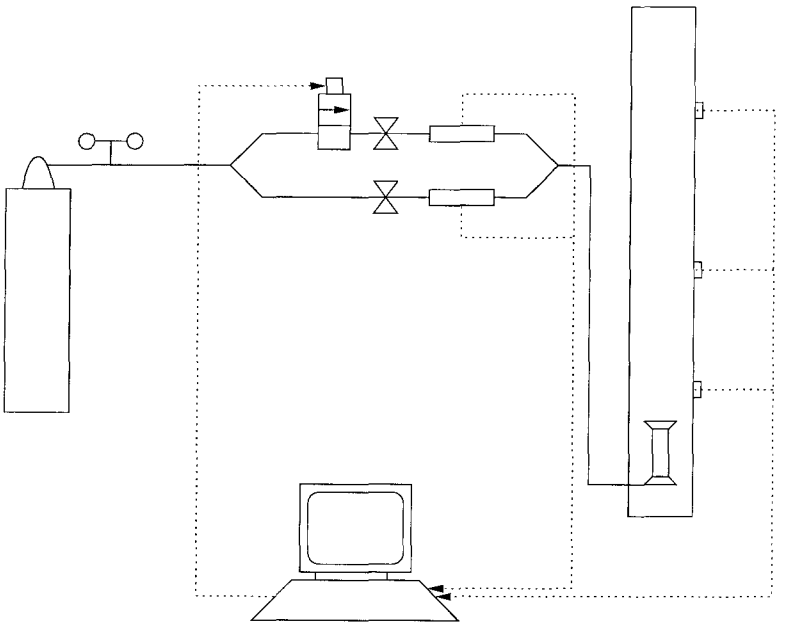

Figure 3.24: Sketch of the experimental setup; the dotted lines are signal connections

by opening momentarily the second line. Timing and duration of the extra fuel release are control parameters. Below we show two examples of a nonlinear control law that take advantage of the particular characteristics of the system at hand.

In figure 3.25 the operating point of the Rijke tube is defined by the methane flow rate of $1.5SLM$. A glance at figure 3.23 reveals that this point is well within the hysteresis region and thus the system can be in any of the two states ('quiet' or 'singing'). The idea now is to expand the operating range of the system into the hysteresis region by forcing a transition from the limit-cycling state into the 'quiet' state. This should be possible as both states are dynamically stable states of the system and thus all we need to do is to 'push' the system out of the region of attraction of the limit-cycle and into the region of attraction of the 'quiet' state. That this can in fact be done is demonstrated in figure 3.25. Here a single pulse (duration: $.5s$) is sufficient to successfully switch from one branch of the hysteresis

loop to the other one.

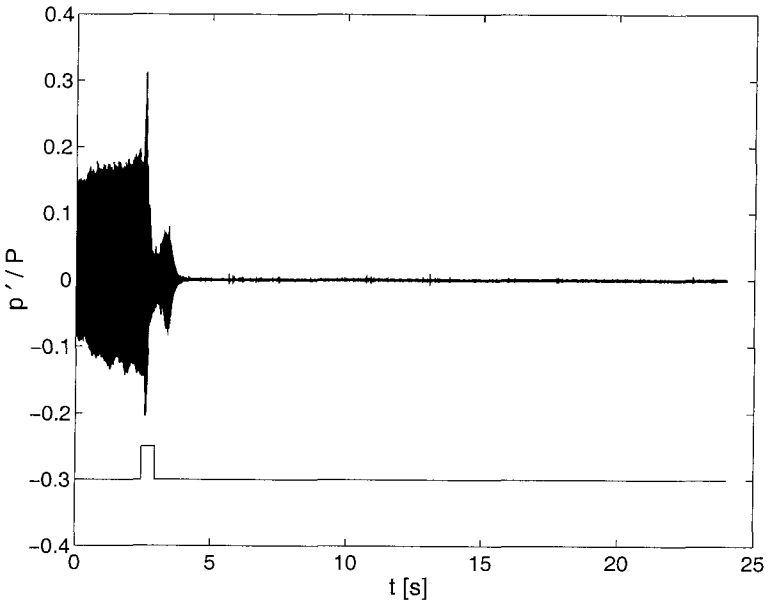

Figure 3.25: Forced transition from large oscillations to the 'quiet' regime in the hysteresis region

A second characteristic of the system is its rather slow growth rate (see figure 3.21). The logarithmic plot in figure 3.26 shows that the initial growth is indeed exponential and if we write $p'/\bar{p} \sim e^{t/\tau}$ we can get an estimate for the time constant τ: $\tau = .32s$. In other words it takes the instability about $.74s$ to grow a factor of 10. Therefore, even if the system is operated in a regime where the 'singing' state is the only dynamically stable state, it takes some time for the pressure oscillations to grow to the limit cycle if they start off at a small amplitude. We have demonstrated above that the Rijke burner can be forced to transition to the 'quiet' state by temporarily adding fuel. Intuitively it should therefore be possible to repeatedly 'kick' the system and keep the amplitude of the instability within a predetermined range. This approach is demonstrated in figure 3.27. The fuel flow rate is $3SLM$ and thus the operating point is to the right of the hysteresis loop. By commanding

the controller to open the secondary fuel line for $.05s$ each time the pressure hits a certain threshold, we effectively suppress the oscillations for a short period of time. Note that the 'quiet' state is dynamically unstable and thus we cannot hope to remain in this state (as opposed to above); instead, the control action needs to be applied repeatedly, that is each time the threshold is reached again.

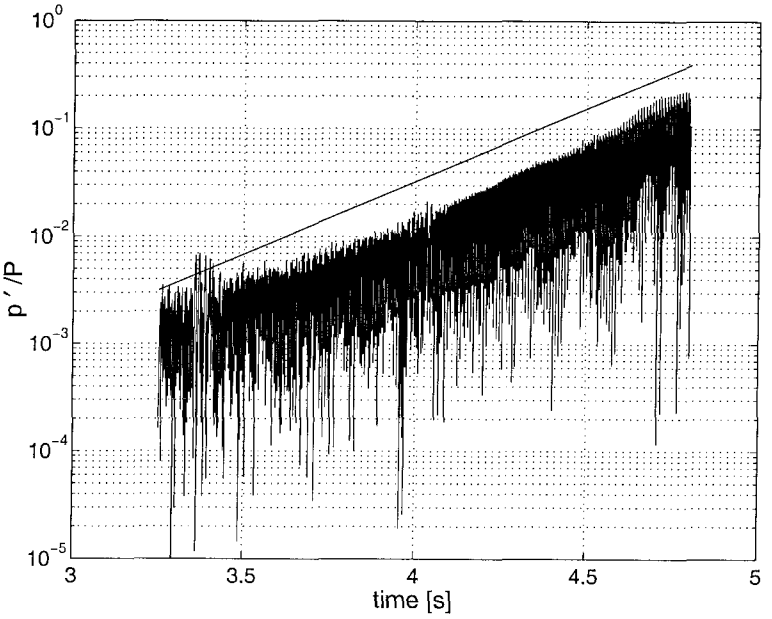

Figure 3.26: Logarithmic plot of the growth phase of the pressure oscillations (part of the trace in figure 3.27)

3.4 Summary

In this chapter we have shown how the analytical framework developed in chapter 2 can be applied to a Rijke tube.

Using a simple one-dimensional transfer function approach, we have shown that the linear stability boundaries can be computed with a low order model (only four modes were used

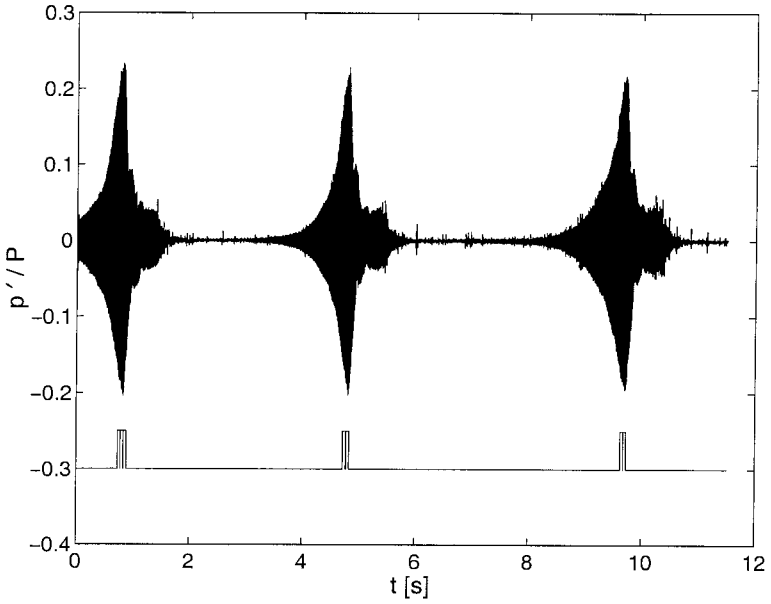

Figure 3.27: Control in the 'unstable' region

in the simulations, giving rise to four coupled second order differential equations).

To correctly capture the nonlinear behavior of the system, a more complex model is needed. It appears that nonlinear heat release effects need to be included; and - based on the flow visualization of the Rijke burner transition - a one-dimensional description of the flow field may not be enough.

The demonstrated possibility of a controlled transition between the stable and unstable branch of the Rijke burner suggests a new approach to designing control laws for combustion systems. However, a deeper knowledge of the nonlinear dynamics - obtained either through an experimental investigation or a more sophisticated model - is required to use this approach.

Chapter 4

Effects of Noise

Observing experimental pressure traces it is obvious that they are not as 'clean' as the ones the model produces. In fact a look at a pressure spectrum shows the presence of a broad background 'noise' across all frequencies. It should be clear that the model, in the way presented up to here, is not capable of producing frequency components different from the modal frequencies. In this chapter we attempt to explain the origins of the noise and show how to integrate it into our model. Finally we analyze how the presence of stochastic sources affects the dynamics of the system. The main purpose here is to investigate some of the behavior that is *possible*. We will not attempt to construct realistic models, but rather explore some aspects of solutions to the oscillator equations with stochastic sources, to aid interpretation and understanding of observed behavior.

From time to time in the past fifty years or so the subject of combustion noise has been an active area of research for brief periods of time. Usually attention has been directed to certain aspects treated at least partly in analogy with the more highly developed subject of aerodynamic noise generated in jets, shear layers and boundary layers. The true origins of the noise observed in combustors remains largely obscure.

Even less attention has been paid to matters relating to connections between noise generated by the combustion field and the dynamical behavior of the chamber containing the reacting flow. Indeed, this aspect of the subject has been so much out of the mainstream of research activities generally that it seems to have been approached more or less independently, and with varying degrees of effort, by only five groups of workers: several coordinated efforts in Russia beginning in the 1960's; Summerfield and his students in the 1970's; Strahle and co-workers in the 1970-80's; Hessler in the 1980's; and Paparizos, Culick and Burnley in the 1990's.

The earliest work by the Russians treating problems of chamber dynamics and combustion instabilities in liquid rocket engines was not known in the West until the early 1990's (Denisov, Kadishevish and Povolotzky 1995). Broadly those efforts led to a practical method of assessing the stability margins of stable liquid rocket engines manufactured in large quantities. In practice, the stability margin of a particular engine could be assessed for practical purposes (e.g., acceptance for launch operations) by analyzing the statistical properties of a single firing of that engine. That method was used routinely instead of the method of 'bombing' with small explosive charges developed by NASA during the Apollo program. Hessler (Hessler 1979, Hessler 1980, Hessler 1982, Duer and Hessler 1984) advocated somewhat related ideas for solid propellant rockets but the approach was not followed in the U.S. to the extent it evidently was in Russia.

Those methods amount to attempts to answer the question, "What information about potential combustion instabilities can be gained from analysis of the pressure record for a firing of a stable motor?" The usefulness of the answer of course depends not only on careful data processing of the record but especially on interpretation of the results of the analysis;

the interpretation in turn depends entirely on understanding the dynamical processes in the combustor.

4.1 Stochastic Sources

According to a general principle most thoroughly discussed by Chu and Kovasznay (1956), it is not enough to consider only acoustic disturbances in the combustion chamber. Chu and Kovasznay (1956) show that any small disturbance in a compressible medium can be synthesized of three kinds of waves or 'modes of motion': acoustic waves, entropy or temperature waves, and vorticity waves. While it is correct that in the limit the acoustic waves carry all the pressure fluctuations and are thus observed as combustion instabilities, the other two wave kinds will affect the dynamics of the system.

In particular, keeping in mind all 3 modes of motion allows one to write down explicitely the contributions from gasdynamics to the functions h and f defined in section 2. It's also the gasdynamical terms that represent the most significant sources of noise, although it is conceivable, as others have pointed out, that other sources contribute noise (Glick 1996–99), such as the randomness associated with combustion of heterogeneous propellants. The major task is to extract from h and f representations of noise sources in such a form that modeling can be done, either theoretically or using experimental results.

In this section a procedure is outlined to incorporate the effects of entropy and vorticity (following Burnley (1996)). Based on the discussion of Chu and Kovasznay (1956) the flow variables (notably the velocity) in the functions h and f are written as sums of contributions associated with each of the three modes of motion. The details of manipulating the various terms in h and f depend crucially on properly respecting the formal ordering procedure

(Culick 1997). The new variables are then inserted in the equations derived by spatially averaging, producing integral representations of noise sources in terms of stochastic flow variables.

In order to obtain numerical results, models of the stochastic variables must be chosen or constructed. In this work white noise behavior is assumed. The analysis produces stochastic differential equations for amplitudes of the acoustic modes assumed to represent a combustion instability. Solving these equations then gives amplitudes reflecting the stochastic or random character of the sources. Results obtained do appear to be realistic but there is no basis for making quantitative comparisons with measurements.

It is important to understand that we are not using this analysis to calculate the noise field in the chamber. To do so would require considering an enormous number of terms in the expansion of the pressure (2.15) in order to cover the broad range of frequencies contained in the spectrum of noise. Rather, we are interested in determining the possible influences of noise on the time-varying amplitudes of the lowest (dominant) modes of the chamber. Hence we will retain only two or three of the set (2.16). The source terms representing noise generated within the volume (part of h) and at the boundary (part of f) will, on the other hand, contain a broad band of frequencies—the precise form depends on the model chosen for the fundamental noise sources.

4.1.1 Three Modes of Motion

Unlike the analysis in chapter 2 in which only the organized oscillatory acoustic field was accounted for, we include here both the deterministic (acoustic) part and the non-deterministic (stochastic or random) part of the motion. According to the principle cited in Chu and

Kovasznay (1956), we can write for weak disturbances

$$p' = p'_a + p'_\Omega + p'_s \tag{4.1}$$

where p'_a, p'_Ω, p'_s are the pressure fluctuations associated respectively with acoustic, vorticity, and entropy waves. Corresponding to (4.1) we may split the velocity, vorticity and entropy fields:

$$\begin{aligned} \vec{u}' &= \vec{u}'_a + \vec{u}'_\Omega + \vec{u}'_s \\ \vec{\Omega}' &= \vec{\Omega}'_a + \vec{\Omega}'_\Omega + \vec{\Omega}'_s \\ s' &= s'_a + s'_\Omega + s'_s \end{aligned} \tag{4.2}$$

In lowest approximation (small amplitude, uniform mean flow) the three types of waves propagate independently and have the properties (Chu and Kovasznay 1956):

Acoustic waves: pressure and velocity fluctuations only

Vorticity waves: velocity and vorticity fluctuations only

Entropy waves: velocity and entropy fluctuations only

Hence to this lowest approximation,

$$\begin{aligned} p' &= p'_a \\ \vec{\Omega}' &= \vec{\Omega}'_\Omega \\ s' &= s'_s \\ \vec{u}' &= \vec{u}'_a + \vec{u}'_\Omega + \vec{u}'_s \end{aligned} \tag{4.3}$$

The density fluctuation for this case of independently propagating waves is

$$\frac{\rho'}{\bar{\rho}} = \frac{1}{\bar{\gamma}} \frac{p'_a}{\bar{p}} - \frac{1}{\bar{c}_p} s'_s \tag{4.4}$$

As in previous applications of spatial averaging (see above, Culick and Yang (1992), Culick (1994) and references cited there) the central idea motivating the structure of the analysis, and the ordering procedure, is the following. The phenomena called generically combustion instabilities are dominated by acoustic waves. Hence the pressure field is represented by the expansion (2.15) with p' identified as the acoustic pressure and we write

$$p' = p'_a(\vec{r};t) = \bar{p}\sum_{j=1}^{\infty}\eta_{aj}(t)\psi_j(\vec{r}) \tag{4.5}$$

The approximation is that $p' \approx p'_a$ in the *left*-hand sides of (2.10), (2.11) and therefore $\eta_n \to \eta_{an}$ in (2.16):

$$\frac{d^2\eta_{an}}{dt^2} + \omega_n^2\eta_{an} = F_n \tag{4.6}$$

To write (4.6) as a system of equations governing the η_{an} as the independent variables requires, as seen above, approximating the flow variables p', $\vec{u}'$, and ρ' appearing in the integrals defining F_n.

4.1.2 Gasdynamical Terms

The forcing function F_n is given in equation (2.17). For the purposes here we must concentrate on the integrals $I_1, \ldots, I_4$ as defined in equation (2.18). The nonlinear contributions I_3 and I_4 eventually generate coupling between the acoustic field and those motions identified as noise. To simplify the following calculations we simply ignore entropy fluctuations (clearly not strictly permissible for analysis of combustors) and substitute (4.2) and (4.4) in the definition of I_3:

$$\begin{aligned} I_3 &= \int\left[(\vec{u}'_a + \vec{u}_\Omega)\cdot\nabla(\vec{u}'_a + \vec{u}'_\Omega) + \frac{1}{\gamma}\frac{p'_a}{\bar{p}}\frac{\partial}{\partial t}(\vec{u}'_a + \vec{u}'_\Omega)\right]\cdot\nabla\psi_n dV \\ &= \left\{\int\left(\vec{u}'_a\cdot\nabla\vec{u}'_a + \frac{1}{\gamma}\frac{p'_a}{\bar{p}}\frac{\partial\vec{u}'_a}{\partial t}\right)\cdot\nabla\psi_n dV\right\} \end{aligned}$$

$$+\int\left(\vec{u}'_a\cdot\nabla\vec{u}'_\Omega+\vec{u}'_\Omega\cdot\nabla\vec{u}'_a+\frac{1}{\gamma}\frac{p'_a}{\bar{p}}\frac{\partial\vec{u}'_\Omega}{\partial t}\right)\cdot\nabla\psi_n dV$$
$$+\int(\vec{u}'_\Omega\cdot\nabla\vec{u}'_\Omega)\cdot\nabla\psi_n dV \tag{4.7}$$

The terms in curly brackets form part of the 'second order acoustics' treated at length in references cited earlier. Within the ordering procedure followed in those works, it is legitimate[1] to replace $\vec{u}'_a$ by the same series expansion as above

$$\vec{u}'_a=\sum_{j=1}^{\infty}\frac{\dot{\eta}_j(t)}{\bar{\gamma}k_j^2}\nabla\psi_j(\vec{r}) \tag{4.8}$$

Note that term by term, the two series (4.5) and (4.8) satisfy the classical linear acoustics equations,

$$\begin{aligned}\bar{\rho}\frac{\partial\vec{u}'_a}{\partial t}+\nabla p'_a &= 0\\ \frac{\partial p'_a}{\partial t}+\gamma\bar{p}\nabla\cdot\vec{u}'_a &= 0\end{aligned} \tag{4.9}$$

Substitution of (4.5) and (4.8) in the curly brackets in I_3 and in all corresponding terms appearing in I_1, I_2 and I_4 leads to the familiar terms nonlinear in the η_{aj} and $\dot{\eta}_{aj}$ quoted above (see equation (2.21)).

Since we have ignored entropy fluctuations, we are assuming here that non-deterministic or stochastic motions (i.e., all non acoustic notions) are contained in the vorticity fluctuations. In solid propellant rockets, two sorts of vorticity may exist: vorticity associated with turbulent motions; and organized vorticity in the form of shear waves generated at burning surfaces (Flandro (1995); Majdalani and van Moorhem (1995)). The second type is also a subject of current research and will be ignored here.

[1]Legitimate, that is, to the order to which those analysis were taken. The substitution is not correct to higher order; finding the correct substitution, or an equivalent procedure, when contributions of higher order in the average Mach number are accounted for, is a subject of current research.

Therefore, the result of this analysis so far is that the part of I_3 that might be identified as a source of noise is

$$(I_3)_{\text{noise}} = \int \left(\vec{u}'_a \cdot \nabla \vec{u}'_\Omega + \vec{u}'_\Omega \cdot \nabla \vec{u}'_a + \frac{1}{\gamma} \frac{p'_a}{\bar{p}} \frac{\partial \vec{u}'_\Omega}{\partial t} \right) \cdot \nabla \psi_n dV + \int (\vec{u}'_\Omega \cdot \nabla \vec{u}'_\Omega) \cdot \nabla \psi_n dV \tag{4.10}$$

Leaving $\vec{u}'_\Omega$ unspecified for the moment, substitute the expansion (4.5) and (4.8) in the integrals. The result contains three kinds of terms having the form

$$(I_3)_{\text{noise}} = \sum_{i=1}^{\infty} \xi_{ni}^{(3)}(t) \eta_{ai}(t) + \sum_{i=1}^{\infty} \xi_{ni}^{(3)v} \dot{\eta}_{ai}(t) + \Xi_n^{(3)}(t) \tag{4.11}$$

It is fairly easy to see from the definitions given in (2.18) that I_4 will generate terms having the same form. Because they are linear, I_1 and I_2 produce terms that represent either linear attenuation, due to interactions between the mean and fluctuating fields but independent of $\vec{u}'_\Omega$; or independent of the acoustic field and linear in $\vec{u}'_\Omega$ that can be symbolically combined with $\Xi_n^{(3)}(t)$. Similar reasoning can be applied to surface integrals in (2.17), and (4.11) is the general form for noise sources at the boundary as well as within the volume.

The result of this reasoning is the following system of acoustic equations that are the system used in previous work (Culick 1995, Culick and Yang 1992, Culick 1994) with the additional source terms representing stochastic or noise sources:

$$\ddot{\eta}_n + \omega_n^2 \eta_n = 2\alpha_n \dot{\eta}_n + 2\omega_n \theta_n \eta_n - \sum_{i=1}^{\infty} \sum_{j=1}^{\infty} [A_{nij} \dot{\eta}_i \dot{\eta}_j + B_{nij} \eta_i \eta_j] + (F_n)_{\text{other}}^{\text{NL}} + \sum_{i=1}^{\infty} [\xi_{ni}^v(t) \dot{\eta}_i + \xi_{ni}(t) \eta_i] + \Xi_n(t) \tag{4.12}$$

We have dropped the unnecessary subscript $(\ )_a$ on η_{an} and we ignore linear coupling of the modes (Culick 1997). In later calculations here we will also ignore the term $(F_n)_{\text{other}}^{\text{NL}}$ representing the influences of other processes not discussed here, notably nonlinear combustion. Note that the linear terms include all linear processes, including linear combustion

dynamics. The combustor is linearly stable if and only if all modes are linearly stable, i.e., α_n negative for all n.

4.1.3 Discussion

We now analyze the extra terms in the oscillator equations. Two of those terms have the form of *multiplicative* noise coupled directly to the oscillators (i.e., the acoustic modes). As well as coupling the modes, some of those terms represent random fluctuations of the damping and spring constant (i.e., the natural frequency) of the modes. This form of coupling between noise and the motion of the system is sometimes called *parametric* excitation. The remaining terms, independent of the oscillators' motions are called *additive*; they are 'external' to the acoustic modes representing deterministic motions in the combustor. It is important to notice that both multiplicative noise terms as well as the additive term appear even though in the limited derivation given here we have only used vorticity waves. If we include entropy waves the same sort of terms appear. One can indeed argue that no matter what disturbances are included, terms having the same form will appear. Of course the exact expression of the terms will change, but since we assume here that they all average out to white noise, no new phenomena will arise. However, by using only one further disturbance (vorticity waves) we have shown that those three terms are indeed *necessary* to capture the whole behavior of the systems. In the literature, noise terms have in general been ignored or at most external disturbances, acting as additive noise, have been considered. We argue that this might lead to an inaccurate description of the system, especially when applied to design an active controller (see chapter 5).

The response or transfer function for a combustor has infinitely many relatively narrow peaks or resonances in its frequency spectrum. Hence a broadband noise field—here we

will assume white noise—is capable of exciting the acoustic modes due to the action of the additive noise contributions. Because natural damping processes become stronger as the frequency increases, only the lowest modes are likely to be excited.

If the combustor is linearly stable, then the noise sources will, according to this picture, excite apparently random motions in the chamber which must contain information about the characteristics of the modes, i.e., of the corresponding oscillators. That is, with appropriate analysis of pressure records, one should be able to solve for the damping ratios α_n, and the natural frequencies ω_n of the modes excited. Finding those characteristics is an example of the general process called system identification (system ID), a well-known activity in several fields. Note that application of system ID requires a model of the system, here a collection of simple oscillators. Examples of system ID applied to combustors with noise and combustion instabilities are discussed in the next section.

There are at least two general questions to be addressed in the subject of noise and combustor dynamics:

1) Is noise, meaning any stochastic or random source, capable of causing the organized oscillatory motions identified as combustion instabilities?

2) What can be learned about the dynamics and stability of a combustor by applying methods of system identification?

In respect to the first question, the implication is that combustion instabilities are forced oscillations, a position advocated for many years by Hessler (Hessler 1979, Hessler 1980, Hessler 1982) and more recently Hessler and Glick (1998). Perhaps the most obvious and unambiguous way to determine whether oscillations are forced (*driven*) or are *self-excited* (i.e., linear instabilities) is based on examining the transient growth periods.

In self-excited oscillations the mechanism responsible for the instability is internal to the system, in our model via the feedback through F_n in equation (4.6). The typical behavior is sketched in figure 4.1(a) showing the initial exponential growth of amplitude (concave upward), evolving into a limit cycle due to the action of nonlinear processes.

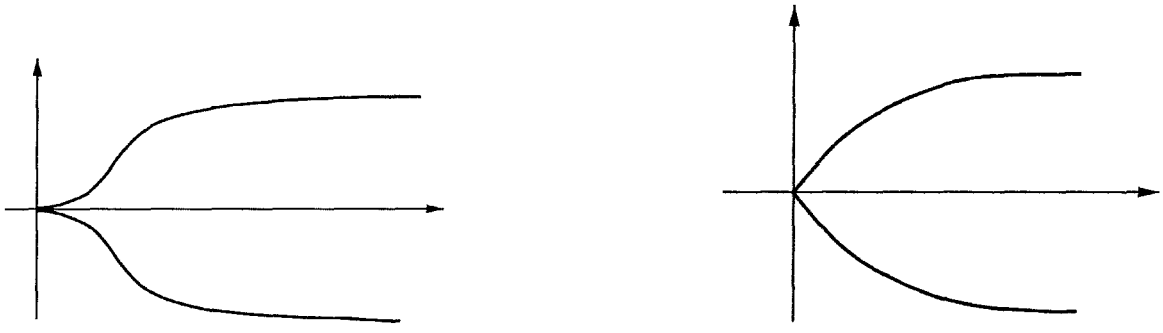

(a) Self-excited system

(b) Driven system

Figure 4.1: Transient growth of driven and self-excited systems

In the case of driven oscillations, the underlying system is dynamically stable and the force F_n is entirely due to external influences (instead of involving the fluctuations, i.e., $\vec{u}'$ and p'). When the external driving starts acting, the amplitude of the oscillation grows as shown in figure 4.1(b): concave *downward.* It finally reaches a constant peak amplitude *without* the action of nonlinear processes. This holds because as $t \to \infty$ the amplitude is set by the condition that the time-averaged power input due to the external force is equal to the time-averaged rate of energy dissipated within the system. In fact, the condition rate of energy gain = rate of energy loss is true also in the limit cycle of self-excited oscillations, but in that case the energy gains and losses are all internal.

The contrast in the transient growths of self-excited and forced oscillations is a fundamental property central to one of the main points of this chapter: data for the transient growth

of combustion instabilities in solid propellant rockets have inevitably had the behavior shown in figure 4.1(a). We are not aware of any data having the form of the sketch in figure 4.1(b). Therefore, we must conclude that combustion instabilities observed in solid propellant rockets are the results of true linearly unstable motions. That conclusion means that there must be internal feedback, a driving force sensitive to the motion itself.

In the following section we examine the question: Can noise alone force significant oscillations in a linearly stable system? The answer depends on just how stable the system is, but our results suggest the same conclusion that Strahle (1978) reached many years ago: *No.* Thus, it seems that all evidence supports the commonly held view that combustion instabilities really are a consequence of unstable conditions.

On the other hand, noise sources certainly do influence both qualitative and quantitative aspects of the oscillations. Simulations in the next section show the most obvious consequence of noise in the system is that the pressure during an oscillation is not a clean sinusoid and hence the peak amplitudes are no longer constant in the motions but are properly described by a probability distribution, the most probable value being that for the amplitude of the deterministic limit cycle.

Question 2 stated above has been partly answered. Calculations in the following section show that much can be learned with system ID if the system is both stable and behaves linearly. Otherwise, assessing the stability margin, or other characteristics, requires deeper investigation of the system's dynamics. In all cases, the matter of uncertainties arising with processing noisy data must be thoroughly addressed.

4.2 Noisy Combustors and System Identification

System identification seems first to have been used in the field of combustor dynamics by several Russian groups as part of their development of liquid rocket engines, beginning perhaps as early as the 1950's but certainly in the 1960's (Agarkov, Denisov, Dranovsky, Zavorokinin, Ivanov, Pikalov and Shibanov 1993). Evidently the approach was used routinely to assess the stability margins of newly fabricated liquid rocket engines.

4.2.1 Two Methods

In section 4.1 it was shown that the addition of non-acoustic velocity perturbations leads to a system of equations of the following kind:

$$\begin{aligned} \ddot{\eta}_n &= \left(2\omega_n\theta_n - \omega_n^2 + \xi_n\right)\eta_n + \left(2\alpha_n + \xi_n^v\right)\dot{\eta}_n + \Xi_n \\ &\quad - \sum_{i=1}^{N}\sum_{j=1}^{N}\left(A_{nij}\dot{\eta}_i\dot{\eta}_j + B_{nij}\eta_i\eta_j + M_{nij}\eta_i\dot{\eta}_j\right) \end{aligned} \tag{4.13}$$

It was mentioned that three distinct kinds of stochastic source terms are present: 'additive noise' – noise as the driving force of an oscillator – as well as 'multiplicative noise'–random perturbations of the growth constants α_n and the frequency shifts θ_n. The multiplicative sources cannot a priori be neglected since any disturbances in the combustion chamber will have an effect on the combustion process as well as the flow field and thus on α_n and θ_n. At this time no successful model of the noisy source terms is known so we choose to approximate them by 'white noise'.

In the following a linearly stable system consisting of four acoustic modes with stochastic sources is simulated. Additive and multiplicative noise terms are included in the simulations and their effect on the resulting pressure oscillations is analyzed. The fundamental mode of the system considered has a frequency of 900 Hz. Realistic values for the parameters

have been taken from Jahnke and Culick (1994) and are given in table 4.1. The simulation generates a pressure trace (here it is assumed that the pressure is recorded at the midpoint of a closed-closed combustion chamber) similar to the one shown in figure 4.2.

mode	1	2	3	4
α_n (1/sec)	-50	-324.8	-583.6	-889.4
θ_n (rad/sec)	12.9	46.8	-29.3	-131.0

Table 4.1: Parameter values used in the simulations

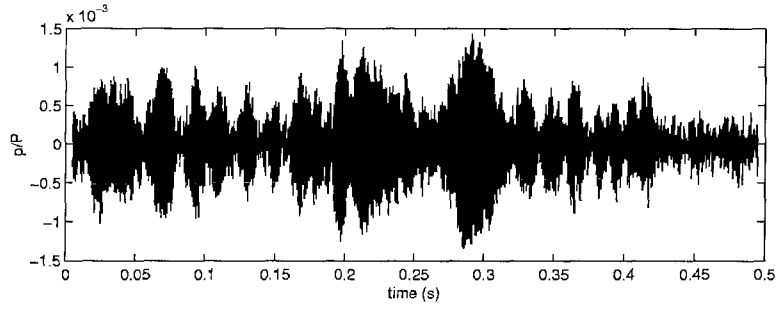

Figure 4.2: Typical simulated pressure trace

In laboratory and field experiments such pressure traces are recorded and are often the only available data. Thus the desire to extract as much information as possible about the system from it. Hessler and Glick (1998) have proposed using 'Burg's Method' (also known as the 'Maximum Entropy Method') to curve-fit the power spectrum of the signal. Some underlying principles of this method are given in appendix B; Figure 4.3 shows its application to the present case. The method is extremely powerful and allows easy determination of both frequencies and growth constants from the experimental data. A great advantage of this method is that no external signal needs to be applied in order to do the system identification. The internally generated 'noise' – resulting from combustion, flow turbulence, ... – is

sufficient to drive the system and identify the acoustic structure.

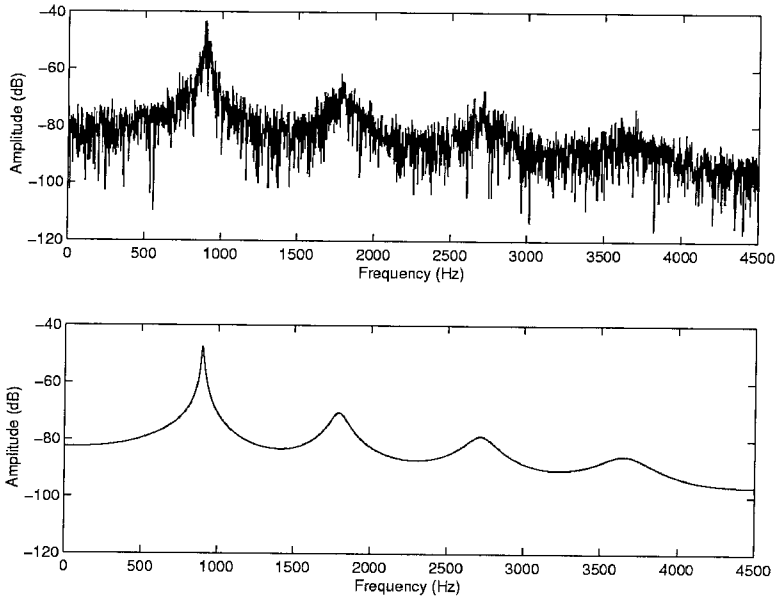

Figure 4.3: Application of Burg's method: Power spectrum of pressure signal shown in Figure 4.2 (top) and its reconstruction using Burg's method (bottom)

A rather common method used experimentally to test the stability of rocket motors is to detonate a small explosive inside the combustion chamber – thus introducing a sharp pressure pulse into the system – and record the decay of that pulse (Harrje and Rearden 1972); see also the example given in the introduction. This approach has been used here in order to compare the achievable results with the method mentioned above. In this case the information is extracted by fitting an exponential decay directly to the signal without making use of the power spectrum. In this method the fitted signal consists of a simple superposition of modes:

$$\frac{p'}{\bar{p}} = \sum_{i=1}^{N} A_i e^{\alpha_i t} \cos(\omega_i t + \phi_i) \tag{4.14}$$

The parameters A_i, α_i, ω_i, and ϕ_i are fitted using a least squares method. For all simulations

reported here, the introduced pulse $p'/\bar{p}$ had an amplitude of 10%; figure 4.4 shows the decaying pulse for the same system used previously and the signal fitted to it.

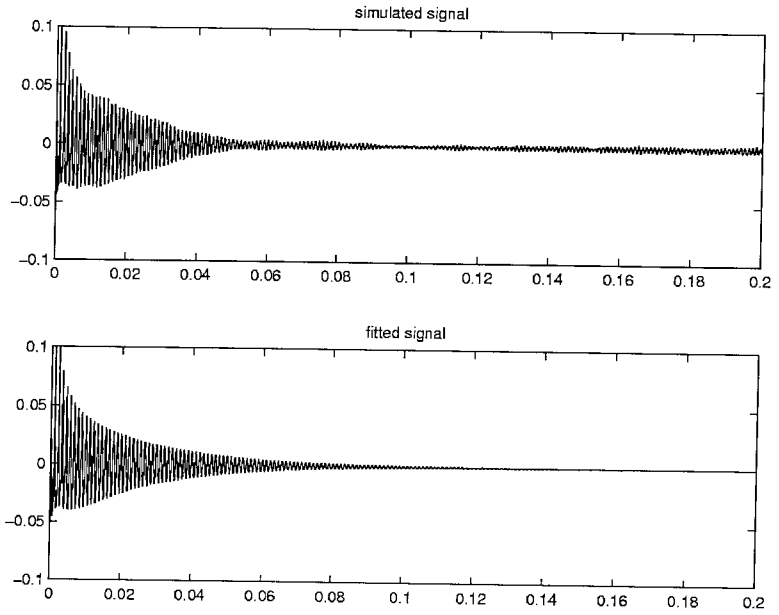

Figure 4.4: Fitting an exponential decay: the reconstructed signal is made up of 4 exponentially decaying oscillators where both decay constants and frequencies get fitted by a least square method to the simulated pressure trace

Both methods are able to detect the frequencies of the modes (and thus the θ's) and the effective α's. Note that they detect the *effective* decay constants, combinations of driving and damping effects. It is not possible to separate those effects by analyzing the data. The following sections contain closer examinations of these two diagnostic methods under various conditions with stochastic sources.

4.2.2 Linear Motions Forced by Additive Noise

In this section both ξ^v and ξ are set to zero and only the influence of the additive noise on the stable linear system is considered.

Due to the random nature of the equations, the simulation is repeated multiple (50) times for each data point using different realizations of the white noise. In that way both mean and standard deviation of the identified parameters can be reported. In the lab such an averaging could be achieved by repeating the experiment or splitting a longer signal into smaller parts (assuming that the 'real' noise is indeed white, i.e., independent of the prior signal). However, this is not always possible and thus it is important to get a good idea about the confidence level associated with the detected parameters.

Noise power for Ξ_n	Average $p'/\bar{p}$
10^1	.005%
10^3	.05%
10^5	.5%

Table 4.2: Relationship between the parameter Ξ and the measurable system output

The random source terms are unknown and are represented in this study by white noise. The strength of the sources are parameters of the system and are defined by their 'noise power' – the height of the power spectral density of the white noise. This 'noise power' is not a measurable quantity; its range has been chosen so that the output of the system, the recorded pressure oscillations, has a reasonable amplitude. Table 4.2 shows how the 'noise power' of Ξ relates to the average pressure fluctuation for the system under consideration. This relation depends on the system as the various source terms need to scale with the relevant characteristics of the system to have an appreciable effect. Thus equation (4.13) shows that ξ^v relates to the magnitude of the growth rate of the least stable mode whereas Ξ scales with the inverse of the growth rate and the inverse of the square of the frequency.

Note that the forcing in the case considered here is given by Ξ which, being white noise, acts at every frequency and in particular at the resonance peak of each mode.

Figures 4.5 and 4.6 show the results of the system identification using Burg's method and the method of pulsing respectively. The main concern being the stability of the system, the results for the growth constants of the various modes are reported in detail along with their standard deviation in tables 4.3 and 4.4.

The values for decay rates and frequency shifts inferred with Burg's method are not influenced by the amplitude of the additive noise sources. This is to be expected since the system analyzed is purely linear and thus changing the amplitude of the (stochastic) driving force is only going to affect the *amplitude* of the final oscillation but does not change any other characteristics of the system. This can also be seen in figure 4.7 which shows the amplitudes of the different modal peaks in the power spectrum against the input noise power. The relation is a linear one and thus the ratio (output power)/(input power) remains constant, meaning that an increase in noise does not lead to a different qualitative behavior of the system.

According to table 4.4 the method of pulsing gives more consistent – the standard deviation between multiple runs is less then 1% – results at low noise levels. At higher noise levels the variance of the results increases dramatically as the decaying pressure pulse gets rapidly 'drowned' by the noise. This effect is especially pronounced for the fast decaying higher modes and is in sharp contrast to the independence of the identification accuracy using the power spectrum. Using this latter method, the values of all decay constants can be given to 20% uncertainty for any noise level.

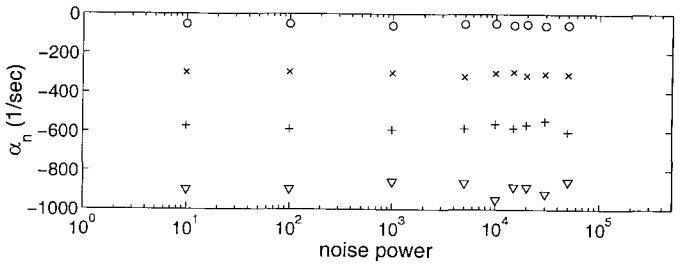

(a) Decay rates

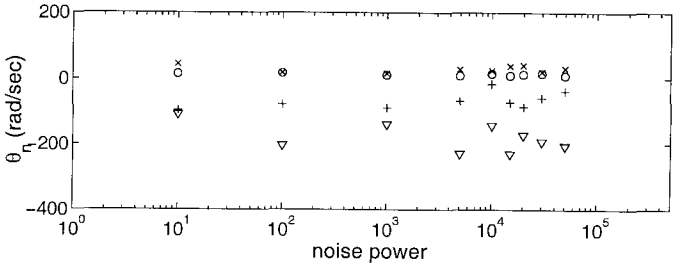

(b) Frequency shifts

Figure 4.5: Using Burg's method for systems with additive noise (1^{st} mode: o, 2^{nd} mode: x, 3^{rd} mode: +, 4^{th} mode: ∇)

Noise	α_1	α_2	α_3	α_4
10^1	-52±12	-298±48	-571±80	-898±108
10^2	-51±16	-297±39	-589±117	-896±188
10^3	-59±14	-301±42	-592±71	-858±137
10^4	-48±10	-301±42	-561±73	-884±159
10^5	-56±18	-309±52	-603±84	-855±145
correct	-50	-325	-584	-889

Table 4.3: Additive noise results for α_i's with Burg's method

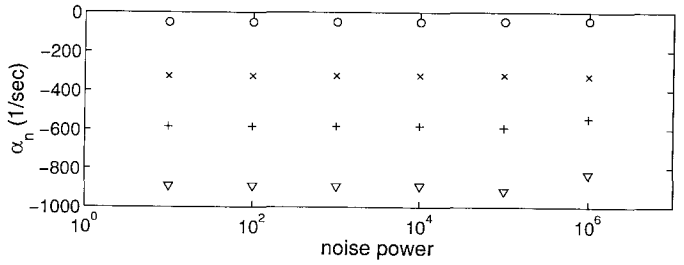

(a) Decay rates

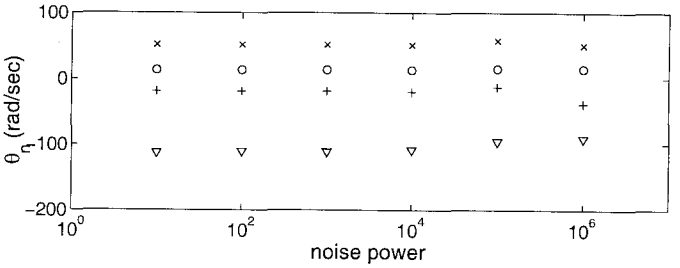

(b) Frequency shifts

Figure 4.6: Using method of pulsing for systems with additive noise (1^{st} mode: $\circ$, 2^{nd} mode: x, 3^{rd} mode: $+$, 4^{th} mode: ∇)

Noise	α_1	α_2	α_3	α_4
10^1	-50±1	-325±1	-584±2	-891±3
10^2	-50±1	-325±1	-585±2	-891±5
10^3	-50±1	-325±2	-585±4	-894±8
10^4	-49±2	-323±3	-584±10	-891±21
10^5	-47±6	-323±16	-592±35	-916±119
10^6	-42±17	-327±62	-544±65	-831±274
correct	-50	-325	-584	-889

Table 4.4: Additive noise results for α_i's with method of pulsing

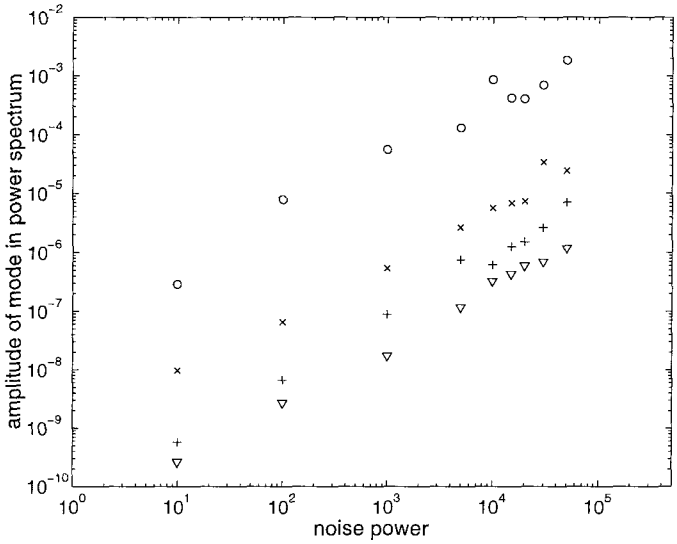

Figure 4.7: Peak amplitudes for all modes in the power spectral density vs. input noise power (1^{st} mode: $\circ$, 2^{nd} mode: x, 3^{rd} mode: $+$, 4^{th} mode: ∇)

4.2.3 Linear Motions with Multiplicative Noise

The numerical experiments are repeated for multiplicative noise. A certain amount of additive noise (noise power 10^4) is also added to excite the otherwise stable system.

There are two distinct kinds of multiplicative noise; in equation (4.13) they are denoted by ξ^v and ξ, causing respectively stochastic fluctuations of the damping and the frequency. Both kinds of source terms are analyzed separately. Figures 4.8 and 4.9, as well as tables 4.5 and 4.6, show the effect of random perturbations of the frequency shift on the identified decay rates of the individual modes using the two different methods. No apparent effect is noticeable – both the mean value and the uncertainty associated with it remain unaffected by the noise source. Comparing with the previous section, it can be seen that the observed scatter is only due to the presence of the additive noise.

At the same time the identification (mean and accuracy) of the modal frequencies (and thus

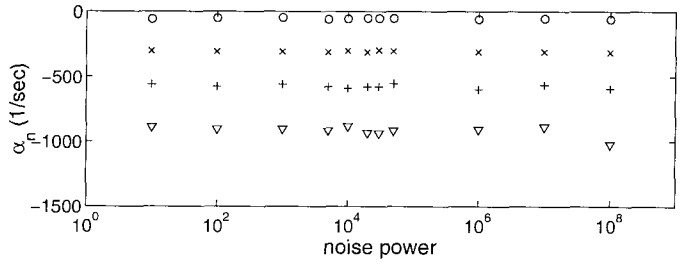

(a) Decay rates

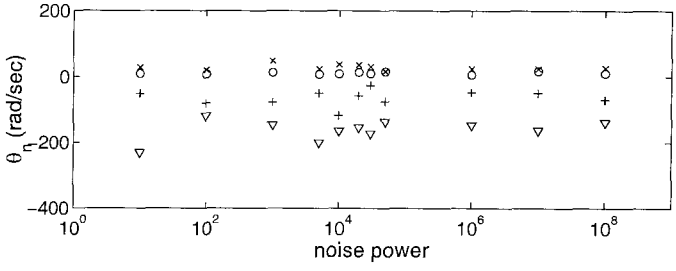

(b) Frequency shifts

Figure 4.8: Using Burg's method in the presence of multiplicative ξ–type noise (1^{st} mode: $\circ$, 2^{nd} mode: x, 3^{rd} mode: $+$, 4^{th} mode: ∇)

Noise	α_1	α_2	α_3	α_4
10^1	-57±14	-301±31	-560±84	-886±98
10^2	-51±13	-307±52	-576±75	-903±126
10^3	-47±11	-307±38	-558±78	-901±117
10^4	-56±16	-300±51	-591±88	-883±150
10^5	-59±18	-310±53	-598±95	-914±128
10^6	-53±15	-310±46	-564±84	-905±172
10^7	-59±19	-313±44	-591±83	-887±124
correct	-50	-325	-584	-889

Table 4.5: Multiplicative (ξ–type) noise results for α_i's with Burg's method

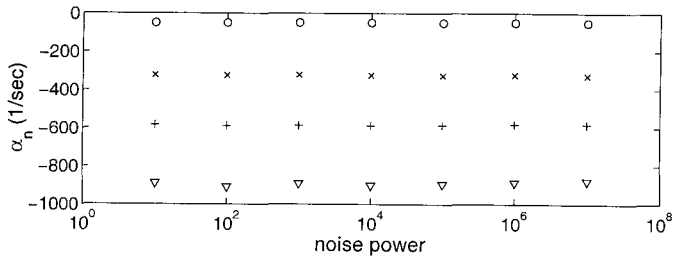

(a) Decay rates

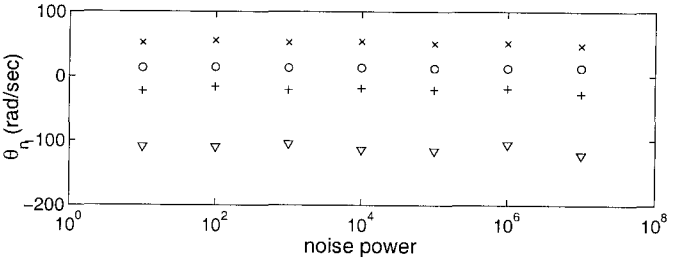

(b) Frequency shifts

Figure 4.9: Using the method of pulsing in the presence of multiplicative ξ–type noise (1^{st} mode: o, 2^{nd} mode: x, 3^{rd} mode: +, 4^{th} mode: ∇)

Noise	α_1	α_2	α_3	α_4
10^1	-50±2	-323±6	-584±9	-889±35
10^2	-50±2	-325±5	-589±8	-908±36
10^3	-50±2	-322±4	-587±10	-891±44
10^4	-50±3	-326±5	-589±8	-902±37
10^5	-49±3	-326±4	-586±12	-895±35
10^6	-50±2	-324±4	-582±15	-886±43
10^7	-49±3	-327±4	-583±11	-877±51
correct	-50	-325	-584	-889

Table 4.6: Multiplicative (ξ–type) noise results for α_i's with method of pulsing

of the frequency shifts) is independent of this sort of parametric noise. This is due to the fact that the length of the analyzed pressure trace is much longer than the fundamental period and therefore the frequency perturbations average out.

The influence of growth rate perturbations is displayed in figures 4.10 and 4.11 and tables 4.7 and 4.8. At low levels the system identification based on Burg's method gives the same results for mean detected growth rates, and their uncertainty, as for the other types of noise. As the noise level grows, however, a shift in the mean values occurs (and thus a wrong determination of the system parameters!), paired with a spreading uncertainty. Finally, as the noise power reaches a critical level, the linear system ID process breaks down.

This type of parametric noise also strongly affects the identification of the system parameters determined by measuring the decaying pulse in the chamber. It should be noted that even at the low noise levels where Burg's method delivered familiar results, the method of pulsing shows rather large standard deviations (25% for the first mode) of the detected parameters when compared with low levels of the other kinds of perturbations (where the error was of the order of 1%). With growing noise level both the shifts of the mean values (growing identification error) and increasing uncertainty are apparent before the identification process completely fails.

At this 'break-down point' the instantaneous growth rate of the first mode (the least stable one) has a finite probability of being positive thus changing the qualitative behavior of the system. As a result the system response undergoes a dramatic change: the pressure signal now exhibits 'spontaneous bursts'. This phenomenon is demonstrated in figure 4.12.

The development of this qualitative change can be seen in the power spectrum. Whereas for both additive noise (figure 4.7) and multiplicative ξ type noise (figure 4.13) the amplitude

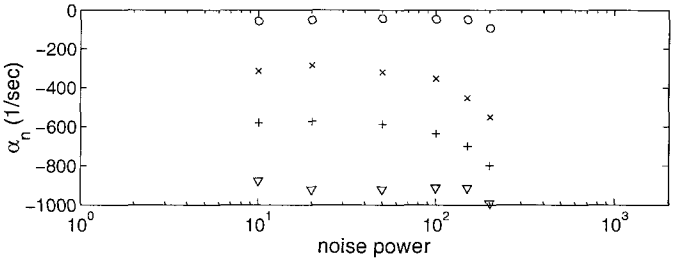

(a) Decay rates

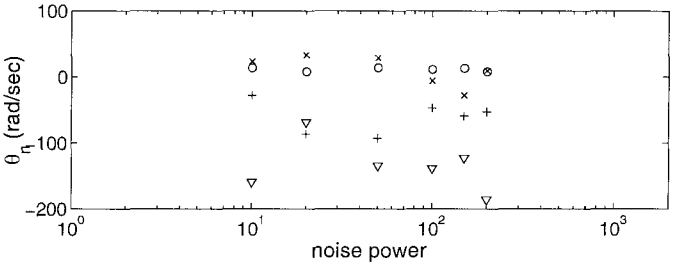

(b) Frequency shifts

Figure 4.10: Using Burg's method in the presence of multiplicative ξ^v–type noise (1^{st} mode: ∘, 2^{nd} mode: x, 3^{rd} mode: +, 4^{th} mode: ∇)

Noise	α_1	α_2	α_3	α_4
10	-56±17	-314±44	-580±81	-877±114
50	-42±11	-320±48	-588±112	-922±249
100	-46±20	-353±82	-636±96	-913±119
150	-48±15	-453±172	-701±146	-913±173
200	-92±170	-551±275	-799±216	-991±189
correct	-50	-325	-584	-889

Table 4.7: Multiplicative (ξ^v–type) noise results for α_i's with Burg's method

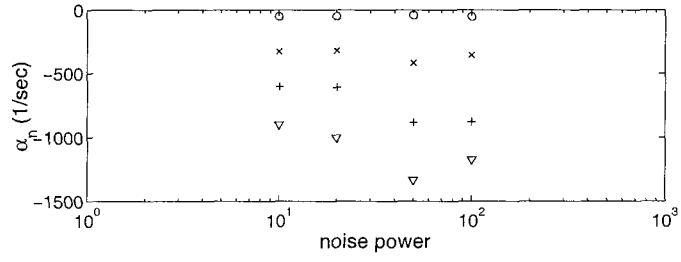

(a) Decay rates

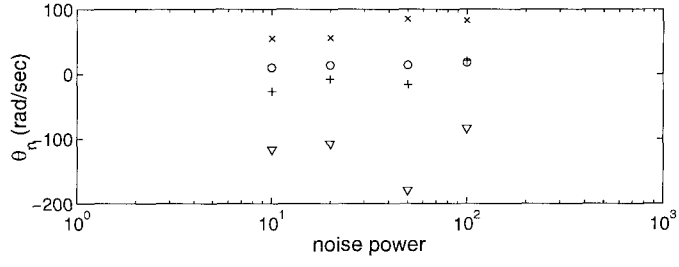

(b) Frequency shifts

Figure 4.11: Using the method of pulsing in the presence of multiplicative ξ^v–type noise (1^{st} mode: $\circ$, 2^{nd} mode: x, 3^{rd} mode: $+$, 4^{th} mode: ∇)

Noise	α_1	α_2	α_3	α_4
10	-51±13	-327±29	-601±41	-899±115
20	-49±12	-319±34	-607±67	-1001±347
50	-41±22	-416±274	-882±542	-1333±762
100	-52±45	-354±201	-878±502	-1171±636
correct	-50	-325	-584	-889

Table 4.8: Multiplicative (ξ^v–type) noise results for α_i's with method of pulsing

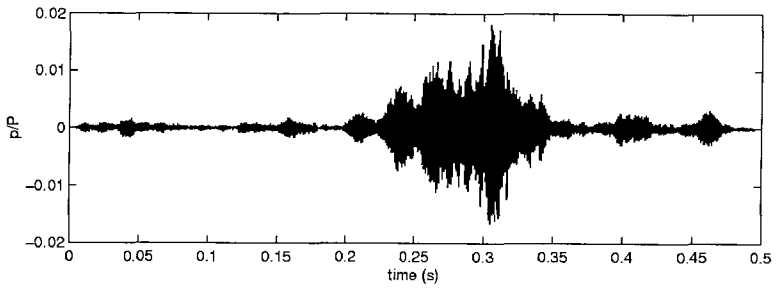

Figure 4.12: Pressure trace in the presence of multiplicative ξ^v– type noise (and the same amount of additive noise as in figure 4.2)

ratios for all the modes remain constant, this is not the case when growth rate perturbations are present. Figure 4.14 clearly shows that this kind of perturbations has its biggest affect on the first mode; its amplitude grows while the other modes remain at a constant level. Therefore, the modal composition of the system response changes with the noise level.

4.2.4 System ID Applied to Limit Cycles with Noise

Up to this point only purely linear systems have been considered. These systems were all stable (an unstable purely linear system is of course unrealistic). To simulate combustion instabilities, nonlinear systems are used, the linear part of which is unstable. The nonlinear terms introduced into the system produce limit cycles, i.e., pressure oscillations of a fixed amplitude. It can be shown (Paparizos and Culick 1989) that in the case of purely longitudinal acoustic modes the second order nonlinearities that need to be retained in equation (4.13) are given by the following terms:

$$\begin{aligned} \ddot{\eta}_n + \omega_n^2 \eta_n &= (2\alpha_n + \xi_n^v)\dot{\eta}_n + (2\theta_n\omega_n + \xi_n)\eta_n + \Xi_n \\ &\quad - \sum_{i=1}^{n-1} \left[C_{ni}^{(1)} \dot{\eta}_i \dot{\eta}_{n-i} + D_{ni}^{(1)} \eta_i \eta_{n-i} \right] \end{aligned}$$

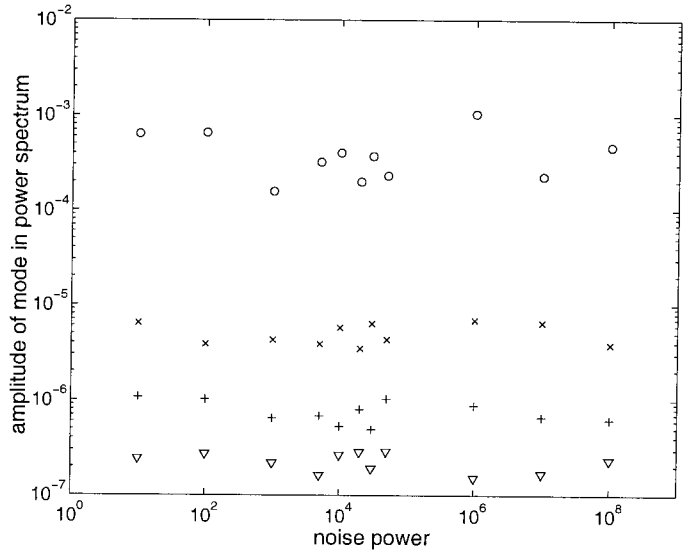

Figure 4.13: Peak amplitudes for all modes in the power spectral density with multiplicative ξ–type noise (1^{st} mode: $\circ$, 2^{nd} mode: x, 3^{rd} mode: $+$, 4^{th} mode: ∇)

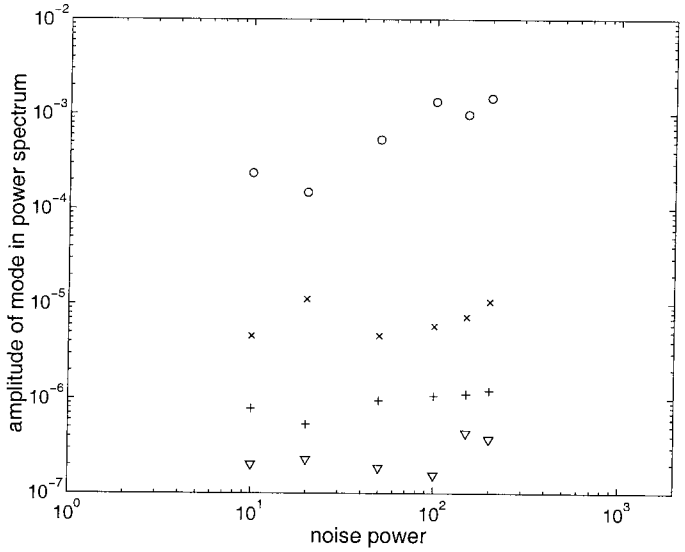

Figure 4.14: Peak amplitudes for all modes in the power spectral density with multiplicative ξ^v–type noise (1^{st} mode: $\circ$, 2^{nd} mode: x, 3^{rd} mode: $+$, 4^{th} mode: ∇)

$$-\sum_{i=1}^{N-n}\left[C_{ni}^{(2)}\dot{\eta}_i\dot{\eta}_{n+i}+D_{ni}^{(2)}\eta_i\eta_{n+i}\right] \tag{4.15}$$

For the calculations that follow the first mode is assumed to be unstable by putting α_1=50; all other values of α_n and θ_n are the same as in table 4.1; figure 4.15 shows a sample trace of an unstable system in the presence of all three kinds of noise sources. The power spectrum of the pressure signal together with a fit using Burg's method is shown in figure 4.16c.

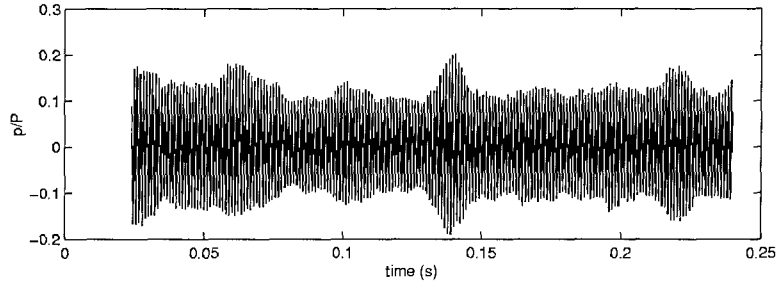

Figure 4.15: Pressure trace in the limit cycle of an unstable system (all three sources of noise are present)

Results obtained by applying the same methods as above have no apparent connection to the (known) parameters. The 'detected' parameters have all (both α_n and θ_n) values close to zero.

The reason for this is that in a limit cycle the average linear growth constants are indeed close to zero because the amplitudes converge towards limiting values from both below (growing) and above (decaying). Thus it is impossible to recover the original linear values since the limit cycle is a strictly nonlinear phenomenon. Since the modes combine to form a limit cycle for the pressure oscillation, the frequencies obviously need to become harmonics of each other which explains the identified frequency shifts. Figure 4.16a shows the pressure trace in the phase-plane and demonstrates that this is indeed a limit cycle.

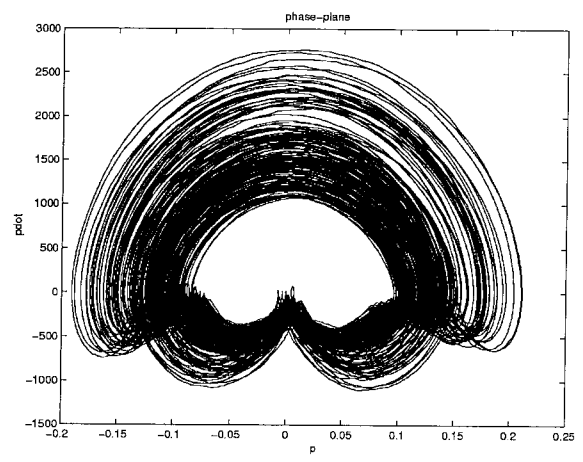

(a) Phase-plane plot of the pressure trace

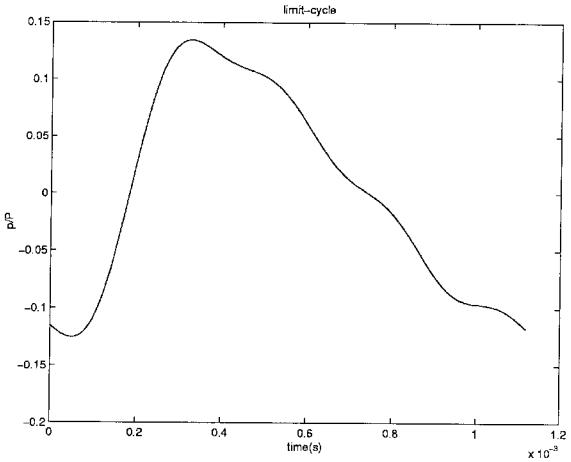

(b) One undisturbed period of the limit cycle

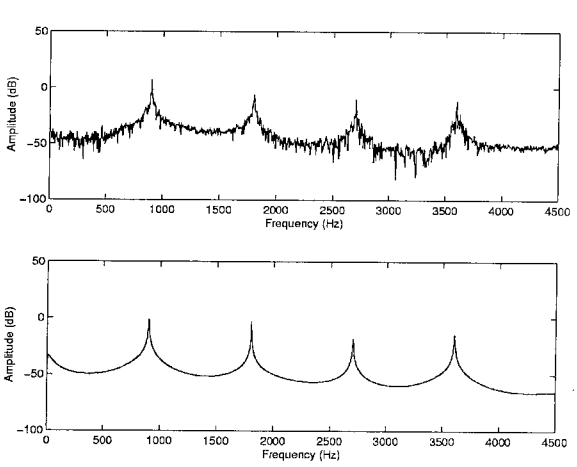

(c) Power spectrum of the system

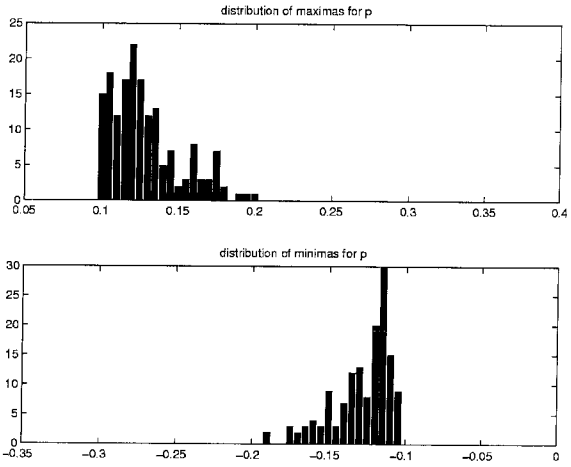

(d) Distribution of pressure maxima and minima

Figure 4.16: Characteristics of the limit cycle in figure 4.15

The limit cycle is a result of the nonlinear interaction between the different modes; linear concepts are therefore only useful when a few modes couple to form the limit cycle, while the other (stable) modes remain essentially uncoupled, obeying the equations of the linear regime. In such a case Burg's method does indeed allow the identification of the decay rate of those uncoupled modes.

Figure 4.16d shows the distribution of pressure maxima and minima in the limit cycle of the simulated pressure trace displayed in figure 4.15. Because these distributions are a direct consequence of presence of the stochastic terms (without random sources the distribution is a delta-function), current research focuses on possible methods of using them to obtain information about the system.

Analyzing these distributions is similar to applying higher order spectral methods to the pressure trace. Vasta and Roberts (1998) describe a method using fourth order spectral quantities to estimate unknown parameters in nonlinear, randomly excited dynamic systems. In a simulated application to a nonlinear oscillator with both nonlinear damping and stiffness and with a Gaussian noise excitation, the approach performs fine. We tried applying the same methods to the problem of combustion instabilities. Initial results showed that the presence of multiple modes made this approach numerically extremely expensive and the parameter estimates were not very accurate. A further disadvantage of the method is that it works only for additive noise; a different or modified analysis needs to be performed if multiplicative noise is present.

If the nonlinear system consists of only one mode, then the equations are linear in the parameters (α, θ) and the approach described by Lieuwen and Lee (2000) can be taken. In that method first and second derivatives of the pressure are estimated from the experimental

data and the values of the parameters are then fitted (by a standard least squares minimization) to the experimental data. As noted by Lieuwen and Lee (2000), this approach fails when other modes are present (even with very small amplitudes) and the method is not able to distinguish between linear and nonlinear effects that control the amplitude and the phase.

4.3 Additional remarks

It has been shown that pressure records, obtained numerically or experimentally, can be easily processed (e.g., by using MATLAB) to identify certain system parameters.

The stable system used in this study can be identified quite robustly by methods based on the power spectra; the method chosen here is the 'maximum entropy method' as proposed by Hessler. The internal noise sources provide sufficient driving to extract the relevant linear characteristics of the system. Burg's method is actually preferable to a method based on introducing a pulse and measuring the decay rates directly, especially in the presence of strong multiplicative noise because it is more robust. That is, it remains applicable to higher noise levels and the standard variation of the measured parameters is constant over a wide range of noise levels. This robustness, however, comes at the price of a higher 'uncertainty' at lower noise levels thus requiring multiple measurements to obtain reliable values of the system parameters. Whereas the standard deviation to be expected in the measurements done by fitting a decaying pulse varies with the strength of the stochastic noise terms (which remain unknown!), it is rather constant (but large, at about 25% for the first – most important – mode) in all cases when Burg's method is used. Thus results obtained from single measurements during motor firings cannot be expected to be very

accurate.

The results obtained for the particular system analyzed can be somewhat generalized by studying a few more cases. The parameters (growth rates and fundamental frequency) used, supposed to illustrate extreme cases, have been arbitrarily chosen. It has been shown above that by using Burg's method constant mean values and standard deviations are found over a wide range of noise levels. In table 4.9 those values are reported for the various systems examined; in these case studies the noise levels have been adapted (see above) such that the output of the systems covers the same range ($p'/\bar{p}$ between .005% and .5%).

actual system					identified parameters			
ω_1	α_1	α_2	α_3	α_4	α_1	α_2	α_3	α_4
900	-50	-325	-584	-889	-52±13	-305±46	-580±81	-880±141
900	-50	-50	-50	-50	-52±13	-51±12	-52±13	-53±13
900	-5	-325	-584	-889	-10±6	-305±46	-580±81	-880±141
900	-5	-50	-50	-50	-11±6	-52±14	-55±15	-54±13
50	-50	-325	-584	-889	-48±12	-122±24	-123±24	-125±25
50	-5	-50	-50	-50	-5±1	-48±5	-50±7	-51±8

Table 4.9: Results of parameter identification for various different systems

A general pattern seems to be evident from table 4.9: at high frequencies it is difficult to detect small decay rates whereas at low frequencies the fast decay rates are impossible to identify. The reason for the latter is easily seen: fast decay rates mean broad peaks in the power spectrum – at low frequencies consecutive modes are close enough together that those peaks overlap, making it impossible to detect their 'width'. In practice such a case

is easily detected by a quick glance at the power spectrum. In case of a high fundamental frequency a wide power spectrum (large frequency range) needs to be fitted; this explains a greater uncertainty in fitting the narrow peaks associated with small decay rates. From the results it is also apparent that it doesn't matter whether the α's are similar or vastly different in value.

These cases confirm that for realistic systems the system parameters *can* be detected by studying a noisy signal; however, the accuracy of the measurement may not be sufficient for practical purposes. The usefulness of the method cannot be determined without further study. Note that the Russian procedure cited at the beginning of this chapter was based on using certain statistical properties of pressure records and did not rely simply on the results of system identification.

The values of the decay rates obtained by any kind of identification process are net values; the values for the gain (growth of the oscillation) due to the combustion process or other sources cannot be inferred without identifying all the losses. Hence the values of the growth constants are particular to a given motor and probably have limited value; there is no apparent way of inferring general behavior of rules without extensive tests (motor size, configuration,...).

It has been shown that the stochastic sources will sustain small amplitude oscillations; however, they do not produce a qualitative change in the power spectrum of the signal in stable systems (with the exception of extraordinary large perturbations of the linear growth rate). There is no evidence that noise alone is capable of forcing true combustion instabilities.

The range of model noise levels used in this study allows identification of decaying pressure

pulses with relatively small errors. This corresponds to experience with motor firings. Thus the values chosen for 'noise power' seem to be realistic and there is no need to extend their range. These noise levels produce extremely small amplitudes of acoustic oscillations, in agreement with the conclusion reached by Strahle (1978). It must be concluded therefore that noise cannot be a basic mechanism for organized oscillations in the combustion chamber. Experimentally observed combustion instabilities thus must be viewed (and analyzed) as true self-excited motions.

For an unstable system none of the methods provides any useful information for growth/decay rates and frequency shifts, because the limit cycle is a purely nonlinear phenomenon: linear concepts such as growth constants therefore become meaningless. In this case a different strategy based on nonlinear concepts needs to be designed. That should be the subject of future research.

On the basis of our simulations reported here, we conclude that the form of system identification suggested by Hessler and his colleagues has limited value for practical purposes. We cannot state at this time whether or not further work in this direction will lead to useful practical methods. For example, some advantage might be taken of earlier Russian procedures developed for liquid propellant rockets. Because of the inability to perform repeated tests with a single motor, the problem treated here is quite different for solid propellant rockets.

Nevertheless, in the general context of understanding the dynamics of combustion systems, investigations of the behavior with stochastic sources form an integral part of the fundamental theory.

Chapter 5

Control with Noise

Even before the development of models including combustor dynamics and feedback control, experimental application of feedback control of combustion instabilities was successfully tested on small systems (mainly using loudspeakers as actuators). Those laboratory demonstrations report examples in which the amplitudes of limit cycles in linearly unstable combustors have been significantly reduced, sometimes even to vanishingly small values (Poinsot, Bourienne, Candel and Esposito 1987, Gulati and Mani 1992). In most cases, the 'practical' controller was a simple proportional feedback or a variation of a PID controller. One might wonder why that simple approach works or, conversely, ask why we need more sophisticated control methods. From a general viewpoint, experiments show that an unstable combustion chamber is a system exhibiting a linear instability (rapidly) growing to a limit cycle (defined by the non-linearities) that typically shows a marked predominant frequency. In terms of dynamical systems, the combustor is characterized by two unstable complex-conjugate poles and then a series of stable poles with relatively large damping. Provided that the combustor is observable and controllable, for this kind of system, a proportional feedback or a PID controller can be successfully tuned to obtain a stable feedback

loop (Franklin, Powell and Emami-Naeini 1995).

Regarding the issue of controllability (and observability) of the system, for the purpose of this argument, we will say that controllability has been proved in practice by the success of the experiments cited. A detailed analysis of this point would allow optimization of the position of actuators and sensors, but that is out of the scope of the present discussion. The need for more sophisticated control methods derives mainly from two aspects: first one might want to impose performance specifications on the controller, for example on the maximum control action, or on the noise or disturbance rejection. Second, combustion systems show a high degree of uncertainty and variability (Lieuwen and Zinn 2000), and a controller 'tuned' on a particular operating point does not guarantee a reliable performance. Third, we have shown in the previous chapter how stochastic sources are necessarily present in the system and that their presence prohibits an exact identification of system parameters. Modern control design methods allow for the introduction of this kind of consideration during the synthesis of the controller.

All the considerations above and the design method presented in the following section are based on a linear model of the combustor. On the other hand, the real system is manifestly nonlinear: the main indication of that is the fact that the pressure oscillations in the combustion chamber rapidly reach a limit cycle. A complete understanding of the dynamics of the combustor would allow tracing the source of the nonlinear behavior observed in the experiments (limit cycles, hysteresis (Isella et al. 1997, Lieuwen and Zinn 2000)) to its origin: nonlinear gasdynamics or nonlinear combustion. In that case nonlinearities in the system could be exploited by an 'ad hoc' form of (nonlinear) control to overcome the main limitations of linear control: requirement of a relatively high control effort and actuation

frequency at the same frequency of the instability. An example of this is given in chapter 3 where the hysteresis of the Rijke tube was exploited to augment the stability range of the system. However, since such a complete model is not available, we decided to limit the analysis to the linear case. Note that the linear part of the model of the combustion chamber presented in chapter 2 is actually a linearization of the full model around the operating point. Since the main purpose here is to keep the system 'stable', i.e., as close as possible to the linearized equilibrium point, the linear model and simulation is a valid and realistic approximation to the real case, provided that the nonlinearities do not give rise to a subcritical bifurcation (Wang 2000). Note that nonlinearities have the effect of limiting the amplitude of the oscillations: hence the linear model is in this sense a 'conservative' approach to the problem (for example, in terms of required control action, we will find an upper limit).

In short, within the present approach, nonlinearities can actually be neglected, except as a formal vehicle for rigorously introducing noise sources (see chapter 4). As a consequence, we will not be able to capture the effects of any instability mechanism different from the linear growth and phase shifting included in the model presented above. On the other hand, the present approach allows for a clear distinction of the effects of uncertainties, intrinsic noise sources, external noise sources, and unmodeled dynamics. The issue of time-delay, another interesting complication in control applications, is treated by Seywert, Isella and Culick (2000) and Isella (2001).

5.1 System Definition

As derived in chapter 2 the following system of equations describes the dynamics of the combustion chamber:

$$\begin{aligned} \ddot{\eta}_n + \omega_n^2 \eta_n &= -\sum_{l=1}^{\infty} [D_{nl}\dot{\eta}_l + E_{nl}\eta_l] \\ &\quad + \sum_{i=1}^{\infty} [\xi_{ni}^{\nu}(t)\dot{\eta}_i + \xi_{ni}(t)\eta_i] + \Xi_n(t) \end{aligned} \tag{5.1}$$

Here we have retained only the linear terms in the acoustic amplitudes (compare with (4.12)). Since we are going to design a controller to eliminate the pressure oscillations (i.e., drive all acoustic amplitudes to zero), this is equivalent to linearizing the nonlinear system around the unstable equilibrium point. Note that the linear terms include all linear processes, including linear combustion dynamics. The linear combustion part has in this formulation been lumped together with the linear gasdynamics into the coefficients E_{nl} and D_{nl}; in fact, it is the linear combustion that makes the system unstable to begin with. As noted by Wang (2000), this is a valid approximation as long as the system presents a supercritical bifurcation at the point of instability. Note also that while the higher order acoustic terms have been neglected, the nonlinear dynamics due to the vorticity and entropy waves are included in the noise terms ξ^{ν}, ξ, and Ξ. The combustor is linearly stable if and only if all modes are linearly stable.

For control applications it is advantageous to reformulate this set of equations in state-space form with state $x = [\eta_1 \dots \eta_\infty \dot{\eta}_1 \dots \dot{\eta}_\infty]^T$, control input u, and output $y = p'/\bar{p}$. The following definitions are needed:

$$A = \begin{bmatrix} 0 & 1 \\ -\Omega^2 - E_{nl} & -D_{nl} \end{bmatrix}$$

$$
\begin{aligned}
B &= \frac{\bar{a}^2}{\bar{p}} \begin{bmatrix} 0 \\ \\ \psi_n(x_{actuator})/E_n^2 \end{bmatrix} \\
C &= [\psi_1(x_{sensor}) \ldots \psi_N(x_{sensor})]
\end{aligned} \tag{5.2}
$$

With this notation, equation (5.1) – without the noise terms – becomes equivalent to

$$
\begin{aligned}
\dot{x} &= Ax + Bu \\
y &= Cx
\end{aligned} \tag{5.3}
$$

Chiefly because of the direct connection between the spatially averaged equations and the form (5.3) favored by the controls community, the procedure leading to equations (2.16) and (5.1) is used almost universally for current work in feedback control of combustor dynamics.

5.2 Robustness

The controller strategy proposed in this section is based on results described in Chou, Chen and Chao (1998) and Biswas (1998). It allows treating parametric uncertainties in the modeling and system identification process; multiplicative noise, in this case intrinsic to the system, arising from vorticity and entropy waves; and residual dynamics neglected in the control design in order to achieve a low order controller in a unified way.

5.2.1 Parameter Uncertainty

Consider the following system (Chou et al. 1998):

$$
\begin{aligned}
\dot{x}_c(t) &= [A_c + \Delta A_c(t)]x_c(t) + A_{cr}x_r(t) \\
&\quad +[B_c + \Delta B_c(t)]u(t) \\
\dot{x}_r(t) &= A_{rc}x_c(t) + A_r x_r(t) + B_r u(t)
\end{aligned}
$$

$$y = [C_c + \Delta C_c(t)]x_c + C_r x_r \tag{5.4}$$

In this description the system has been split into two parts: the controlled dynamics (state x_c) which will be used in the design of the controller and the residual dynamics (state x_r) which are neglected in that design. The reasoning behind this splitting is that we want to achieve a controller that is as simple as possible. This desire leads to a need for a low order model of the system; the controlled dynamics describe that low order system (which at the minimum needs to include all unstable modes) whereas the residual modes describe those parts of the original system that the designer chooses to disregard (the higher acoustic modes which are strongly attenuated in the combustion chamber). In principle this residual system is infinite dimensional since it stems from the pressure expansion (2.15) but as above we will truncate it to N modes.

The uncertain parameters of the controlled system are assumed to be bounded ($|\ |$ denotes the modulus matrix):

$$\begin{aligned} |\Delta A_c(t)| &\leq Q^{(A)} \\ |\Delta B_c(t)| &\leq Q^{(B)} \\ |\Delta C_c(t)| &\leq Q^{(C)} \end{aligned} \tag{5.5}$$

$Q^{(A)}$, $Q^{(B)}$ and $Q^{(C)}$ are nonnegative constant matrices that describe the highly structured uncertainty of the parameters.

Now consider a controller based on a Kalman filter (used to reconstruct the state from the measured output, i.e., the pressure signal from the sensor) with estimator gain L and feedback gain K:

$$\dot{\hat{x}}_c(t) = A_c\hat{x}_c(t) + B_c u(t) + L[y(t) - C_c\hat{x}_x(t)]$$

$$u(t) = -K\hat{x}_c(t) \tag{5.6}$$

Then the controlled nominal closed-loop system is described by H_c and its interaction with the residual system is governed by H_{cr} and H_{rc} (note that H_{cr} and H_{rc} have been changed to allow for the presence of A_{cr} and A_{rc} when compared to Chou et al. (1998)).

$$\begin{aligned} H_c &= \begin{bmatrix} A_c - B_cK & -B_cK \\ 0 & A_c - LC_c \end{bmatrix} \\ H_{cr} &= \begin{bmatrix} A_{cr} \\ LC_r - A_{cr} \end{bmatrix} \\ H_{rc} &= [A_{rc} - B_rK \quad -B_rK] \end{aligned} \tag{5.7}$$

In this work we just quote the theorem proven by Chou et al. (1998). The proof is rather elaborate and uses several lemmas from controls theory; the reader is referred to the cited reference for details. To state the final result, which relates the closed-loop stability of the system to the uncertainties in the nominal parameters, we first need to give a few definitions. Define the matrices G_c and G_r as follows:

$$\begin{aligned} G_r &\geq [\sup |g_{ik}^{(r)}(j\omega)|] \\ G_c &= [\sup |g_{ik}^{(c)}(j\omega)|] \end{aligned} \tag{5.8}$$

Where $\omega > 0$ and $g_{ik}^{(r)}$ and $g_{ik}^{(c)}$ are the ikth elements of $(j\omega I - A_r)^{-1}$, respectively $(j\omega I - H_c)^{-1}$. Also define the uncertainty matrix U as

$$U = \begin{bmatrix} Q^{(A)} + Q^{(B)}|K| & Q^{(B)}|K| \\ Q^{(A)} + Q^{(A)}|K| + |L|Q^{(C)} & Q^{(B)}|K| \end{bmatrix} \tag{5.9}$$

According to Chou et al. (1998) (with the trivial extension to include A_{cr} and A_{rc}), the closed-loop system will be stable if the matrices H_c and A_r are stable matrices and the

following inequality

$$\rho[\, G_c U \;+\; G_c\, |H_{cr}|\, G_r\, |H_{rc}|\,] < 1 \tag{5.10}$$

is satisfied (here $\rho[\,]$ denotes the spectral radius).

5.2.2 Multiplicative Noise

Now consider the system below (Biswas 1998):

$$\begin{aligned} \dot{x}(t) &= [A + \xi^{(A)}(t)]x(t) + [B + \xi^{(B)}(t)]u(t) \\ y &= [C_c + \xi^{(C)}(t)]x \end{aligned} \tag{5.11}$$

Here $\xi^{(A)}$, $\xi^{(B)}$, and $\xi^{(C)}$ are random time functions. Lacking precise information about their nature (as in many practical applications and consistent with the assumptions in chapter 4), they are assumed to be described by Gaussian white noise processes with zero mean and can be characterized through the quantities $\Xi^{(AA)}$, $\Xi^{(BB)}$, $\Xi^{(AB)}$, and $\Xi^{(CC)}$ where ($E[\,]$ denotes the expected value)

$$\begin{aligned} \Xi_{ij}^{(AA)} &= \sum_{k=1}^{N} E[\xi_{ki}^{(A)}(t)\xi_{kj}^{(A)}(t)] \quad 1 \le i,j \le n \\ \Xi_{ij}^{(BB)} &= \sum_{k=1}^{N} E[\xi_{ki}^{(B)}(t)\xi_{kj}^{(B)}(t)] \quad 1 \le i,j \le N_u \\ \Xi_{ij}^{(AB)} &= \sum_{k=1}^{N} E[\xi_{ki}^{(A)}(t)\xi_{kj}^{(B)}(t)] \quad \begin{matrix} 1 \le i \le N \\ 1 \le j \le N_u \end{matrix} \\ \Xi_{ij}^{(CC)} &= \sum_{k=1}^{N} E[\xi_{ki}^{(C)}(t)\xi_{kj}^{(C)}(t)] \quad 1 \le i,j \le N_y \end{aligned} \tag{5.12}$$

As before a controller with estimator gain L and feedback gain K is considered.

Following the approach taken by Biswas (1998), we consider the process $\{V(t), t \ge 0\}$ defined by

$$V(t) = \frac{1}{2}||x(t)|| + \frac{1}{2}||\hat{x}(t) - x(t)|| \tag{5.13}$$

Using Ito's lemma (Øksendal 1998) we can write down an expression for dV which we can then integrate over $(0,t)$ and take the expectation. We get (see Biswas (1998) for further details):

$$E[V(t)] = E[V(0)] + \int_0^t \left([x\ \hat{x} - x], H[x\ \hat{x} - x]^T \right) d\theta \tag{5.14}$$

Here H is the expected closed-loop matrix and is defined as

$$H = \begin{bmatrix} H_{11} & H_{12} \\ H_{21} & H_{22} \end{bmatrix} \tag{5.15}$$

$$\begin{aligned} \text{where } H_{11} = {} & A + BK + \Xi^{(AA)} + \Xi^{(AB)}K \\ & + (\Xi^{(AB)}K)^T + K^T\Xi^{(BB)}K \\ & + L^T\Xi^{(CC)}L \\ H_{12} = {} & BK + \Xi^{(AB)}K + K^T\Xi^{(BB)}K \\ H_{21} = {} & (\Xi^{(AB)}K)^T + K^T\Xi^{(BB)}K \\ H_{22} = {} & A - LC + K^T\Xi^{(BB)}K \end{aligned}$$

Now, choose K and L so that

$$(\zeta, H\zeta) \leq -\gamma||\zeta||^2, \mathrm{Re}(\gamma)) > 0 \tag{5.16}$$

Then we have

$$E[V(t)] \leq E[V(0)]e^{-2\gamma t} \tag{5.17}$$

Therefore, we conclude that the closed-loop system is exponentially mean square stable if there exist K and L such that the matrix H is negative definite.

5.2.3 Controller Design

We can combine both approaches (i.e., account for bounded parameter uncertainty and random Gaussian noise perturbations) by including the Ξ-terms in equation (5.15) in the uncertainty of the closed-loop matrix H_c in equation (5.8). Thus by redefining the uncertainty matrix U,

$$U = \begin{bmatrix} U_{11} & U_{12} \\ U_{21} & U_{22} \end{bmatrix} \tag{5.18}$$

$$\begin{aligned}
\text{where } U_{11} = {} & Q^{(A)} + Q^{(B)}|K| + \Xi^{(AA)} + \Xi^{(AB)}|K| \\
& + (\Xi^{(AB)}|K|)^T + |K|^T\Xi^{(BB)}|K| \\
& + |L|^T\Xi^{(CC)}|L| \\
U_{12} = {} & Q^{(B)}|K| + \Xi^{(AB)}|K| + |K|^T\Xi^{(BB)}|K| \\
U_{21} = {} & Q^{(A)} + Q^{(A)}|K| + |L|Q^{(C)} \\
& + (\Xi^{(AB)}|K|)^T + |K|^T\Xi^{(BB)}|K| \\
U_{22} = {} & Q^{(B)}|K| + |K|^T\Xi^{(BB)}|K|
\end{aligned}$$

and fulfilling equation (5.10), robust stability can still be guaranteed.

Up to this point we have derived conditions that L and K need to fulfill without specifying how to design them. Note that the controller is to be designed for the nominal, undisturbed plant; we can then check equation (5.10) to make sure it is also effective on the perturbed system - or we can use that equation to see how much noise or parameter variation our controller can handle.

The design of the controller depends of course on the performance we wish to achieve. Any method can be used: Biswas (1998) uses a pole-placement technique, and here we follow Chou et al. (1998) in using a standard LQG method.

LQG is advantageous because it allows for the inclusion of additive system noise ($\xi^{(x)}$) as well as sensor noise ($\xi^{(y)}$). Thus the complete system we try to control is given by:

$$\begin{aligned}
\dot{x}_c(t) &= [A_c + \Delta A_c(t) + \xi^{(A)}(t)]x_c(t) + A_{cr}x_r(t) \\
&\quad + [B_c + \Delta B_c(t) + \xi^{(B)}(t)]u(t) + \xi^{(x)} \\
\dot{x}_r(t) &= A_{rc}x_c(t) + A_r x_r(t) + B_r u(t) \\
y &= [C_c + \Delta C_c(t) + \xi^{(C)}(t)]x_c + C_r x_r + \xi^{(y)}
\end{aligned} \tag{5.19}$$

In using this method we minimize the performance index J given by

$$J = \int_0^\infty \left[x_c^T(t)Qx_c(t) + \rho_c u^T(t)Ru(t)\right] dt \tag{5.20}$$

In this case ρ_c is the design parameter that will be changed to fulfill condition (5.10). Since we want to reduce the pressure oscillations at a specific location x_p, it is natural to choose Q such that $x_c^T Q x_c$ represents our best estimate of p' at this point

$$Q = \bar{p}^2 \cdot \begin{bmatrix} \psi_1^2(x_p) & 0 & 0 \\ 0 & \ddots & 0 \\ 0 & 0 & \psi_N^2(x_p) \end{bmatrix} \quad \text{and} \quad R = 1 \tag{5.21}$$

5.3 Numerical Example

In the following we will briefly demonstrate the described design procedures on a particular example. The example has been chosen solely because it has been used previously in the literature (Haddad, Leonessa, Corrado and Kapila 1997, Culick and Yang 1992, Yang, Sinha and Fung 1992). The methods used are obviously much more general and can be applied to any linearized (combustion) system – as mentioned previously, *all* processes, including combustion, have been linearized and are embedded in the model parameters.

The numerical example used is the same one as given in Haddad et al. (1997). The combustion chamber is assumed to be cylindrical of length L and only longitudinal modes are considered. The chamber is closed on the upstream end and has a nozzle at the downstream end which acts as an acoustically closed boundary. The sensor detecting the instability is a microphone located at x_s whereas the actuator used to control the pressure oscillations is a loudspeaker located at x_a. The internal dynamics of the loudspeaker are modeled as a second order system and included in the state-space formulation, i.e., they form an integral part of A_c in equation (5.19) through augmentation of the state x_c. In this way the actuator dynamics are accounted for in the design of the controller. In this example the actuator (and sensor) are treated as perfectly known systems; within the framework described here it is straightforward to include uncertainties or noise in those systems too. Note that the model of the actuator as a 'loudspeaker', a second order system with a high gain, is actually more general than it seems. If we wanted to represent an injector, the same model would still apply, with a longer time delay, and some difference in the numerical value of the parameters, but substantially the same structure, i.e., second order dynamics and very high gain (Neumeier, Nabi, Arbel, Vertzberger and Zinn 1997, Isella 2001).

The linearized model of the combustion chamber is characterized through the parameters E_{nl} and D_{nl} which are given (after non-dimensionalization of time by $\frac{\pi L}{\bar{a}}$) in table 5.1 for the first 4 longitudinal modes – the parameters are originally taken from Yang et al. (1992) and are typical for solid propellant rockets. In this design study we only consider uncertainty in the parameters E_{nl} and D_{nl} and noise in those terms given in equation (5.1). In other words there is no noise or uncertainty in the sensing or actuation process and the stochastic sources act (as described by the model) as random perturbations of E_{nl} and D_{nl}. Thus we

D_{nl}	$n=1$	$n=2$	$n=3$	$n=4$
$l=1$	-.01	.007	-.001	.007
$l=2$	.01	.1	.007	-.001
$l=3$	-.01	.01	.75	.008
$l=4$	.02	-.005	.01	1.5

E_{nl}	$n=1$	$n=2$	$n=3$	$n=4$
$l=1$	-.005	-.005	.0025	.0016
$l=2$	-.0025	-.015	.01	.01
$l=3$	-.005	.0	-.02	.02
$l=4$	.01	.02	.02	-.025

Table 5.1: Combustion chamber parameters

put (keeping the notation of the previous section)

$$Q^{(B)} = 0 \quad Q^{(C)} = 0$$
$$\Xi^{(AB)} = 0 \quad \Xi^{(BB)} = 0 \quad \Xi^{(CC)} = 0 \tag{5.22}$$

Furthermore we assume that all stochastic sources (due to the vorticity and entropy modes in the chamber) are uncorrelated and have the same variance σ^2. Finally we assume that the parameter uncertainties can all be described by a single variable ϵ. These assumptions are only made to simplify the expressions as we can now write:

$$\begin{aligned} Q^{(A)} &= \epsilon \cdot \begin{bmatrix} 0 & 0 \\ |E_{nl}| & |D_{nl}| \end{bmatrix} \\ \Xi^{(AA)} &= N \cdot \sigma^2 \cdot 1 \end{aligned} \tag{5.23}$$

A controller was designed using an LQG technique by taking only 1 mode (the unstable first mode) into consideration. It is assumed that the complete system is given by 4 modes and thus the remaining 3 modes are considered to give the residual dynamics. Basing the controller on a minimal set of modes is desired as it reduces the order of the controller and thus allows for easier implementation.

Figure 5.1 shows the response of the reduced and complete system to the controller (turned

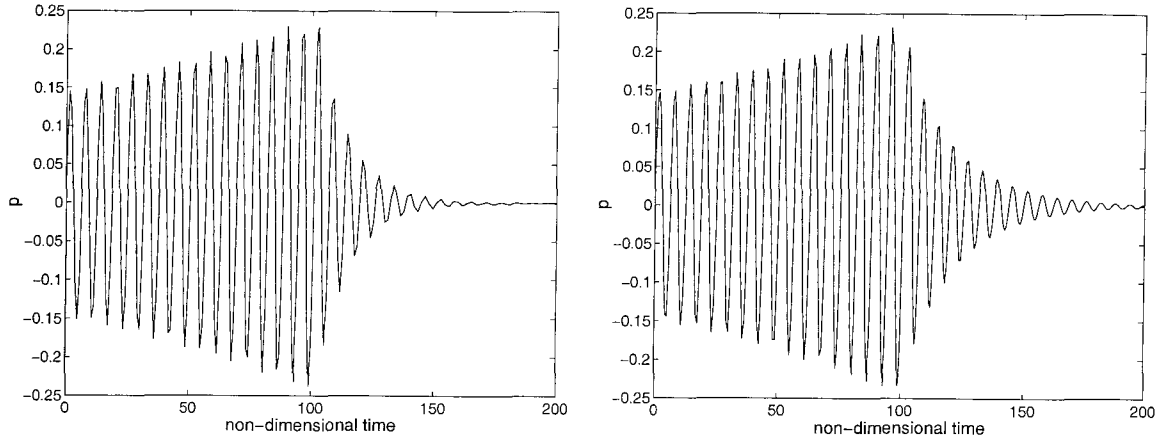

(a) Nominal system (only 1 mode)

(b) Complete system (all 4 modes)

Figure 5.1: System response to controller action

on at $\tilde{t} = 100$). As expected the presence of the extra modes (not considered in the design) in the full system reduces the performance of the controller (slower decay).

Figure 5.2 shows the guaranteed stability limits (in terms of ϵ and σ) of the controller. The solid line is the limit predicted by equation (5.10) for the truncated system where only 1 mode is used in the simulation. In other words: this is the stability limit in terms of ϵ and σ that we obtain if we consider the controlled system (based on which the controller was designed) only, ignoring any effects of the residual modes. The other lines describe the stability region as more modes are added in the simulation, i.e., as the system approaches the 'complete' system. We see that the stability region shrinks as additional modes are introduced into the simulation while the same controller (based on 1 mode) is retained. Since in the example given here we assume that the complete dynamics are described by 4 modes, stability for the 'complete' system with this controller is guaranteed only in the dark shaded region in the lower left corner of the plot. In this extreme case (where we considered only one mode to base the controller on) the area changes are drastic, but as

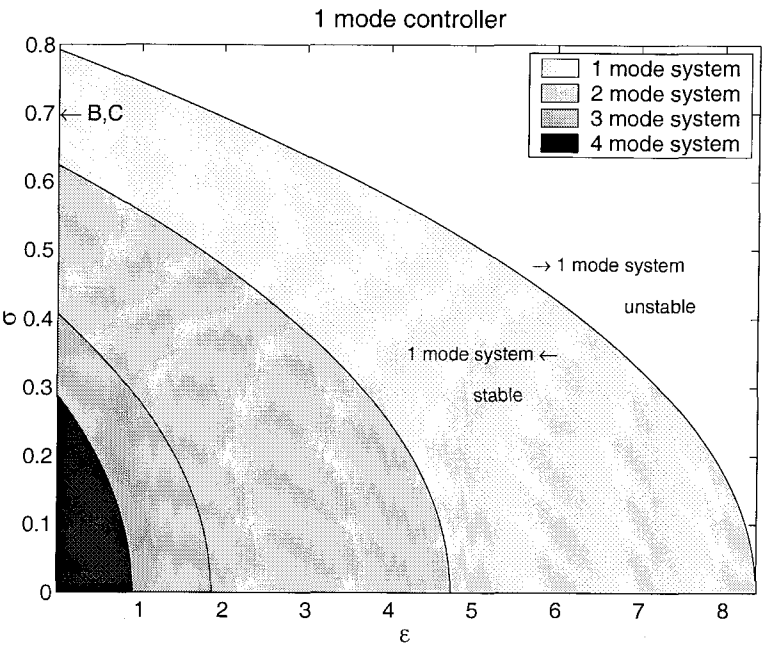

Figure 5.2: Guaranteed stability limits for closed-loop system in $\sigma - \epsilon$ plane (noise variance and uncertainty) depending on number of residual modes considered

the neglected modes become more heavily damped their influence grows smaller (as can be seen by the lines moving closer together). If more modes were to be added, the stability limits would converge to form the final region (in the $\sigma - \epsilon$ plane) in which the low-order controller is still guaranteed to be effective.

Similar plots are shown in figure 5.3. Just as in figure 5.2 only the first mode of the system is controlled. The left plot assumes that there are no uncertainties in the parameters (i.e. $\epsilon = 0$) and shows the guaranteed stability limits in terms of the two different multiplicative noises σ ($\sigma^2 = E(\xi\xi)$) and σ^ν ($(\sigma^\nu)^2 = E(\xi^\nu\xi^\nu)$) – refer to equation (5.1) and note that ξ and ξ^ν are one-dimensional in this example. The second plot (figure 5.3b) assumes that no noise sources are present ($\sigma = 0$) and investigates the stability limits in terms of the uncertainty in the parameters E_{ni} and D_{ni}. Again, since we consider only 1 mode for the

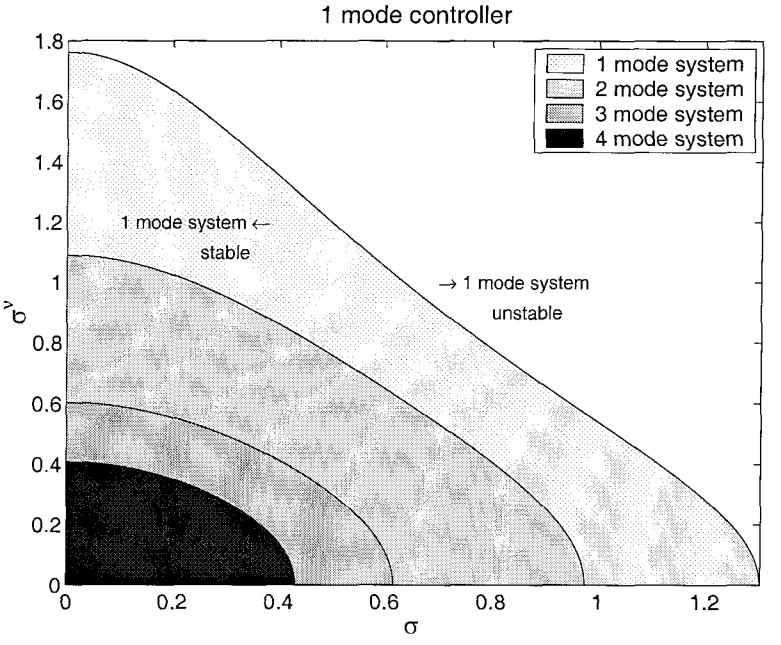

(a) Only multiplicative noise

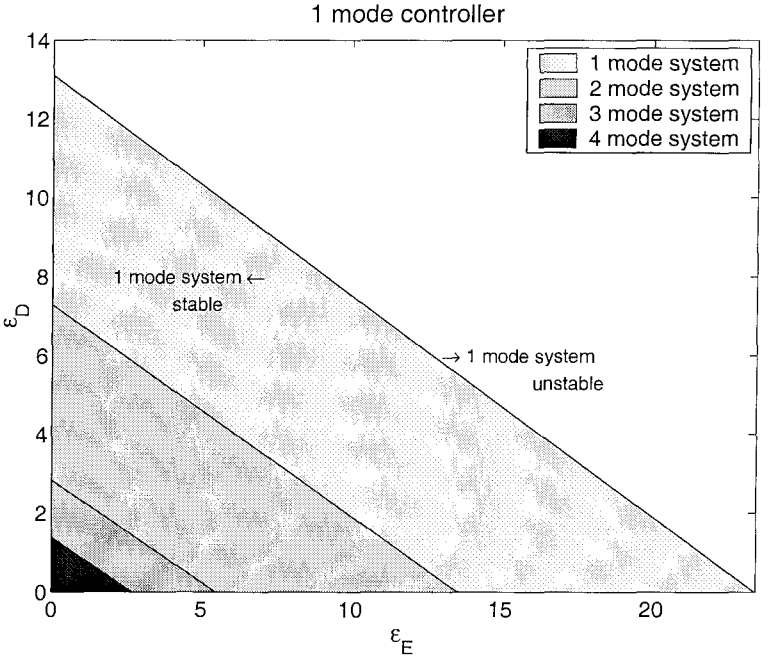

(b) Only parameter uncertainty

Figure 5.3: Guaranteed stability limits for closed-loop system when either $\epsilon = 0$ or $\sigma = 0$, depending on number of residual modes considered

controlled system, this uncertainty is entirely described by two values: ϵ_E (for E_{ni}) and ϵ_D (for D_{ni}). As in figure 5.2 the guaranteed stability region in both instances shrinks when more and more of the ignored dynamics are taken into account.

Figure 5.4 illustrates the effect the (stable) residual system can have in the presence of noise. The same controller (based only on the unstable first mode) is used in all three cases. In case A (low noise) the controller is able to stabilize the full system (all 4 modes included in the simulation); however, at a higher noise level (case B) the pressure oscillations do not decay to zero. Note that this noise level is well within the stability limits as predicted with the truncated (1 mode) system and thus underlines the importance of the neglected dynamics. If the simulation is performed with the reduced system, the instability does indeed decay as anticipated (case C).

5.4 Summary

We have shown how uncertainties, noise, unmodeled dynamics and time-delay can be included in the controller design for combustion instabilities.

A clear distinction has been made between the uncertainty and the noise. This is necessary as the parameter uncertainty can be bounded; e.g., in practical applications we might know that in the operating range of interest the various parameters are located within certain numerical bands. In contrast, true noise sources can in general not be bounded, and thus do not fit in the common control frameworks; they are characterized by their mean values, which we include in the system parameters and by their variation.

Explicit consideration of the neglected modes allows studying their influence on the controller robustness. This is especially important since in most experimental implementations

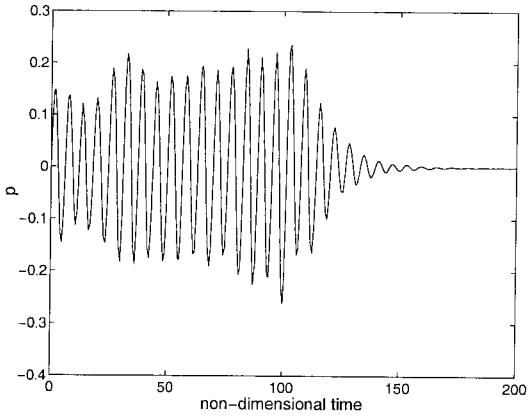

(a) case A (complete system)

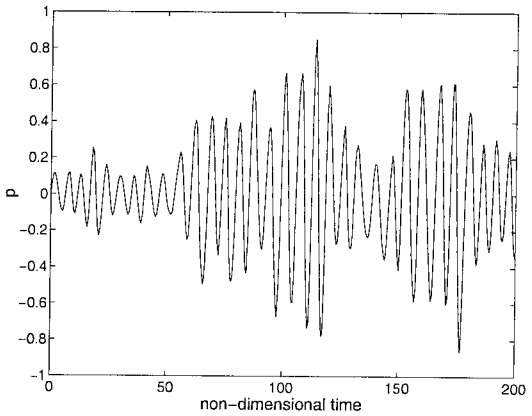

(b) case B (complete system)

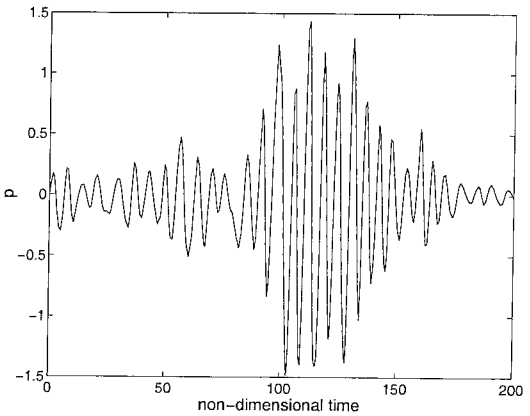

(c) case C (reduced system)

Figure 5.4: Time simulations of various cases as defined in figure 5.2

to date the controller has been designed by taking only the unstable mode(s) into account. In the example given here only the first mode is unstable and it is in fact possible to stabilize the system by solely controlling this one mode. Note that the controller is designed to accommodate large uncertainties (or noise) since we anticipate that the residual modes will affect the dominant first mode. This is the way unmodeled dynamics are traditionally handled: by including them in the uncertainties of the system. The framework presented here shows how much of that uncertainty can be attributed to the neglected modes. In the example given, the damping of the ignored modes (notably the second one) is rather small and thus we see that the actual parameter uncertainty ϵ (or noise intensity σ) that the controller can tolerate declines dramatically as additional modes are considered. Therefore, we conclude that the residual dynamics dominate the uncertainty unless the neglected modes are highly damped.

Future work in this area should include testing of the concepts on an experimental combustor; and system identification to define better models of real actuators, in particular injectors and fuel flow modulators. More analysis is also needed to characterize (and eventually take advantage of) nonlinearities naturally present in combustion chambers. That these nonlinearities can indeed be successfully exploited to achieve control has been demonstrated in chapter 3.3.2.

Chapter 6

Concluding Remarks

In this work we have attempted to discuss several issues that arise in the context of control of combustion instabilities.

The general analytical framework most commonly used in the literature was explained and compared to a different approach developed at Georgia Tech. We have pointed out that any results obtained with low-order models need to be carefully evaluated within the limits of the underlying assumptions and simplifications. The difficulties arise due to the spatial averaging and subsequent truncation of the modal expansion. Therefore, we suggest to simplify the system of partial differential equations as much as possible, eliminating all dependent variables, before applying any Galerkin-type projections to finally arrive at ordinary differential equations. It is equally important to carefully define the order in the small quantities to which the expansions (and thus the system of ODE's) is valid. In the case of combustion instabilities there are two independent parameters which determine the order of validity: the magnitude μ of the mean flow which characterizes the strength of the combustion and the magnitude ϵ of the velocity fluctuations in the combustion chamber which measures the importance of the instability.

This analytical framework has been applied to a Rijke tube. The formulation presented here is particularly attractive since the coefficients of the differential equations are expressed in terms of transfer functions of the heat source. Thus we can easily introduce various heat sources (flames, heaters, ...) as long as we know how they react to incoming pressure or velocity waves. Conversely we can study the influence of changes in those transfer functions on the overall dynamical behavior of the Rijke tube system.

We have shown that transfer functions found in the literature can account for the sudden appearance of large amplitude pressure oscillations. This phenomenon is also observed in experiments. However, we were not able to explain the experimental fact of a hysteresis with our model. The most likely reason for this is that while the model includes nonlinear gasdynamics, the description of the heat source by means of transfer functions is purely linear. Thus any nonlinear effects (e.g., the amplitude of the limit cycle) are either purely gasdynamical or result from the interaction of the heat source with the flow field. Furthermore, we have only retained terms up to the second order in the fluctuating quantities and higher order terms might introduce additional dynamical behavior. Another explanation for the observed hysteresis could be the simple fact that some of the underlying model parameters change once the system becomes unstable and only return to their initial value after the system has returned to its original state.

Even though the nonlinear behavior is currently not completely understood, we have demonstrated how we can take advantage of certain nonlinear features (e.g., hysteresis) in designing a control law that expands the stability region of the system. Further studies in this direction could quantify the savings (in term of control effort) that the exploitation of the nonlinear features can achieve. An obvious advantage of the control strategy presented

here for the Rijke burner (the same strategy has also been successfully implemented on a dumb combustor (Isella et al. 1997)) is the fact that the control action can take place at frequencies much lower than the frequency of the underlying instability - this facilitates the implementation of active control schemes in industrial systems where high frequency actuators seem impractical.

We did analyze some of the nonlinearities by introducing 'noise' into the system. We showed how the presence of vorticity waves leads necessarily to the appearance of three distinct disturbance fields. Therefore, we included multiplicative as well as additive noise into our simulations. We also argued that those three terms capture all possible first order effects of any disturbance attacking the system. We have shown the quantitative and qualitative differences in the pressure oscillations that result from the presence of these stochastic sources. We conclude that if a sufficient level of true internal noise is present (i.e., if it is not drowned by measurement noise from the instruments used to record the pressure trace) then linear stability margins can be inferred with reasonable accuracy from the results of single experimental runs. This could conceivably even be done online thus detecting changes in the stability characteristics during operation of the system. This monitoring could provide an early warning as to when the operating limits are reached and preventive actions (additional fuel injection, increase of damping, ...) could be taken to stop the pressure oscillations from growing to critical levels. While these margins are an important quantity to know, single runs do not give any information about the nonlinear stability of the system ('triggering').

Combining all of the above we realize that any control law that wants to have a chance of being able to suppress pressure oscillations needs to be robust to internal disturbances as

well as changes in the parameter values. Furthermore, only low-order control laws are viable in industrial applications and thus the system needs to be truncated (simplified) before the controller is designed. We have derived an analytical expression that guarantees the linear stability of the closed-loop system given all of those problems.

Directions of Future Work

As mentioned before a thorough understanding of the nonlinear behavior of various combustion systems might lead to a more efficient and better design of control algorithms.

In order to get this understanding experiments and analytical models giving the response of different heat sources to incoming pressure and velocity waves would be necessary. By different heat sources we mean laminar flames, wrinkled flamelets and turbulent flames, since those appear in the industrial applications.

A physically based model, as opposed to white noise, of the stochastic sources (vorticity waves, entropy waves, and others) would also be of considerable interest. This could lead to a better understanding of the pressure amplitude distributions which would help in predicting occurrences of triggering and in identifying system parameters through analyzing the recorded pressure traces.

Appendix A

Bifurcations

We provide here a short introduction, by no means complete, to bifurcations and limit-cycles, intended primarily to explain various terms used in this work. The reader is referred to the literature (Strogatz 1996, Wiggins 1996) for further details.

Simple Example

As an example to illustrate the various types of bifurcations that we encounter in the context of our studies of combustion instabilities, we consider a two-dimensional system in polar coordinates (r, ϕ) with uncoupled radial and angular dynamics. For simplicity we also assume that $\dot{\phi} = 1$, providing a constant angular speed. For a particular choice of radial potential, the radial dynamics of this simple example are described by:

$$\dot{r} = \alpha r - \beta r^3 - r^5 \tag{A.1}$$

A limit-cycle is defined as an isolated closed trajectory in the state-space (in this example a circle in the $r - \phi$ plane), meaning that neighboring trajectories either spiral towards or away from the limit cycle. If all neighboring trajectories approach the limit cycle, it is stable

(attracting); otherwise it is unstable (repelling) or semi-stable (this case is exceptional and we don't consider it here).

Supercritical Hopf Bifurcation

We put $\beta = 1$ in equation (A.1) and let α be the free parameter (α is the linear growth rate in this example). Figure A.1 plots equation (A.1) in the phase plane for two different

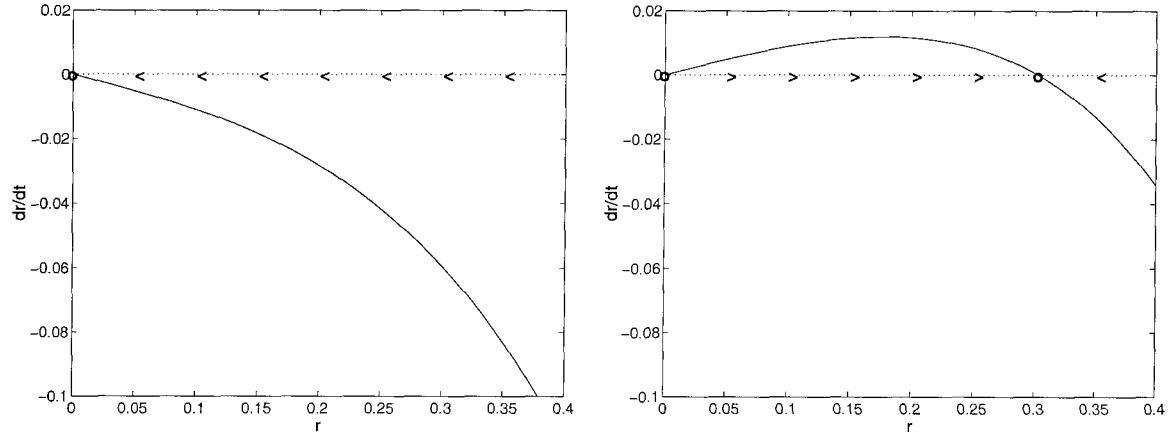

(a) $\alpha = -.1$

(b) $\alpha = .1$

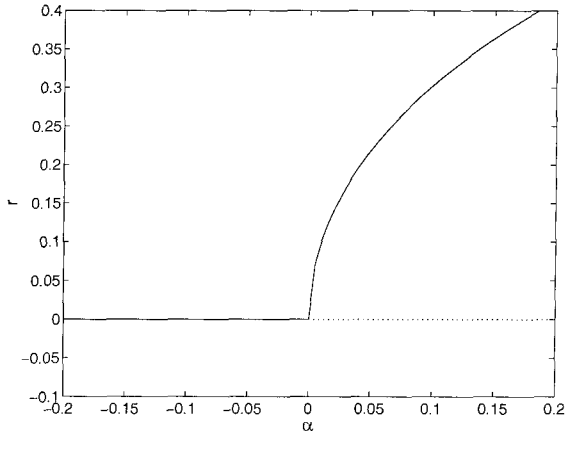

(c) r vs. α

Figure A.1: Supercritical Hopf bifurcation

α's and shows the solution to $\dot{r} = 0$ as a function of α (stable solutions are plotted with a solid line and unstable solutions are represented by a dotted line).

Note the qualitative change that happens as α crosses 0. If $\alpha < 0$, the origin ($r = 0$) is stable, i.e., if the system starts out at any value of r it will spiral towards the origin (as indicated by the arrows in the figure). However, with $\alpha > 0$, the origin becomes unstable and r tends toward a finite value, producing a limit cycle. The limit cycle appears and starts to grow as the origin changes stability; such a behavior is characteristic for a supercritical Hopf bifurcation.

Subcritical Hopf Bifurcation

Now we change β to -1 in equation (A.1). Figure A.2 plots the modified equation (A.1) in the phase plane as α crosses 0.

As before, the origin loses its stability as α changes from negative to positive. But contrary to the behavior found above, even while the origin is stable there exist two other solutions to $\dot{r} = 0$, giving rise to a stable and an unstable limit cycle. We ignore the stable limit cycle for the moment. As α approaches 0 from below the unstable limit-cycle gets continuously smaller, shrinking the region of attraction of the origin (all trajectories that will eventually converge towards the origin). Finally, when the origin becomes unstable, the unstable limit cycle disappears completely. Such a behavior, where an unstable limit cycle closes in on the origin is called a subcritical Hopf bifurcation.

Note that whereas a small disturbance would collapse back to the origin for $\alpha = -\epsilon$, it will jump towards the finite amplitude limit cycle for $\alpha = \epsilon$. This limit cycle is peculiar to this example and need not be present for a subcritical Hopf bifurcation to occur (i.e., the trajectories could grow without bound). But obviously if, as in our case, r is to represent

the amplitude of the pressure oscillation, such an unrestrained growth is unrealistic.

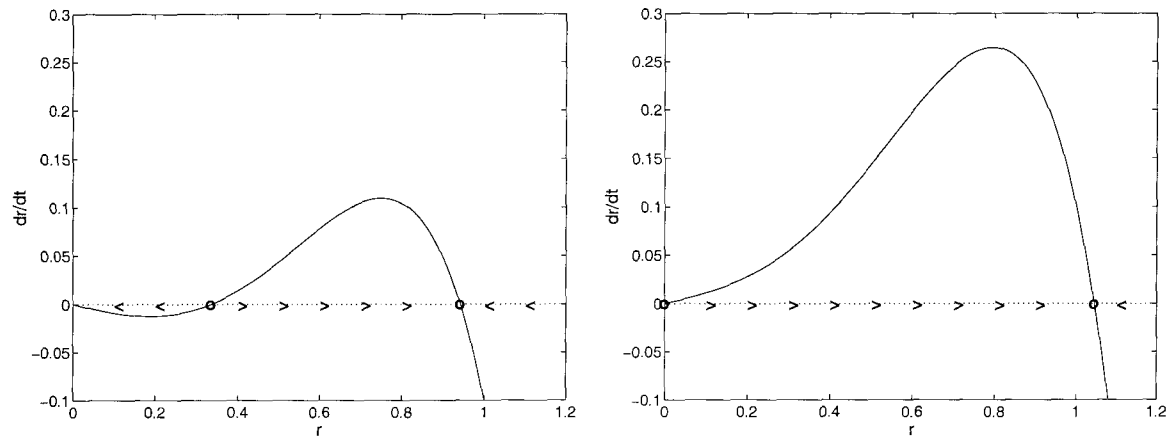

(a) $\alpha = -.1$ (b) $\alpha = .1$

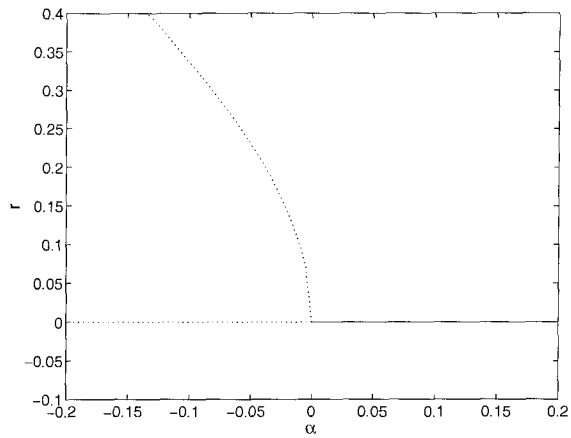

(c) r vs. α

Figure A.2: Subcritical Hopf bifurcation

Nevertheless, if a subcritical Hopf bifurcation is present, a 'catastrophic' event occurs as the parameter crosses the stability limit: suddenly a large amplitude oscillation arises (or the motion of the system blows up). For this reason a system featuring dynamics corresponding to a subcritical bifurcation is hard to predict and control: small changes in the operating

condition can lead to a very different behavior of the system.

Saddle-Node Bifurcation

With $\beta = -1$ another type of bifurcation occurs at $\alpha = .25$. It is responsible for the two limit cycles mentioned above. This type of bifurcation where 'out of nowhere' limit cycles appear is called a saddle-node bifurcation. Figure A.3 illustrates this behavior.

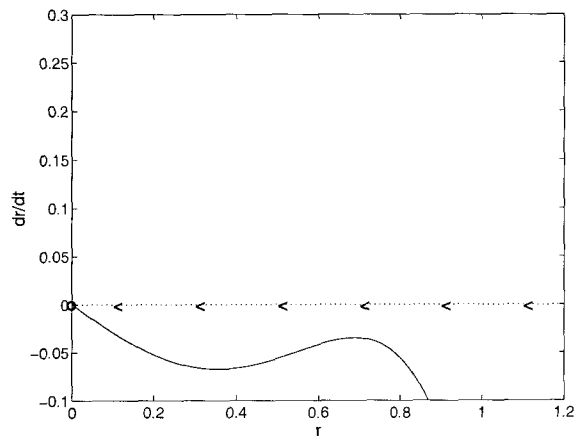

(a) $\alpha = -.3$

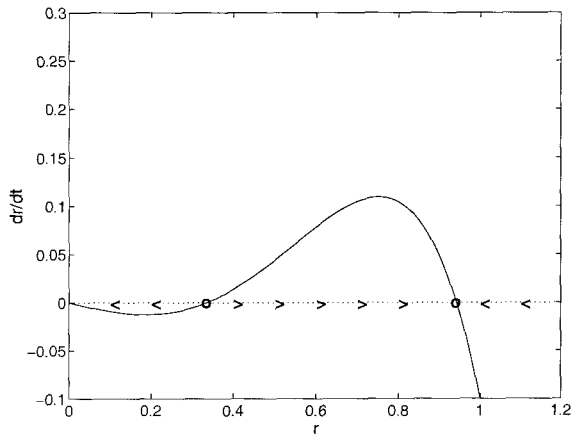

(b) $\alpha = -.1$

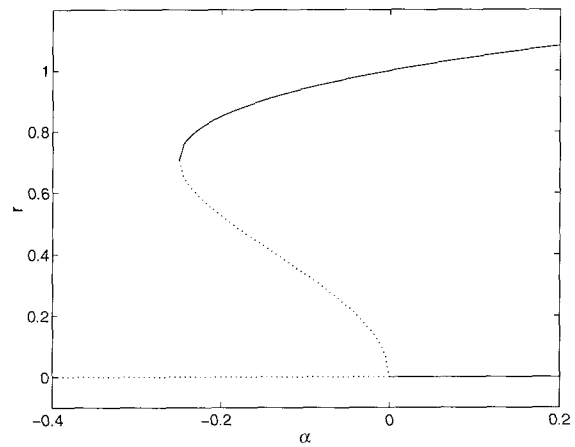

(c) r vs. α

Figure A.3: Saddle-node bifurcation

In the study of combustion instabilities such a saddle-node bifurcation always appears in conjunction with a subcritical Hopf bifurcation; together both explain the phenomena of 'triggering' and hysteresis. Triggering occurs if, after the saddle-node bifurcation, a disturbance is larger then the unstable limit cycle and thus continues to grow towards the finite amplitude limit cycle (refer to figure A.2a); note that disturbances smaller than the amplitude of the unstable limit cycle just decay towards the origin. Hysteresis occurs because while the origin loses its stability at $\alpha = 0$ and large amplitude oscillations arise at that value, we cannot simply turn off those oscillations by bringing $\alpha < 0$ – instead we need to decrease α to its value at the saddle-node bifurcation before the oscillations disappear.

More Modes

The restriction to essentially one dimension in the previous example (all dynamics are in r) gives the wrong impression that higher powers of r (e.g., up to 5^{th} power) are needed to explain triggering. In combustion instabilities several modes participate in the dynamics, which are described by coupled differential equations. The following example of two coupled equations demonstrates that complicated dynamics do not require these high powers.

As before we consider the system in polar coordinates; assume that radial and angular dynamics are uncoupled; and put $\dot{\phi}_1 = const$ and $\dot{\phi}_2 = const$. Thus we have two modes oscillating at a constant frequency and their amplitudes r_1 and r_2 are governed by the following system of equations:

$$\begin{cases} \dot{r_1} = \alpha_1 r_1 + r_1^2 - r_1 r_2 - r_2^2 \\ \dot{r_2} = -r_2 - r_2^2 + r_1 r_2 + r_1^2 \end{cases} \tag{A.2}$$

α_1, the linear growth rate of the first oscillator, is the parameter in this example. The second oscillator is linearly stable ($\alpha_2 = -1$). The amplitudes r_1 and r_2 are plotted as a

function of α_1 in figure A.4 - showing a subcritical Hopf bifurcation and the possibility for triggering.

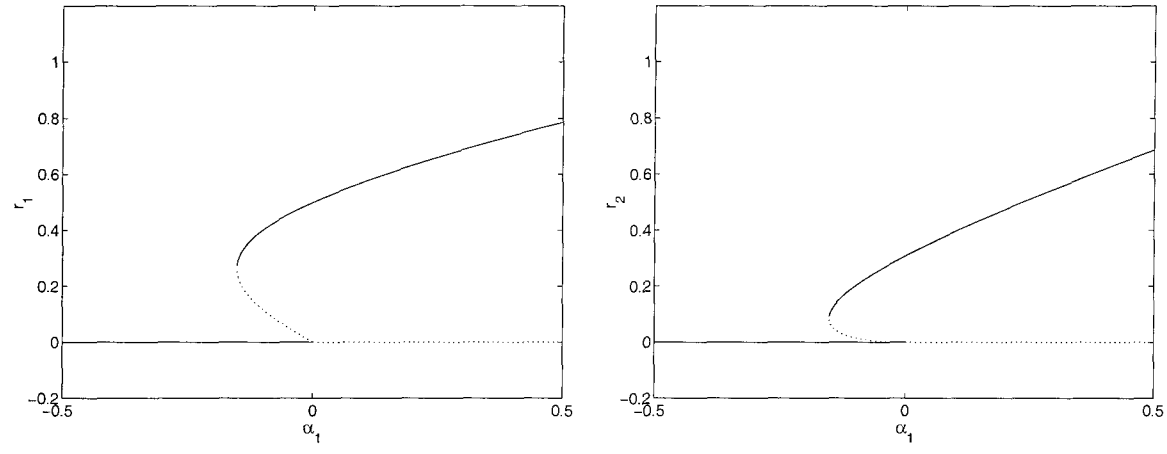

(a) r_1 vs. α_1 (b) r_2 vs. α_2

Figure A.4: Bifurcation diagram for 2 modes example

The complete equations describing combustion instabilities are obviously more complicated (see chapter 2 for details) and their possible dynamical behavior is the subject of current research. Ananthkrishnan (2000a) and Ananthkrishnan (2000b) gives an interesting discussion of the qualitative dynamics of longitudinal acoustic modes in a uniform cylindrical combustion chamber.

Appendix B

Burg's Method

Burg's method is one of many used in Digital Signal Processing to estimate power spectrums and thus can be found in most textbooks (Haddad and Parsons 1991). The method is rather elaborate and only a few brief remarks are given here.

Burg's method has the advantage of yielding a high frequency resolution, being always stable and computationally efficient. The method is associated with 'maximum entropy spectrum estimation'. This is based on extrapolating a known segment of autocorrelation values $r_{xx}(0)$, $r_{xx}(1)$, ..., $r_{xx}(p)$ of a sequence $x(n)$ to indices for which the autocorrelation values are not known. Once the complete autocorrelation function is known, the power spectrum $S(f)$ can be computed by

$$S(f) = \frac{1}{2W} \sum_{n=-\infty}^{+\infty} r_{xx}(n)\, e^{-i2\pi fnT} \tag{B.1}$$

Here W is one half the sampling frequency and $T = 1/f_s$ is the spacing between samples. Given the first values of the sequence r_{xx} there is an infinite number of possible extrapolations that will yield a valid power spectrum. The maximum entropy method enforces the condition that no new information is added to the underlying sequence, i.e., the fewest

possible assumptions about the signal outside the available data are made. This is done by maximizing the 'entropy'.

Entropy is a measure of uncertainty about any set of events. The entropy $H(x)$ of a continuous random variable with probability density function $f(x)$ is defined in information theory as

$$H(x) = -\int_{-\infty}^{+\infty} f(x)\ \log f(x)\ dx \tag{B.2}$$

Between the power spectrum $S(f)$ and the average entropy per sample point the following relation can be demonstrated:

$$H(x) = \ln\sqrt{2\pi e} + \frac{1}{4W}\int_{-W}^{W} \ln S(f)\, df \tag{B.3}$$

Maximizing the entropy under the constraint that $S(f)$ gives the known autocorrelations yields the solution:

$$S(f) = \frac{P}{\left|1 + \sum_{k=1}^{p} a_k e^{-i2\pi fk}\right|^2} \tag{B.4}$$

To evaluate the parameters Burg's method makes use of the similarity of the equations satisfied by the a_k and those for linear predictors. This parallel leads to the constraint that the parameters satisfy the Levinson-Durbin recursion, which can be solved very efficiently. This similarity also shows that the maximum entropy method models the signal as the output of an autoregressive process.

Once the a_k's are known, frequencies and decay rates of the various modes are obtained by looking at the imaginary and real part of the roots of $1 + \sum a_k z^k$.

A critical part of the method is the determination of the order p. This order is not known a priori - a low order will not give enough frequency information whereas too big an order might lead to 'line splitting' making identification of the modes impossible. We have chosen

to follow Hessler's (Hessler and Glick 1998) recommendation stating that to identify N modes an approximate order of $4N + 1$ should be chosen. Our experience shows that this order works fine as long as the sampling frequency of the signal is not too high compared with the highest mode.

Since Burg's method is one of the standard methods in Digital Signal Processing, it is included in most commercially available software packages. In this work we have made use of the Signal Processing Toolbox, an extension of MATLAB.

Appendix C

Review of Work on Dynamics and Control of Combustion Instabilities at the Massachusetts Institute of Technology

At the Jet Propulsion Center we have made an effort to review the work of other research groups on the subject of control of combustion instabilities. The report on the research done at the Massachusetts Institute of Technology is included here in this appendix. Other reviews in this ongoing effort describe the work at Cambridge University, included in (Poncia 1998), and at the Georgia Institute of Technology, included in (Isella 2001).

C.1 Introduction

In 1995 a group at MIT started a concerted effort in the subject of controlling combustion instabilities. The investigations by the group led by A.M. Annaswamy and A.F. Ghoniem have resulted in a number of publications that are reviewed in this document (as far as they are available).

While their activity started by developing a kinematic model for a laminar premixed flame, the main interest of the MIT group is the application of modern control techniques to combustion instabilities.

The approach taken by the MIT group is outlined in their first publication (Annaswamy and Ghoniem 1995). It discusses the general needs and requirements for active control and presents a survey of the field before going on to describe their model and some attempts at control (see below).

Since all the publications follow the same structure (description of the model including the flame response followed by control application example) and are quite repetitive, the various papers are broken up in this summary and the outline given by Annaswamy and Ghoniem (1995) is closely followed.

C.2 The Model Equations

C.2.1 Acoustic Model

The model of combustion instabilities in the MIT study is based on the 'classical' approach of deriving a wave equation for the pressure perturbation that is then expanded into the acoustic mode shapes of the combustor ($p' = \bar{p}\sum_{i=1}^{N}\eta_i(t)\psi_i(x)$). The longitudinal acoustic modes are assumed to be the dominant ones and thus the whole modeling is done in one dimension only. This leads to a second order differential equation for each mode retained:

$$\ddot{\eta}_i + \omega_i^2\eta_i + \sum_{j=1}^{N} d_{ij}\dot{\eta}_i = b_i\dot{Q}' + b_{Mi}Q' \tag{C.1}$$

In this equation the terms involving the coefficients b_{Mi}, c_{Mi}, and d_{ij} result from the presence of the mean flow and a mean heat release in the chamber. The earlier MIT publications neglect the mean flow (effectively putting these coefficients to 0). Starting with Annaswamy, El Rifai, Fleifil, Hathout and Ghoniem (1998) these effects are properly accounted for.

The right-hand side of equation (C.1) requires a model for the heat release Q'. As we will

see below, the proposed model makes use of the perturbed velocity at the flame u'_f. Using the linearized momentum equation we get (where the coefficients c_{Mi} are again due to the mean flow):

$$u'_f = \sum_{i=1}^{N} (c_i \dot{\eta}_i + c_{Mi} \eta_i) \tag{C.2}$$

C.2.2 Heat Release / Flame Response

The combustion process in the chamber is modeled by a laminar premixed flame. The model (used in all of their work) is developed by Fleifil, Annaswamy, Ghoneim and Ghoniem (1996). A simple expression for the fluctuating heat release due to flow oscillations in the chamber is derived.

The following assumptions are made:

- The flame is modeled as a thin axisymmetric interface (cylindrical combustion chamber) that separates the reactants from the products.
- The flame propagates at constant speed, the laminar flame speed S_u, in the direction normal to its surface.
- Neglect expansion and vorticity generation across the flame.
- The flame is insensitive to pressure perturbations.

A further approximation about the curvature of the flame is made but Fleifil et al. (1996) show that while this approximation simplifies the equations substantially it has a negligible effect on the final expression for the heat release fluctuation (see equation (C.4) below). With those assumptions the 'G-equation' (used previously by various other authors in the combustion literature) describing the flame surface is valid. G is a scalar function that

changes sign at the flame front and its evolution is governed by:

$$\frac{\partial G}{\partial t} + \vec{u} \cdot \nabla G - S_u |\nabla G| = 0 \tag{C.3}$$

This equation is linearized and, assuming a velocity perturbation that's harmonic in time, can be directly integrated using the Laplace transform to obtain an expression for the instantaneous flame surface area. Assuming furthermore that the total heat release rate Q is directly proportional to this area (which implies that ρ is constant), the result can be formulated in the familiar (n-τ) model: $Q'(t) = nu'_f(t - \tau)$. Both interaction index n and time delay τ are functions of the 'flame Stroudhal number' $G = \omega R/S_u$ (R is the radius of the chamber); see figure C.1. It should be noticed that τ is independent of the amplitude u_1 of the velocity perturbation.

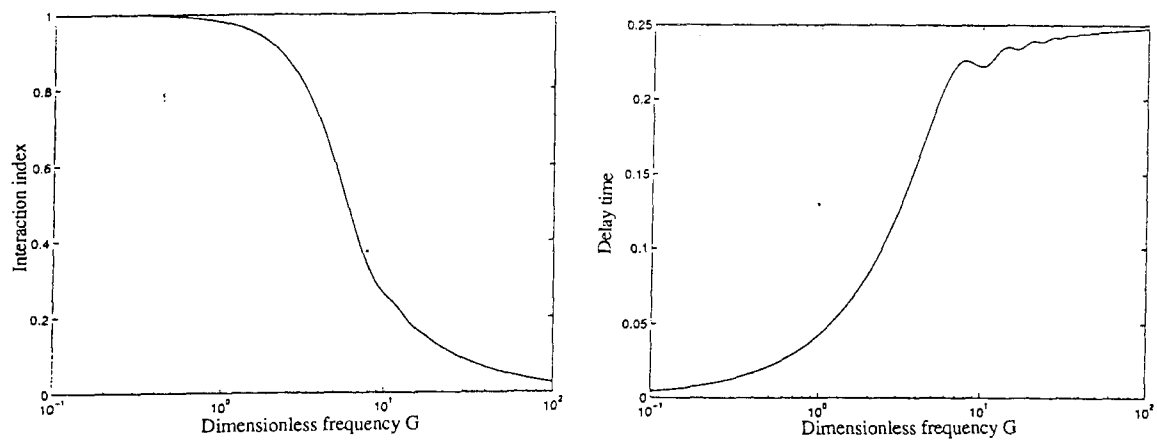

Figure C.1: Flame model in n-τ framework

The calculations were done for two different cases: one assuming a uniform velocity perturbation along the radius of the duct, the second (corresponding to the figure) assuming a perturbed pipe flow profile. The results are very similar which leads to the conclusion that the acoustic velocity field can be approximated for practical purposes by a uniform perturbation.

The (n-τ) description can be readily converted in a transfer function framework by writing $Q' = H(j\omega)u'_f$. The H derived through the intermediate step with n and τ can be nicely approximated by a first order model (see figure C.2). Thus the following differential equation can be used to relate the unsteady heat release rate to the velocity perturbation:

$$\frac{dQ'}{dt} + \beta_1 Q' = \beta_2 u'_f \tag{C.4}$$

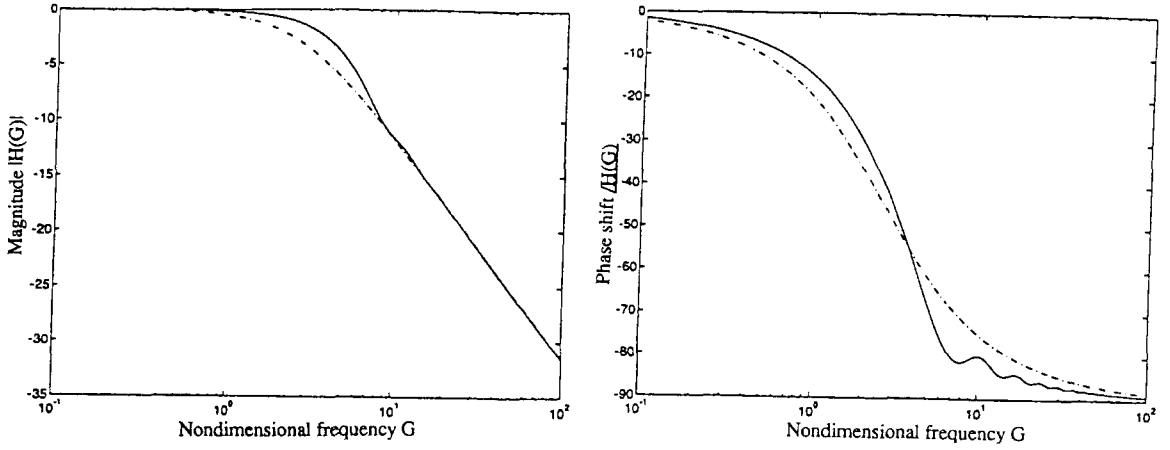

Figure C.2: Flame model in transfer-function framework

In (Annaswamy, Fleifil, Hathout and Ghoniem 1997) equation (C.4) is obtained analytically and a better expression for the coefficients β_1 and β_2 (relating them to the flame parameters) is derived by recognizing that the effect of high frequencies on the flame dynamics is negligible and thus u' can be taken to vary slowly with time.

The differential relation (C.4) is at the heart of the MIT model and distinguishes it from other works in combustion control. It is obviously only an approximation but it seems to do a good job as it leads to instabilities in the correct modes when compared to experiments. It is however only a linear model and as such cannot explain the limit-cycles observed in the experiments (since it is combined with a linear model of the acoustics of the chamber).

An attempt to correct this deficiency is done by Rumsey, Fleifil, Annaswamy, Hathout and Ghoniem (1998a) where the equation C.4 is modified to

$$\frac{dQ'}{dt} + \beta_1 Q' = \beta_2 f(u'_f) \tag{C.5}$$

The non-linear function f is introduced *ad hoc* into (C.5). Rumsey et al. (1998a) identifies two mechanisms that lead to limit-cycle behavior: a change of phase between u' and Q' or a change in gain between those two quantities.

Three different variations of f are analyzed (the phase change is associated with the sign change of f; the first example does present a small gain change too; however, Rumsey et al. (1998a) argue that the phase change is the dominant mechanism here):

- phase change: $f(u) = c_1 u - c_2 u^3$ or $f(u) = \begin{cases} k_1 u & : \quad |u| \leq u_0 \\ (k_1 + k_2)u_0 - k_2 u & : \quad u < u_o \end{cases}$
- gain change: $f(u) = \begin{cases} u & : \quad |u| \leq u_0 \\ u_0 & : \quad u < u_o \end{cases}$
- gain and phase change: $f(u) = \frac{u(t-\tau)}{1+\epsilon|u(t-\tau)|}$

Physical explanations for the three variations are given as follows:

- The phase change could be due to the fact that at small velocity amplitudes the heat release is dominated by propagation whereas at higher velocity levels the heat release is dominated by convection (no further details on this are given by Rumsey et al. (1998a)).
- The gain change could be due to a 'saturation' effect in the heat release.
- The third functional form arises if the nonlinearity is attributed to the mixing effects at the injection nozzle and the time-delay to convection.

The linear model is further refined by Fleifil, Hathout, Annaswamy and Ghoniem (2000). In that paper equation (C.4) is once again verified using a more detailed analysis. In particular the implicit assumption that the density ρ is constant is removed and a dependence of the heat release on the equivalence ratio ϕ is introduced. The following form replacing (C.4) is obtained:

$$\frac{dQ'}{dt} + \omega_f Q' = A_d \frac{\bar{\beta}}{\bar{\alpha}} \bar{u} \left[\frac{u'}{\bar{u}} + \frac{\rho'}{\bar{\rho}} + \mu \frac{\phi'}{\bar{\phi}} + \Lambda_\phi \frac{\dot{\phi}'}{\bar{\omega}_f \bar{\phi}} + \Lambda_u \frac{\dot{u}'}{\bar{\omega}_f \bar{u}} \right] \tag{C.6}$$

C.2.3 Coupling / Stability

The combustor dynamics are described by equations (C.1), (C.2) and (C.4) which together describe the coupling between the chamber acoustics and the flame dynamics.

It should be noted that the heat release model introduces a linear coupling between the modes, even in the case without mean flow. The formal appearance of the coupling terms arrives through the introduction of the velocity perturbation at the flame, equation (C.2) into the heat release expression on the right-hand side of equation (C.1). This coupling is thoroughly discussed by Annaswamy et al. (1997) and Hathout et al. (1998).

From the equations given above the stability of the modes (positive or negative damping) can be assessed. This obviously depends on the location of the flame. Annaswamy et al. (1997) show that this model reproduces stability results obtained experimentally by Lang, Poinsot and Candel (1987).

As mentioned, the coupling between the modes is due (in the absence of mean flow and mean heat release) entirely to the heat release fluctuations. This effect is analyzed for the 2-mode case under a simplified flame model: $\dot{Q}' \sim u'$. This simplification is appropriate at acoustic frequencies since, according to equation (C.4), the heat release lags the velocity fluctuation by $\pi/2$ at those frequencies. Incidentally this also shows that the internal dynamics of

the flame are almost irrelevant in determining the stability of the system, at least given this model. It is shown that the stability/instability characteristics, i.e., growth rates and resonance frequencies, of the system are only slightly affected by this linear coupling (in fact they are of second order in the coupling parameters).

While the coupling thus introduced does not majorly change any characteristics of the uncontrolled system and thus could be neglected to calculate stability limits of combustion chambers, it does affect the zeros of the system transfer function in a direct way. This has an effect on the controller design (see below).

C.3 Control Effort

In order to do control, sensor(s) and actuator(s) need to be added to the combustor. For the bulk of their work, the MIT group chooses a microphone (located at x_s) as sensor and a loudspeaker (located at x_a) as actuator. The most recent publications use secondary fuel modulation for the actuating process; no specific dynamics are attributed to the injection process besides adding a time lag to the system (see below).

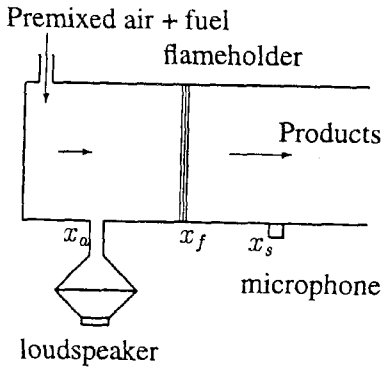

Figure C.3: System used to derive model

The addition of the loudspeaker modifies equations (C.1) and (C.2) slightly, acting as a

source of mass and energy. To account for this $+b_{ci}\dot{v}_a$ is added to the RHS of (C.1) and $+k_{a0}\alpha_r v_a$ is added to the RHS of (C.2). Here v_a is the velocity of the loudspeaker diaphragm and $k_{a0} = 0$ if $x_a > x_f$ and unity otherwise (i.e., it describes the relative position of actuator and flame).

Finally the diaphragm itself presents some dynamics as it responds to an input voltage u_a across the loudspeaker. These dynamics are modeled by a second order system:

$$m_l\ddot{x}_a + b_l\dot{x}_a + k_l x_a = k_1 u_a \tag{C.7}$$

Combining all the equations, the complete model can be written in operator form as:

$$p' = W(s)G_l(s)u_a \tag{C.8}$$

$W(s)$ is of order $2N+1$ (N: number of modes retained) and includes the effects of acoustic modes, flame dynamics, and all coupling effects therein. $G_l(s)$ denotes the actuator dynamics of (C.7). The complex poles of $W(s)$ correspond to the acoustic modes and the real pole of $W(s)$ corresponds to the flame dynamics. The complex zeros of $W(s)$ represent the coupling between the modes and the real zero stems again from the flame dynamics.

The general approach to the control problem is outlined by Annaswamy and Ghoniem (1995) (at this early point of their studies the dynamics of the actuator were still ignored, thus putting $G_l(s)$=1).

In case of a single mode analysis a simple first order phase-lead controller can be used to stabilize the system. It is recognized that this is primarily due to the fact that $W(s)$ is minimum phase, a fact which might not hold in the presence of multiple modes.

Therefore, a 2-modes case is also analyzed. If the parameters are chosen appropriately ($\omega_1 < \omega_{zero} < \omega_2$) the phase angles at the two acoustic frequencies can be almost 180^o apart.

Thus the phase variations of the controller $G_c(s)$ need to be shaped appropriately and a higher order compensator is needed. Strategies suggested by Annaswamy and Ghoniem (1995) are pole-placement, LQR and, in case the operating conditions change, an adaptive controller.

Annaswamy and Ghoniem (1995) then successfully test this general approach on two simulated experiments: a Rijke tube and a premixed combustor rig.

Rumsey, Fleifil, Annaswamy, Hathout and Ghoniem (1998b) present a nice overview of the evolving effort at MIT and shows how they started designing controllers with the simple linear model and then built a bench top combustor rig to test the controllers in a laboratory environment. Figure C.4 shows a diagram of the test facility and figure C.5 shows the experimental response of the system, obtained when applying three different kinds of controllers: proportional control, a phase-lead controller and an LQG controller.

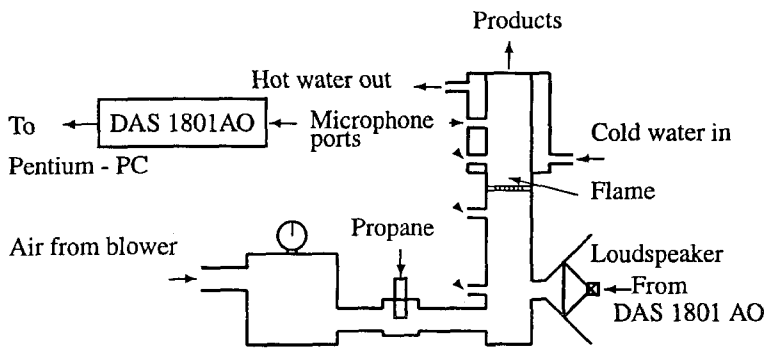

Figure C.4: Schematic of combustor rig

C.3.1 The Need to Model the Linear Coupling

In Annaswamy et al. (1997), the focus is on the effect that the linear mode coupling induced by the flame model has on the controller design. Note that in this study the actuator has

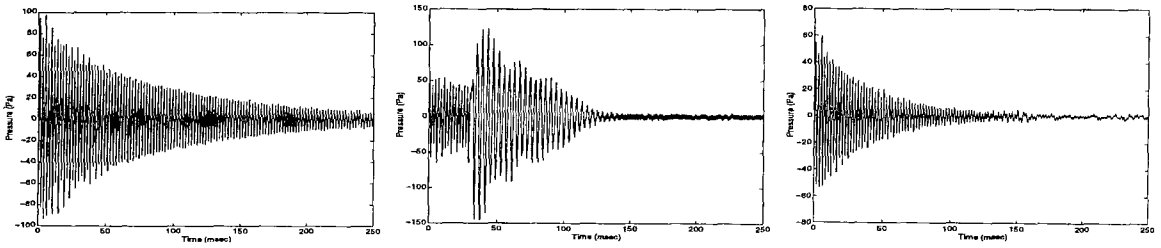

Figure C.5: Results obtained with (from left to right): proportional control, phase-lead control, and LQG control

no dynamics; this assumption has no effect on the conclusions drawn.

Whereas the change of poles of the system due to the coupling is of second order in the coupling parameters, the change in the zeros of the system is of first order in those coupling parameters. Furthermore, the zeros depend directly on the sensor location x_s and the actuator location x_a. Depending on the combination of flame location, x_s and x_a, the system can be non-minimum phase and the zero frequency can be close to a resonance frequency. This result has repercussions on the control design as it introduces extra phase shifts between the control signal and the pressure signal.

To demonstrate the effect the coupling has, a numerical simulation (using two modes) is performed for two different combinations of actuator/sensor location (labeled A/B and A/C respectively). See figure C.6 for a pole/zero map of the transfer functions W_c of both systems (note that the A/C configuration is non-minimum phase). The point of the paper is to show that it is not enough to know the damping and the frequency of each mode but that the coupling between the modes needs to be considered when the controller is designed. Therefore, poles/zeros of the models of both configurations are also shown for the case in which the coupling terms are simply ignored, giving the transfer functions W_u.

Designing a simple phase-lead controller and an LQR controller for both configurations,

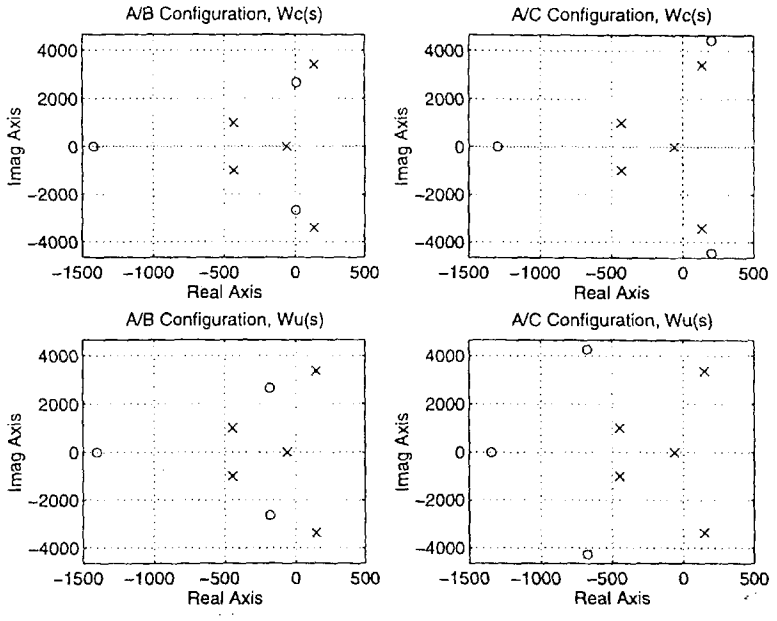

Figure C.6: Poles (x) and zeros (o) of the systems studied

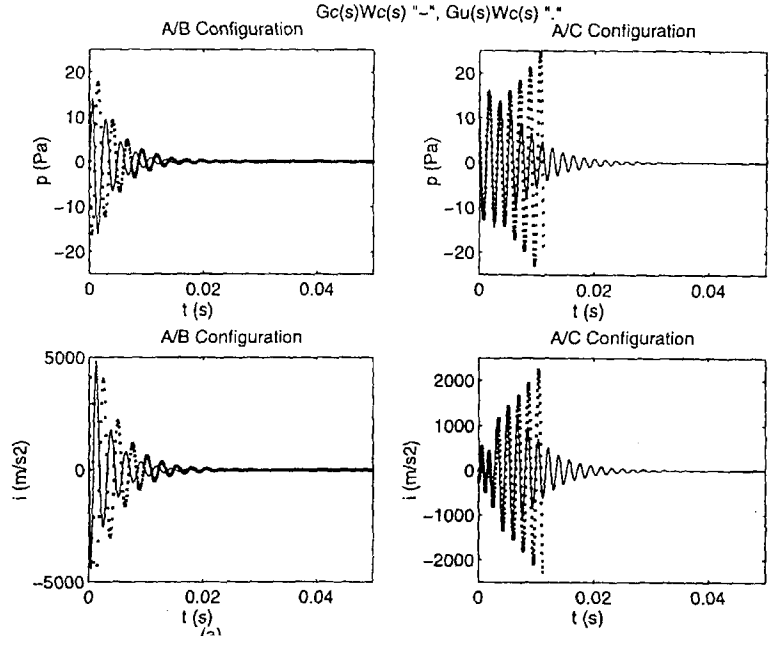

Figure C.7: Results obtained with controllers whose design is based on the coupled (solid) and uncoupled (dashed) model

they show that a design based on the uncoupled model (i.e., on W_u) might not be effective in case the system is non-minimum phase; see figure C.7. The reason is of course the extra phase shift introduced by the left-hand plane zeros which are not accounted for in the design.

Fleifil, Hathout, Annaswamy and Ghoniem (1998) analyze the two mode case once again, with a single sensor and single loudspeaker as actuator. It is shown that in case of an end-mounted loudspeaker there is no 'antiresonance damping' (i.e., the zeros are on the imaginary axis) and thus the effect of linear coupling is negligible. In the case of a side-mounted speaker, the linear coupling between the modes as well as actuator/sensor location affect the system and can make it non-minimum phase.

Hathout, Fleifil, Rumsey, Annaswamy and Ghoniem (1997) also include a discussion of the 'zero dynamics' showing that collocation of sensor and actuator does not guarantee a minimum phase transfer function, and that even when sensor and actuator are in separate locations the zeros can be stable. The properties of the zeros must therefore be considered separately for each case.

C.3.2 The Need to Model All Frequencies Correctly

Fleifil et al. (1998) attempt to explain the results of some experiments (Lang et al. 1987, Gulati and Mani 1992) which reported that the dominant acoustic instability can be suppressed by active control, but that secondary peaks at different frequencies which were not excited in the uncontrolled combustor appear.

This effect is particular to the controlled problem and can be explained by splitting the

acoustic field inside the chamber into three contributions:

$$p' = p'_h + p'_{direct} + p'_{indirect} \tag{C.9}$$

In this decomposition p'_h is the component of the pressure due to the homogeneous part of the heat release (i.e., the part of the heat release that would be present without the actuator); p'_{direct} is the contribution of the actuator on the acoustic pressure, and $p'_{indirect}$ is the effect on the pressure of the change in the heat release due to the action of the actuator. p'_h and p'_{direct} govern the phase lag between control input and control output in the acoustic frequency range whereas $p'_{indirect}$ introduces an extra phase lag at frequencies comparable to the flame characteristic frequency which is lower than the acoustic frequency. It is the combination of these different phase lags which is responsible for unexpected behavior if the controller is designed with only the unstable acoustic mode in mind (instead of considering the entire frequency range).

Examples are given for an end-mounted and side-mounted loudspeaker where the parameters for the numerical simulations have been chosen to replicate the experiments of Gulati and Lang respectively. Results of the simulations are shown in figure C.8 and are in qualitative agreement with the experiments.

For each case the exact reason for the appearance of the secondary peaks is given, i.e., the contributions of each of the three pressure components and their interplay with the controller are analyzed. Note that these peaks can occur even though, as in the end-mounted case, p'_{direct} is zero; that is, the actuator is not directly contributing to this mode.

It is noteworthy that the actuator in the model used by Fleifil et al. (1998) does not present any internal dynamics and therefore does not introduce any extra resonances in the system. This deficiency is remedied by Hathout et al. (1998) where this analysis of the

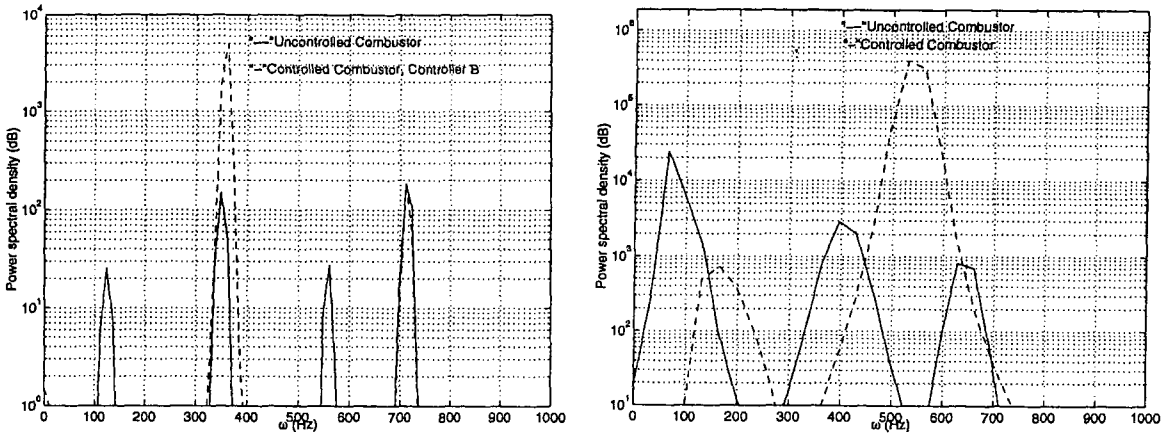

Figure C.8: Simulation results of experiments reported by Gulati (left) and Lang (right)

mutual influences of the combustor dynamics and the controller is repeated in more detail. Furthermore, Hathout et al. (1998) argue (and show) that the appearance of secondary peaks can be avoided if an LQR approach is used to design the controller. The reason for the effectiveness of the LQR design is that by construction the control input is minimized over the whole frequency range as opposed to just the unstable frequency. Hathout et al. (1998) compare the LQR controller with a phase-shift controller in both time and frequency domain and show that the LQR design can indeed successfully suppress the secondary peaks in the experimental setup of both Gulati and Mani (1992) and Lang et al. (1987).

C.3.3 The Need for Robust Control

Annaswamy et al. (1998) do a sensitivity analysis of the system to parameter variation (such as effective combustor length, laminar burning velocity, mean flow speed and mean heat addition). The effects of these parameters on unstable frequency and growth rate are shown for a numerical example; more important than the change in these observable quantities, however, is their effect on the overall transfer function relating pressure and control input.

For the combustor considered by Annaswamy et al. (1998), the perturbed transfer function is shown in figure C.9.

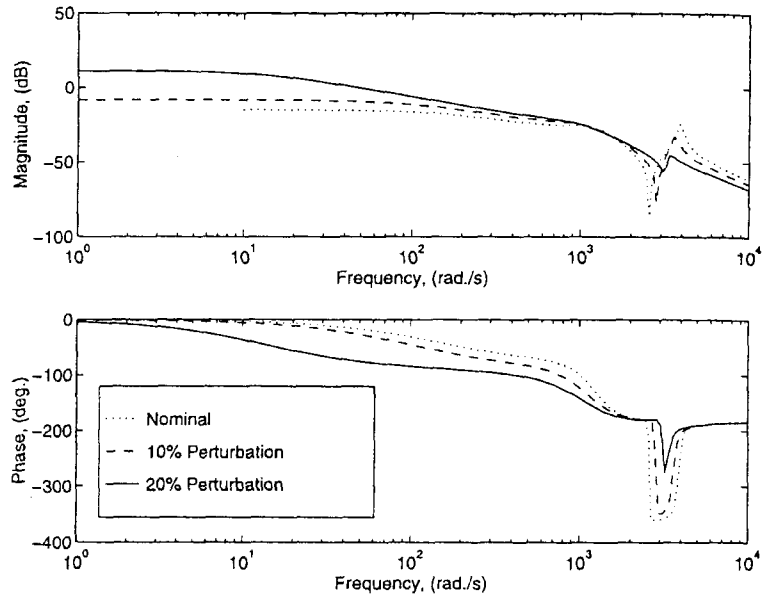

Figure C.9: Gain-phase characteristics for nominal and perturbed parameter values

Using the nominal transfer function, a model fixed phase-lead controller is designed. This controller achieved satisfactory performance even when some of the parameters were perturbed up to 60%. However, perturbing the effective length or the combustor zeros by 20% resulted in an unstable response. The reason is that both of those perturbations introduce significant phase variations in the vicinity of the unstable frequency.

To accommodate such a variation, a self-tuning phase lead compensator is designed. This adaptive controller has actually a similar structure as the fixed controller except that a varying gain $k_0(t)$ is added.

The complete controller has the following form (γ_k and a are adaptive parameters that

determine the speed of the adaptation):

$$u_a = k_0(t)X + \dot{k_0}X_f \tag{C.10}$$

$$\dot{k_0} = -\gamma_k p' X_f \tag{C.11}$$

$$X = k_c \frac{s+z_c}{s+p_c} p' \tag{C.12}$$

$$X_f = \frac{1}{s+a} X \tag{C.13}$$

Results obtained with this controller are shown in figure C.10 along with the time variation of the tuning gain k_0. Note that once convergence is achieved, $\dot{k_0} = 0$, this controller becomes indeed a fixed phase lead controller.

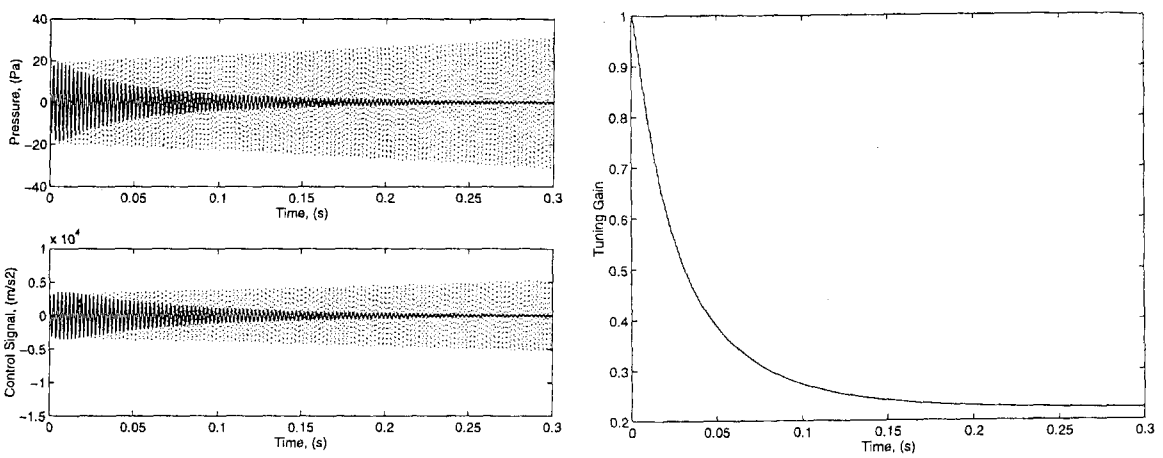

Figure C.10: Performance of self-tuning controller vs. fixed controller

Annaswamy et al. (1998) also compares this adaptation method to the LMS algorithm. In that algorithm Q' is fed back (instead of p' for the self-tuner) and the filtered signal X_f is constructed in a different way (in the equation $X_f = W(s)X_t$, $W(s)$ is determined by the combustor model at a chosen stable or unstable operating point). These differences result in numerical instabilities which lead to failure of the LMS controller.

C.3.4 No Need to Consider Nonlinearities?

Rumsey et al. (1998a) add the nonlinearities described in equation (C.5) to the system and show that these lead to limit-cycle behavior. They also show that a describing function analysis can be performed in order to estimate the limiting amplitude of the pressure amplitudes.

An LQG controller was designed based on the *linear* model (with two modes). The simulations demonstrate that this controller performs fine even with the nonlinearities present. If the nonlinear system is recast in a different form (by writing $f(u) = u - g(u)$), the resulting closed-loop system can be described by figure C.11. The following theorem is proven: if (i) W_{cl} is strictly positive real and (ii) $g(x)x > 0$ for all $x \neq 0$ and $g(0) = 0$, then the closed-loop system is asymptotically stable. Thus if the combustion process satisfies these conditions, a linear controller is sufficient. In practice this may not be easily verifiable.

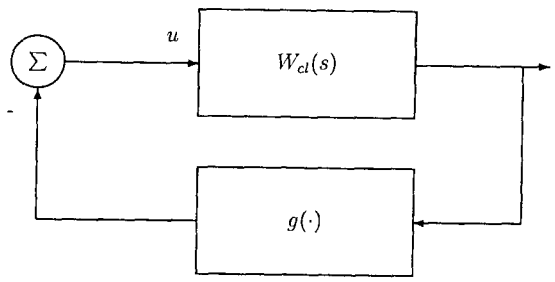

Figure C.11: Nonlinear feedback system

Hathout et al. (1997) use an optimal control strategy based on a state estimator to design an LQG controller. The design of the controller is based on the linear 2-modes model of a bench top combustor rig. The controller thus obtained controls the simplified transfer function model (obviously, since it was designed for this specific case) as well as the full PDE system (where no model decomposition has been done). This shows the validity of the

model and the robustness of the controller. Furthermore, this controller is also applied to the actual experiment and shown to perform in a satisfactory manner (see figure C.5, right). The bench top combustor exhibited limit-cycle behavior thus indicating the nonlinearity did not affect the performance of the linear design and the robustness of the design. The same result was also reported by Rumsey et al. (1998b) for other controllers (see figure C.5, left and center).

C.3.5 Time Delay

Fleifil et al. (2000) analyze the bulk mode of a combustor. They assume that the pressure oscillations lead to equivalence ratio fluctuations at the nozzle exit which are then convected to the flame. This creates a time delay τ_c in the system and the equation needed to describe this phenomenon is given by:

$$\frac{d^2p'}{dt^2} - \Gamma p'(t - \tau_c) + \omega^2 p' = 0 \tag{C.14}$$

This equation leads to stability bands (see figure C.12, τ_{ac} is the acoustic mode time scale); the time delay needs to lie within certain values for the system to be stable.

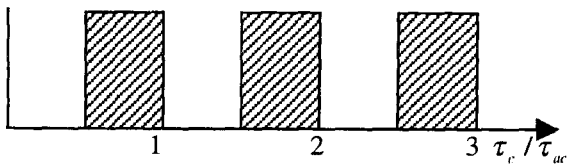

Figure C.12: Stability bands (shaded area is unstable)

If now an external modulation of the equivalence ratio is considered as control actuation (by secondary fuel injection), equation (C.14) is modified by replacing the RHS with $\gamma \frac{d\phi'_c}{dt}$. Therefore, as the system is unstable in some bands of frequency given the time delay τ, the

easiest way to control is to change the resonance frequency. This is achieved successfully by using an integral controller:

$$\frac{d\phi_c'}{dt} = -k_c p' \tag{C.15}$$

Niculescu, Annaswamy, Hathout and Ghoniem (2000) provide very detailed guidelines to cope with time-delay in generic second and third order systems. The analyzed system is described by either of the following two equations where τ represents a discrete (lump) delay and k, k_1, k_2 are parameters:

$$s^2 + 2\rho\omega_0 s + \omega_0^2 + ke^{-s\tau} = 0 \tag{C.16}$$

$$s(s^2 + 2\rho\omega_0 s + \omega_0^2) + (k_1 s + k_2)e^{-s\tau} = 0 \tag{C.17}$$

Niculescu et al. (2000) give explicit analytical expressions that the parameters (ρ, ω_0, k) need to satisfy for the system to be (un)stable independent of the value of τ. They then proceed to explore delay-dependent properties: switches from stability to instability and reversals of those switches. Once again explicit expressions for the values of parameters and conditions on when a single or more switches/reversals occur are given. These conditions provide guidelines for control designs; unfortunately, no applications are described in the paper.

C.3.6 Can Open-Loop Control Work?

Prasanth, Annaswamy, Hathout and Ghoniem (2000) discuss the merits of open-loop control. Obviously, such a control scheme would be easier to implement on a real system than a closed-loop scheme and thus deserves to be carefully considered. Open-loop strategies have been successful in experimental devices, e.g., by using low frequency pulsing of secondary fuel.

Prasanth et al. (2000) argue that the general class of models that describe a combustion instability are of the following form (the values of the parameters $\xi_0, \omega, k_1, k_2, \tau$ depends on the mechanism responsible for the instability - Prasanth et al. (2000) derives this equation for a case with both convective delay between the supply of fuel and its burning at the flame location, and a propagation delay of the flame surface into the reactants flow):

$$\ddot{\eta} + 2\xi_0\omega\dot{\eta} + (\omega^2 - k_1)\eta + k_2\eta(t-\tau) = 0 \tag{C.18}$$

Since the most promising control action is injection of secondary fuel, they focus on a control strategy that switches with a period T and pulse width $0 \leq W_p \leq 1$ between equivalence ratios ϕ_i, i.e.,

$$\phi(t) = \begin{cases} \phi_1 & : \quad nT \leq t < nT + W_pT \\ \phi_2 & : \quad nT + W_pT \leq t < (n+1)T \end{cases} \tag{C.19}$$

Note that all the parameters depend on the value of the equivalence ratio and that, given a desired operating condition of ϕ_{av}, there need to exist possible operating points $\phi_1 < \phi_{av} < \phi_2$ with $\phi_{av} = W_p\phi_1 + (1 - W_p)\phi_2$. Prasanth et al. (2000) use the small gain theorem from control theory to derive a linear matrix inequality (LMI) that the system needs to fulfill in order to be asymptotically stable and then apply that condition to the cases of stable-stable (both operating points ϕ_1 and ϕ_2 are stable) and stable-unstable (one of the operating points is unstable) switching. For the first case they show that one needs to switch sufficiently slowly so that any transients induced by the switching die down. For the second case the fraction of time spent at the unstable operating point is relevant to the overall stability and not all ϕ_{av} can be achieved; an iterative algorithm to find the appropriate W_p and T is given.

Prasanth et al. (2000) argue that this approach with the LMI can also be applied for non-ideal (i.e., not instantaneous) switching or in the presence of a hysteresis in the combustor

dynamics.

To show that such an open-loop strategy works, numerical simulations are done with parameter values suitable to simulate the experiment done by Richards, Janus, Robey, Cowell and Rawlins (1999). The simulations are shown in figure C.13 (a noise vector w has been added to the system dynamics to represent disturbances) and seem to match with the experimental results. The average operating point ϕ_{av} is unstable in both cases, the switching frequency between ϕ_1 and ϕ_2 is indicated at the top of the plots.

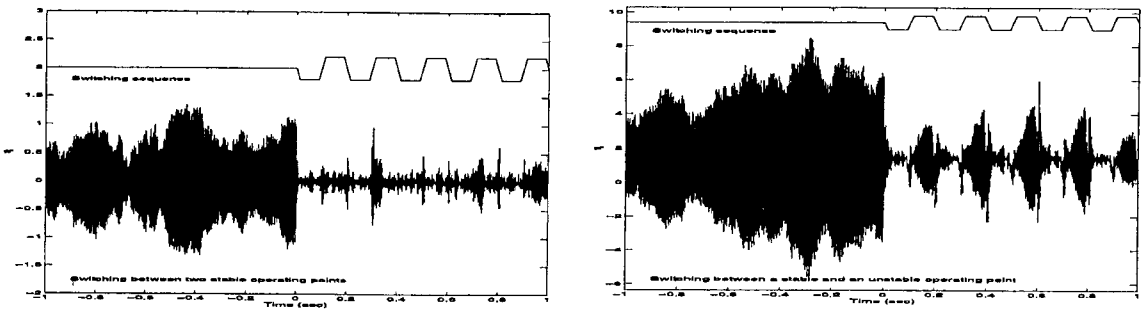

Figure C.13: Simulations of open-loop equivalence ratio switching between two stable points (left) and a stable and an unstable operating point (right)

C.4 Comments

It is obvious that the main focus of the MIT group is the application of control. Their model of combustion instabilities is not novel at all (contrary to what they claim) and has been used to a much larger extent by other researchers. In fact, only a one-dimensional analysis is used; presumably the work can be extended to incorporate tangential or radial modes by a more general application of the method of spatial averaging (as done for instance by Culick or Zinn). It should also be noted that only linear gasdynamics are used and thus any

behavior produced by nonlinear gasdynamics (such as limit-cycles) cannot be captured.

The flame response is the most distinguishing feature of their model when compared to other works in the combustion instability control literature, with the notable exception of Dowling who has used the same heat release dynamics, based on the MIT work. While the governing differential equation has been derived under severe restrictions, it seems to be applicable to all the applications given. However, the applications are very limited in scope (basically they are Rijke tubes) and the bench top combustor used at MIT has been constructed in such a way as to fit the model!

Up to the work by Fleifil et al. (2000) the premixed flame is held in place by a perforated plate and is supposed to be rather flat. In Fleifil et al. (2000) equation (C.6) is derived for an extended flame but in that paper no flame dynamics are used (!) as the heat release rate does not respond to acoustic fluctuations at the flame but rather to equivalence ratio variation at the fuel nozzle. Assuming that the fuel nozzle in the feed system is choked, the instantaneous equivalence ratio is related to u' via $\phi = \bar{\phi}[1 - u'/\bar{u}]$. This paper is therefore different from the rest of the work (the flame dynamics are replaced by a time delay) and might indicate a new direction of their research.

The linear flame model described by equation (C.4) when used in conjunction with the chamber acoustics compares well with experiments in predicting the correct unstable frequencies. Note that even though the linear coupling introduced through the heat release is stressed in the MIT work, the fact that their model predicts the unstable modes is not by itself an indication that they got the model right since the effect of this coupling on the uncontrolled system is negligible.

The analysis of the influence of time delay seems very limited at this point. While their

approach (Niculescu et al. 2000) does indeed provide explicit limits on the system parameters, the expressions given are only valid for low-order systems and are restricted to a one mode analysis. It is doubtful that such an analysis can be done for a more complex (and thus realistic) system.

The various controllers designed in the MIT work are all based on a 2-modes model. The 'trick' to write the complete system in an input-output framework and use a transfer function allows them to explain various problems occurring when applying control. This approach is very simple, and classical control concepts (gain & phase margin) can easily be applied in this way. Moreover, the effect of changes in actuator/sensor location can be readily assessed. Except for the self-tuning controller, the controllers used (proportional, integral, phase-lead, LQG) are not very sophisticated. But even the adaptive controller varies only one single parameter in order to adapt to a perturbed plant (i.e., accommodate model uncertainties). Nevertheless, all of these controllers, which have been designed for a low-order linear model, perform successfully on the real bench top combustor.

The analysis of open-loop control schemes gives a way to determine a suitable frequency and pulse width for using a pulsed secondary fuel source. The conclusions drawn are rather obvious (especially for the stable-stable switching), but nevertheless a framework to analyze this type of control actions is provided. It should be noted, however, that the numerical simulations reported (figure C.13) are misleading inasmuch as they are only linear simulations. The apparent presence of a limit cycle is only due to the forcing by the added noise term; the average operating point is in fact (marginally) unstable. No simulations including nonlinearities are given: thus the claim that this analysis can be used in the presence of hysteresis is not really proven. Furthermore, the discussion is based on a single

mode, lumped-parameter model which might be too restrictive for actual systems.

The MIT work is obviously far from finished and some of the subjects (time-delay, nonlinearities) have barely been touched. However, the published papers show a steady progression in their effort and the ongoing work at MIT seems to become more elaborate. Note that the papers cited in this review reference other papers or conference presentations by the MIT group. These other sources have either not been published or are verbatim copies of the works reviewed here and are therefore not included in this report.

Bibliography

AGARD (ed.) (1996). *Active Combustion Control for Propulsion Systems*, AGARD-R-820. NATO Advisory Group for Aerospace Research and Development, Propulsion and Energetics Panel, 6-9 May, Athens, Greece.

Agarkov, A., Denisov, K., Dranovsky, M., Zavorokinin, I., Ivanov, V., Pikalov, V. and Shibanov, A. (1993). Injector flame stabilization effects on combustion instability.

Ananthkrishnan, N. (2000a). Qualitative dynamics of nonlinear acoustic waves in a combustion chamber, i: Mode truncation and triggering, *Documents on Active Control of Combustion Instabilities*. California Institute of Technology, Jet Propulsion Center.

Ananthkrishnan, N. (2000b). Qualitative dynamics of nonlinear acoustic waves in a combustion chamber, ii: Second mode and dual mode instability, *Documents on Active Control of Combustion Instabilities*. California Institute of Technology, Jet Propulsion Center.

Annaswamy, A. and Ghoniem, A. (1995). Active control on combustion systems, *IEEE Control systems magazine* **15**(6): 49–63.

Annaswamy, A., El Rifai, O., Fleifil, M., Hathout, J. and Ghoniem, A. (1998). A model-based self-tuning controller for thermoacoustic instability, *Combustion science and*

technology **135**(1-6): 213–240.

Annaswamy, A., Fleifil, M., Hathout, J. and Ghoniem, A. (1997). Impact of linear coupling on the design of active controllers for the thermoacoustic instability, *Combustion science and technology* **128**(1-6): 131–180.

Biswas, S. (1998). Robust stabilization of linear systems in the presence of gaussian perturbation of parameters, *Optimal Control Applications and Methods* **19**: 271–286.

Burnley, V. (1996). *Nonlinear combustion instabilities and stochastic sources*, PhD thesis, California Institute of Technology.

Burnley, V. and Culick, F. (2000). Influence of random excitations on acoustic instabilities in combustion chambers, *AIAA Journal* **38**(8): 1403–1410.

Candel, S. (1992). Combustion instabilities coupled by pressure waves and their active control, *24th International Symposium on Combustion* pp. 1277–1296.

Carrier, G. (1954). *Quarterly of Applied Mathematics* **12**: 383.

Chou, J., Chen, S. and Chao, C. (1998). Robust stabilization of flexible mechanical systems under noise uncertainties and time-varying parameter perturbations, *Journal of Vibration and Control* **4**: 167–185.

Chu, B.-T. and Kovasznay, L. (1956). Nonlinear interactions in a viscous heat-conducting compressible gas, *Journal of Fluid Mechanics* **3**(5): 494–514.

Clanet, C., Searby, G. and Clavin, P. (1999). Primary acoustic instability of flames propagating in tubes: cases of spray and premixed gas combustion, *Journal of Fluid Mechanics* **385**: 157–197.

Clavin, P., Pelce, P. and Longting, H. (1990). One-dimensional vibratory instability of planar flames propagating in tubes, *Journal of Fluid Mechanics* **216**: 299–322.

Culick, F. (1971). Nonlinear growth and limiting amplitude of acoustic oscillations in combustion chambers, *Combustion science and technology* **3**(1): 1–16.

Culick, F. (1994). Some recent results for nonlinear acoustics in combustion chambers, *AIAA Journal* **32**(1): 146–169.

Culick, F. (1995). Nonlinear acoustics in combustion chambers with stochastic sources, *Documents on Active Control of Combustion Instabilities.* Guggenheim Jet Propulsion Center, California Institute of Technology.

Culick, F. (1997). A note on ordering perturbations and the insignificance of linear coupling in combustion instabilities, *Combustion Science and Technology* **126**(1–6): 359–379.

Culick, F. and Yang, V. (1992). Prediction of the stability of unsteady motions in solid propellant rocket motors, nonsteady burning and combustion stability of solid propellants, *Progress in Astronautics and Aeronautics* **143**: 719–779.

Denisov, K., Kadishevish, A. and Povolotzky, J. (1995). Full-scale component and engine stability testing using spectral analysis, *Progress in Astronautics and Aeronautics* **169**: 529–544.

Duer, J. and Hessler, R. (1984). Forced oscillation theory and applications, *20th AIAA/ASME/SAE/ASEE Joint Propulsion Conference.* AIAA Paper No. 84-1356.

Flandro, G. (1995). Effects of vorticity on rocket combustion stability, *Journal of Propulsion and Power* **11**(4): 607–625.

Fleifil, M., Annaswamy, A., Ghoneim, Z. and Ghoniem, A. (1996). Response of a laminar premixed flame to flow oscillations: A kinematic model and thermoacoustic instability results, *Combustion and flame* **106**(4): 487–510.

Fleifil, M., Hathout, J., Annaswamy, A. and Ghoniem, A. (1998). The origin of secondary peaks with active control of thermoacoustic instability, *Combustion science and technology* **133**(4-6): 227–265.

Fleifil, M., Hathout, J., Annaswamy, A. and Ghoniem, A. (2000). Reduced order modeling of heat release dynamics and active control of time-delay instability, *38th Aerospace Sciences Meeting Conference and Exhibit.* AIAA paper No. 2000-0708.

Franklin, G., Powell, J. and Emami-Naeini, A. (1995). *Feedback Control of Dynamic Systems*, Addison Wesley.

Glick, R. (1996–99). Numerous private conversations and semi-private e-mails.

Gulati, A. and Mani, R. (1992). Active control of unsteady combustion-induced oscillations, *Journal of Propulsion and Power* **8**(5): 1109–1115.

Haddad, R. and Parsons, T. (1991). *Digital Signal Processing—Theory, Applications and Hardware*, Computer Science Press.

Haddad, W., Leonessa, A., Corrado, J. and Kapila, V. (1997). Robust reduced-order control of combustion instabilities, *Proceedings of the 1997 IEEE International Conference on Control Applications.* Hartford, CT.

Harrje, D. and Rearden, F. (1972). *NASA SP194.*

Hathout, J., Annaswamy, A., Fleifil, M. and Ghoniem, A. (1998). A model-based active control design for thermoacoustic instability, *Combustion science and technology* **132**(1-6): 99–138.

Hathout, J., Fleifil, M., Rumsey, J., Annaswamy, A. and Ghoniem, A. (1997). Model-based analysis and design of active control of thermoacoustic instability, *Proceedings of the 1997 IEEE International Conference on Control Applications*. Hartford, CT.

Hessler, R. (1979). Studies of motor instability problems, *16th JANNAF Combustion Sub-Committee Meeting*.

Hessler, R. (1980). Prediction of finite pressure oscillations in stable rocket motors, *17th JANNAF Combustion Sub-Committee Meeting*.

Hessler, R. (1982). Forced oscillation prediction, *19th JANNAF Combustion Sub-Committee Meeting*.

Hessler, R. and Glick, R. (1998). Application of maximum entropy method to passively extract motor stability information, *Workshop 'Measurement of Thermophysical and Ballistic Properties of Energetic Materials'*. Politecnico di Milano, Milan, Italy.

Holmes, P., Lumley, J. and Berkooz, G. (1996). *Turbulence, Coherent Structures, Dynamical Systems and Symetry*, Cambridge University Press.

Hong, B., Yang, V. and Ray, A. (1998). Robust feedback control of combustion instability with model uncertainty, *36th Aerospace Sciences Meeting, Reno, Nevada*. AIAA paper No. 98-0354.

Isella, G. (2001). *Modeling and simulation of combustion chamber and propellant dynamics and issues in active control of combustion instabilities*, PhD thesis, California Institute of Technology.

Isella, G., Seywert, C., Culick, F. and Zukoski, E. (1997). A further note on active control of combustion instabilities based on hysteresis, *Combustion science and technology* **126**(1-6): 381–388.

Jahnke, C. and Culick, F. (1994). Nonlinear energy transport between longitudinal acoustic modes in cylindrical combustion chambers, *30th AIAA/ASME/SAE/ASEE Joint Propulsion Conference.* AIAA Paper No. 94-3190.

Lang, W., Poinsot, T. and Candel, S. (1987). Active control of combustion instability, *Combustion and Flame* **70**: 281–289.

Lieuwen, T. and Lee, D. (2000). Nonlinear modeling of combustor dynamics using experimental data, *36th AIAA/ASME/SAE/ASEE Joint Propulsion Conference and Exhibit.* AIAA paper No. 2000-3464.

Lieuwen, T. and Zinn, B. (2000). Experimental investigation of limit cycle oscillations in an unstable gas turbine combustor, *38th Aerospace Sciences Meeting and Exhibit.* AIAA paper No. 2000-0707.

Lores, M. and Zinn, B. (1973). Nonlinear longitudinal combustion instability in rocket motors, *Combustion Science and Technology* **7**: 245–256.

Majdalani, Y. and van Moorhem, W. (1995). The unsteady boundary layer in solid rocket motors, *31st AIAA/ASME/SAE/ASEE Joint Propulsion Conference.* AIAA Paper No. 95-2731.

McIntosh, A. (1987). Combustion-acoustic interaction of a flat flame burner system enclosed within an open tube, *Combustion Science and Technology* **54**: 217–236.

McManus, K., Poinsot, T. and Candel, S. (1993). A review of active control of combustion instabilities, *Progress in Energy and Combustion Science* **19**(1): 1–29.

Merk, H. (1957). *Applied Scientific Research* **A6**: 317.

Neumeier, Y., Nabi, A., Arbel, A., Vertzberger, M. and Zinn, B. (1997). Open-loop performance of a fast-response, actively controlled fuel injector actuator, *Journal of Propulsion and Power.*

Nicoli, C. and Pelce, P. (1989). One-dimensional model for the rijke tube, *Journal of Fluid Mechanics* **202**: 83–96.

Niculescu, S., Annaswamy, A., Hathout, J. and Ghoniem, A. (2000). Control of time-delay induced instabilities in combustion systems, *to be published.*

Øksendal, B. (1998). *Stochastic differential equations : an introduction with applications*, Springer.

Paparizos, L. and Culick, F. (1989). The two-mode approximation to nonlinear acoustics in combustion chambers. i. exact solutions for second order acoustics, *Combustion Science and Technology* **65**(1–3): 39–65.

Pelce, P. and Rochwerger, D. (1992). Vibratory instability of cellular flames propagating in tubes, *Journal of Fluid Mechanics* **239**: 293–307.

Poinsot, T., Bourienne, F., Candel, S. and Esposito, E. (1987). Suppression of combustion instabilities by active control, *Journal of Propulsion* **5**: 14–20.

Poncia, G. (1998). *A study on thermoacoustic instability phenomena in combustion chambers for active control*, PhD thesis, Politecnico di Milano.

Powell, E. (1970). *Nonlinear combustion instability in liquid-porpellant rocket engines*, PhD thesis, Georgia Institute of Technology.

Powell, E. and Zinn, B. (1971). A single mode approximation in the solution of nonlinear combustion instability problems, *Combustion Science and Technology* **3**: 121–132.

Prasanth, R., Annaswamy, A., Hathout, J. and Ghoniem, A. (2000). When do open-loop strategies for combustion control work?, *36th AIAA/ASME/SAE/ASEE Joint Propulsion Conference and Exhibit.* AIAA paper No. 2000-3350.

Pun, W. (2001). *Heat driven pressure oscillations*, PhD thesis, California Institute of Technology.

Raun, R., Beckstead, M., Finlinson, J. and Brooks, K. (1993). A review of rijke tubes, rijke burners and related devices, *Progress in Energy and Combustion Science* **19**: 313–364.

Rayleigh, L. (1896). *The Theory of Sound*, Mcmillan.

Richards, G., Janus, M., Robey, E., Cowell, L. and Rawlins, D. (1999). Control of flame oscillations with equivalence ratio modulation, *AIAA Journal of Propulsion and Power* **15**: 232–240.

Rijke, P. (1859). Notiz über eine neue Art, die Luft in einer an beiden Enden offenen Röhre in Schwingungen zu versetzen, *Annalen der Physik* **107**: 339–343.

Rowley, C., Colonius, T. and Murray, R. (2000). Pod based models of self-sustained oscillations in the flow past an open cavity, *6th AIAA/CEAS Aeroacoustics Conference.* AIAA paper No. 2000-1969.

Rumsey, J., Fleifil, M., Annaswamy, A., Hathout, J. and Ghoniem, A. (1998a). Low-order nonlinear models of thermoacoustic instabilities and linear model-based control, *MIT Adaptive Control Laboratory Report.*

Rumsey, J., Fleifil, M., Annaswamy, A., Hathout, J. and Ghoniem, A. (1998b). The role of active control in suppressing thermoacoustic instability.

Seywert, C., Isella, G. and Culick, F. (2000). Active feedback control of combustor dynamics with time delay and noise, *36th AIAA/ASME/SAE/ASEE Joint Propulsion Conference and Exhibit.* AIAA paper No. 2000-3124.

Strahle, W. (1978). Combustion noise, *Progress in Energy and Combustion Science* **4**: 157–176.

Strogatz, S. (1996). *Nonlinear Dynamics and Chaos*, Addison Wesley.

Vasta, M. and Roberts, J. (1998). Stochastic parameter estimation of non-linear systems using only higher order spectra of the measured response, *Journal of Sound and Vibration* **213**(2): 201–221.

Wang, Y. (2000). *Effects of actuator limits in bifurcation control with applications to active control of fluid instabilities in turbomachinery*, PhD thesis, California Institute of Technology.

Wiggins, S. (1996). *Introduction to Applied Nonlinear Dynamical Systems and Chaos*, Springer Verlag.

Yang, V., Sinha, A. and Fung, Y. (1992). State-feedback control of longitudinal combustion instabilities, *Journal of Propulsion and Power* **8**(1): 66–73.

Zinn, B. and Powell, E. (1970a). Application of the galerkin method in the solution of combustion-instability problems, *XIXth International Astronautical Congress* **3**: 59–73.

Zinn, B. and Powell, E. (1970b). Nonlinear combustion instability in liquid-propellant rocket engines, *Thirteenth Symposium (International) on Combustion.* Salt Lake City, Utah.